Ultrafine Particle Loss in Aerosol Diluters

A THESIS
SUBMITTED TO THE FACULTY OF THE GRADUATE SCHOOL
OF THE UNIVERSITY OF MINNESOTA
BY

Aaron Michael Collins

IN PARTIAL FULFILLMENT OF THE REQUIREMENTS
FOR THE DEGREEE OF
MASTER OF SICENCE

David B. Kittelson, Advisor

December 2010

Acknowledgements

First and foremost I would like to thank Prof. Kittelson for his help and support through this process. I would also like to extend my thanks to all of the students and staff in the Center for Diesel research, with a special thanks to Anil Bika, Luke Franklin, Jake Swanson and André Olson. I would also like to thank Gina Cuneo for her never ending support of all my pursuits in life. Without her support, this work may have never been completed.

Finally I would like to thank Professor Benjamin Y. H. Liu for his finical support of this work as well as for the time he spent to help mentor a young engineer.

Abstract

Measurements of high concentration aerosols typically require some method to reduce the concentration of the aerosol to a measureable method. One common method is to use an aerosol diluter to reduce the aerosol concentration by a known value. Particle loss within the aerosol diluters can result in values of dilution that are particle size dependent and vary from the idealized volumetric dilution value.

Experiments were performed to measure the sub-100nm particle loss within aerosol diluters. The diluters tested include the TSI 3302, MSP 1100, a "leaky filter" laboratory diluters and a newly developed Orifice Diluter. Particle loss within aerosol diluters was found to be a significant effect, with up to 50% of the dilution being due to particle loss. Particle loss within the aerosol diluters was found to be primarily diffusion driven and loss within the diluters increased with decreasing particle diameter. A new terms was derived to describe particle loss within the aerosol diluters where diluter penetration describes the percentage of particle loss within an aerosol diluter.

Further investigation into particle charge found a significant reduction in particle penetration when the aerosol was singly charged. This can result as much as a 40% enhancement in particle loss.

Diluter penetration curves for the TSI 3302,MSP 1100, "leaky filter" and Orifice Diluters were then used to correct measurements of high concentration diesel aerosol. Correction methodology was found to be highly sensitive to the measured size distribution of the diesel aerosol. With accurate size distribution measurements the agreement between diluter and CPC combinations was corrected to less than 3% at a

concentration of 1.57E5 cm^{-3} with a geometric mean diameter (GMD) of 50.0nm . As the GMD was reduced for the aerosol agreement among diluters was reduced, with a resulting agreement of ±4% at a GMD of 36.5 nm and ±25% at a GMD of 16.3nm. The decrease in agreement is due to the accuracy in the size distribution measurements.

Table of Contents

List of Figures

List of Tables

Chapter 1

Introduction

1.1 Relevance to Society

High concentrations of ultrafine particles, defined as having an effective diameter less than 100nm, have raised concerns about air pollution and health effects associated with exposure. On area of concern is the health effects associated with exposure and inhalation of ultrafine particles. Although the mass associated to ultrafine particles is typically relatively small when compared to PM2.5 standards, research indicates that the high surface area to mass ratio makes these particles more efficient for delivery of hazardous substances (Stoeger, 2006; Oberdörster,2000). Work by Bateson and Schwartz(2001) also showed high levels of ultrafine particles are especially dangerous to the elderly, developing children and those with pre-existing cardiopulmonary disease.

Typical roadway and urban aerosol ultrafine particle concentration can vary between 40,000 to 500,000 particle/cm^3(Kittelson 2004; Westerdahl 2005). Typically this measurement is made using a condensation particle counter(CPC) also sometimes referred to as a Condensation Nuclei Counter(CNC). The CPC allows for single particle counting of aerosols using condensation growth and an optical detector, for a more detailed description see section 1.5.2. This method of measuring ultrafine particles, however, is typically constrained by the upper concentration measurement limit of the device. Typical CPC concentration limits for the single counting mode are in the range 10^4 to 10^5 particles/cm^3, well below some roadway aerosol concentrations. To extended

the upper concentration limit, aerosol dilution is used to reduce the inlet concentration of the CPC to an acceptable range. Knowing the dilution ratio and the inlet concentration to the CPC allows for the true concentration to be back calculated.

Dilution ratios are traditionally calculated using the volumetric flow rates within the diluter to determine the overall reduction in concentration; this is termed the volumetric dilution ratio. Unfortunately the assumption surrounding the use of volumetric flow rates as the dilution ratio assumes that there are no particle losses internal to the diluter. If particle losses are present, this introduces an additional complexity as the particle dilution ratio may not the same as the volumetric dilution ratio.

The objective of this body of work is to investigate the relationship between the volumetric dilution and particle dilution ratios in the ultrafine particle size range for common commercial and laboratory diluters. The diluters tested include the TSI 3302, MSP 1100, "Leaky Filter" and an Orifice diluter. Parameters such as particle size and aerosol charge are investigated over the particle size range of 9 nm to 100 nm Additionally, using the measured particle dilution ratio, high concentration diesel aerosol concentration measurements are made and inter agreement among diluter and CPC combinations are compared.

1.2 What is Aerosol Dilution?

Aerosol dilution is simply the act of reducing the concentration of an aerosol in a known ratio. An aerosol is defined as liquid or solid particles suspended in gas. The reduction in the number of particles in a given stream is typically achieved by the introduction of a particle free flow reducing the concentration.

The general premise of any dilution system is described by Figure 1-1. The incoming particle laden flow, Q_{in} at N_{in} concentration, combines with a diluting flow, Q_{dil} at concentration N_{dil}, to provide a flow at Q_{out} with a concentration of N_{out}. Some size dependent particle losses within the system may occur, as shown by $N_{loss}(dp)$.

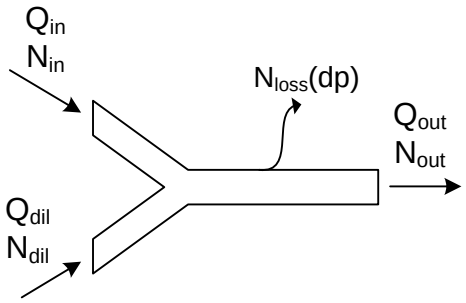

Figure 1-1
General Flow System for an Aerosol Diluter

The Dilution Ratio is then described as the ratio of the inlet concentration to the outlet concentration

$$DR = \frac{N_{in}}{N_{out}} \qquad \textbf{Equation 1-1}$$

where DR is the dilution ratio, N_{in} is the inlet concentration and N_{out} is the outlet concentration.

Using a simple conservation of particle number solution for Figure 1-1 the resulting particle number balance is as follows

$$N_{in}(dp)Q_{in} + N_{dil}(dp)Q_{dil} + \left(\frac{\partial N}{\partial t}\right)_{coag,evap} - N_{loss}(dp) = N_{out}(dp)Q_{out} \qquad \textbf{Equation 1-2}$$

Assuming a constant pressure and temperature yields a mass balance for the flows to be

$$Q_{in} + Q_{dil} = Q_{out} \qquad \textbf{Equation 1-3}$$

Using the assumption that the dilution flow is particle free , $N_{dil} = 0$, and ignoring the effects of coagulation, evaporation and wall loss, such that $\left(\frac{\partial N}{\partial t}\right)_{coag,evap} = N_{loss} = 0$, the resulting substation into Equation1-1 yields

$$DR_{vol} = \frac{N_{in}}{N_{out}} = \frac{Q_{in} + Q_{dil}}{Q_{in}} \qquad \textbf{Equation 1-4}$$

This is termed to volumetric dilution ratio based solely on the assumptions of particle number conservation in the system and that the dilution flow is particle free. It is termed the volumetric dilution ratio since its only dependency is on the volumetric flows of the inlet flow and dilution flow.

However, if particles were to be lost from the system, such that $N_{loss} \neq 0$ but Equation 1-3 remains valid, then Equation 1-2 can be rewritten such that

$$\frac{N_{out}(dp)}{N_{in}(dp)}\left(\frac{Q_{in} + Q_{dil}}{Q_{in}}\right) = 1 - \frac{N_{loss}(dp)}{N_{in}(dp)Q_{in}} \qquad \textbf{Equation 1-5}$$

Using the previous definition of dilution, Equation 1-1, we can define $DR_{particle}$ such that it is the dilution ratio when particle losses are present. This yields

$$DR_{particle}(dp) = \frac{N_{in}(dp)}{N_{out}(dp)} \qquad \textbf{Equation 1-6}$$

Subsisting Equation 1-4 and Equation 1-6 into Equation 1-5 then can yield the Diluter Penetration, P*(dp)*, such that

$$\frac{DR_{vol}}{DR_{particle}(dp)} = 1 - \frac{N_{loss}(dp)}{N_{in}(dp)Q_{in}} = P(dp) \qquad \textbf{Equation 1-7}$$

For values of P*(dp)* less than unity, this describes a system in which particles are being lost in the system resulting in an increase the $DR_{particle}$ when compared to DR_{vol}. For values of P(dp) greater than unity, describes a system in which particle generation is occurring such that the resulting particle dilution ratio is less than that of the volumetric dilution ratio. This is not typical of diluters as they are typically made of inert materials, however, some instances of dilution at elevated temperatures could result in particle production.

A graphical representation of this relationship can be found in Figure 1-2, where a hypothetical diluter with a fixed volumetric dilution ratio of 10 has a particle dilution ratio that increases with decreasing particle diameter. As shown by Figure 1-2 the resulting diluter penetration decreases as the values of volumetric dilution and particle dilution diverge.

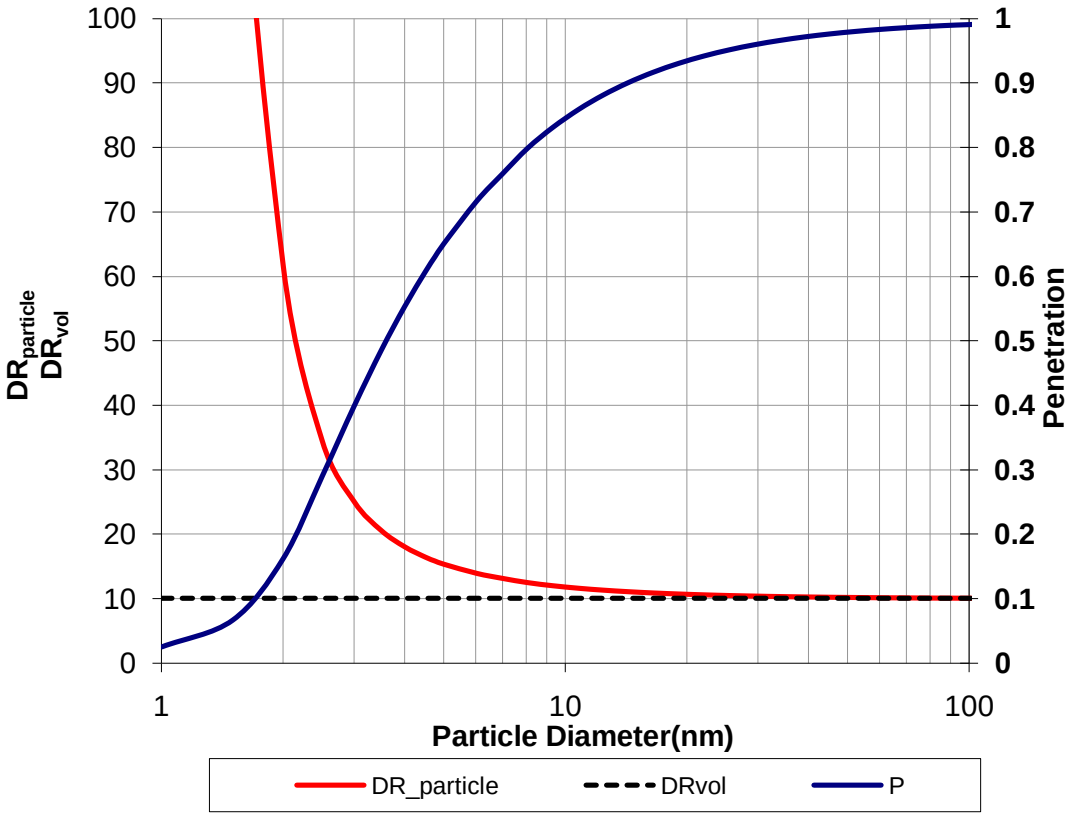

Figure 1-2
Example Diluter Performance Curves

1.3 Common Methods of Dilution

Although in practice there are variety of methods of aerosol dilution including rotary disk diluters and porous tube diluters, the two most commonly used types of diluters used are the bifurcating diluter and mixing diluter.

1.3.1 Bifurcated Diluter

The bifurcated flow diluter is a passive diluter that requires a source of vacuum, typically the sample flow of an instrument, to draw the aerosol through two branches of the diluter. A majority flow passes through an absolute filter, with a smaller minor flow

bypassing the flow as shown in Figure 1-3. Typically the ratio of the flow is controlled via a flow restriction placed in the bypass flow loop. Increasing the restriction to flow results in an increase in the dilution flow through the filter, whereby decreasing the restriction allows more flow to bypass the filter. The flow restriction can range in construction but is typically a small diameter capillary or orifice.

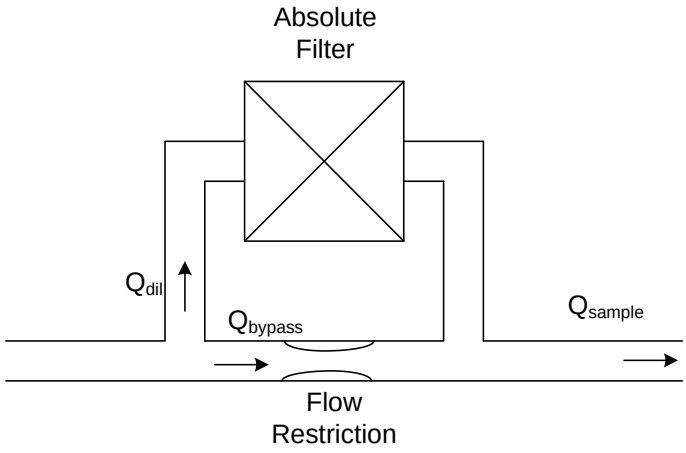

Figure 1-3
Schematic of a Bifurcated Flow Diluter

Volumetric dilution ratio for this device is determined via

$$DR_{vol} = \frac{Q_{bypass} + Q_{dil}}{Q_{bypass}} = \frac{Q_{sample}}{Q_{bypass}} \qquad \textbf{Equation 1-8}$$

where Q_{sample} is the total flow exiting, and entering, the diluter, Q_{dil} is the particle free dilution air, and Q_{bypass} is the aerosol flow to be diluted.

1.3.2 Mixing Diluter

The mixing style diluter uses a particle free dilution air to mix with a sample flow to reduce the aerosol concentration. Typically the dilution flow is provided by a compressed air source, or driven by a blower. Commonly a mixing diluter that use a compressed air flow, and air entrainment to provide the inlet flow is called an ejector diluters. A schematic of a mixing style diluter can be found in Figure 1-4.

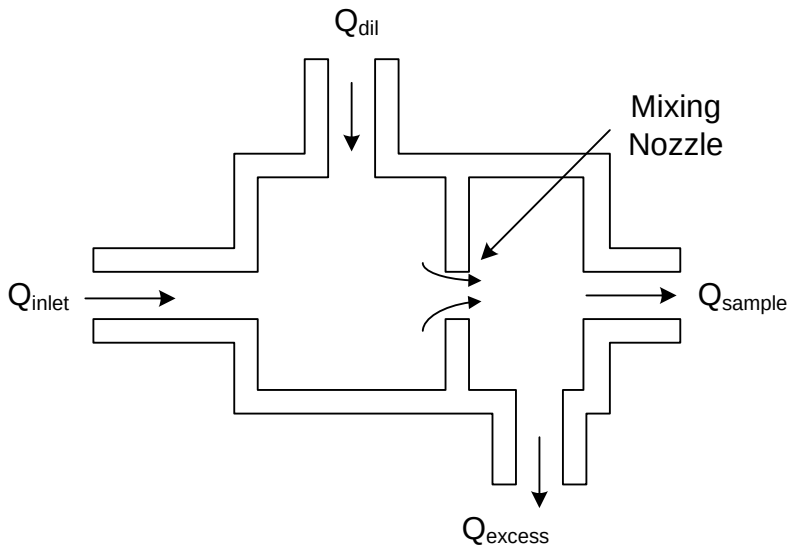

Figure 1-4
Schematic for a mixing style diluter

One key assumption when using this style of diluter is spatially homogenous flow exiting the mixing nozzle, resulting in the same concentrations in both the sample flow and excess flow. Using this assumption the volumetric dilution ratio is found to be the same as described by Equation 1-4.

1.4 Literature Review

A variety of methods of dilution have been developed for laboratory and industrial use. Applications for the dilution include diesel engine exhaust, smoke stack emissions and laboratory measurements of coagulation and condensation of fine and ultrafine particles.

Work by Fuchs and Sutugin(1965) in the measurement of the rate of coagulation required the measurement of high concentration aerosols upstream and downstream of a coagulation chamber. The need for dilution was a requirement of the method in which the aerosol concentration was measured. Aerosol measurement was done using a particle size magnifier(PSM) and a nephlometer, in which the PSM was limited to aerosol concentrations below 10^5 cm^{-3}. The dilution system used to avoid the concentration measurement limit was a bifurcated flow diluter in which a majority of flow would go through a large surface area absolute filter. A minor flow would then go through a capillary tube bypassing the filter with the exit of the capillary flow tube into the filtered major flow. Figure 1-5 shows the general schematic of the diluter used. One important thing done by Fuchs and Sutugin(1965) was the measurement of pressure drop across the capillary tube to determine the bypass flow rate in order to determine the volumetric dilution ratio. Although it was indicated that the particle dilution ratio varied from the volumetric dilution ratio, and further noted that it was size dependent, no values of penetration are given. Dilution ratios generated by a single diluter or a combination of diluters ranged from 7:1 to 1500:1

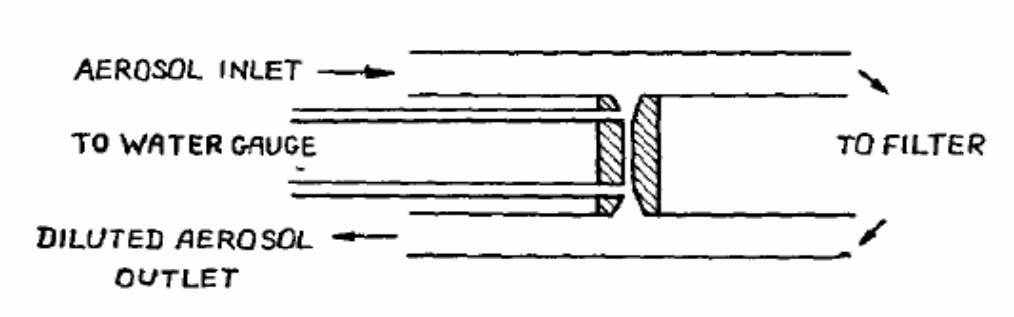

Figure 1-5
Capillary Tube Diluter [Fuchs, Sutugin; 1965]

A similar diluter was used by Delattre and Friedlander(1978) for the measurement of high concentration sulfuric acid droplets formed by a turbulent free jet using an electrical aerosol analyzer. Again a bifurcated diluter is used in which a majority of the sample flow goes through and absolute filter, while the minor flow bypasses the diluter via a capillary tube to be re-introduced into the filtered major flow. As with Fuchs et al(1965) the capillary flow is measured via the pressure drop to determine the volumetric flow. This method allowed for a final dilution ratio of 6400:1. Furthermore Delattre et. al(1978) calculated the theoretical losses in the capillary tube and determined the losses of 10 nm particles to be 17% and for 15 nm the losses were calculated to be 8%.

Work by Kittelson et al.(2002) to measure diesel engine generated aerosol required the use of a "leaky filter" diluter to measure the concentration using a Condensation Particle Counter(CPC). The "leaky filter" diluter is similar to those produced by Fuchs et al.(1965) and Delattre et al.(1978), in which the flow is bifurcated with a major flow going through a absolute filter and a minor flow bypassing the filter. One difference, however, is that this was placed inside of a capsule HEPA filter, thus preventing the ability to accurately measure the capillary tube pressure drop to determine

the minor flow. To determine the dilution ratio the concentration of an ammonium sulfate aerosol was measured both with and without the diluter placed upstream of the CPC(Kittelson 2002). It was noted, that the dilution ratio determined this way varied from day to day, and furthermore they attributed it to poor mixing which they solved by using a mixing tube and orifice. No work was done to characterize the losses within the capillary tube or correct the results for losses within the diluter.

Brockmann et al(1984) used the method of air entrainment to provide dilution. A small particle laden sample flow is entrained into a much larger particle free flow. The mixture of these two flows provides the necessary dilution. The major flow in this case is provided by a compressed air, or other gas, and is monitored via rotameters. The sample flow is pulled through a small diameter capillary tube and flow rate through the tube determined via the pressure drop across the tube. Dilution ratios that could be produced by the device were from 300-4000.

Work by Brockmann et al(1984) used the equation given by Gormley and Kennedy(1949) to predict the diffusion deposition inside the sample capillary. Furthermore, the work of Chen and Comparin(1976) was used to estimate the losses at the entrance of the sample tube which is not accounted for in Gormley and Kennedy(1949). Using the work of Chen and Comparin(1976) it was determined that particle losses in the entrance of the capillary tube were not a significant factor. The final results showed that for 2 nm particles, penetration varied from 80% to below 20% over the operational range of the diluter. No direct measurements were made to compare the predicated penetration theory to actual penetration.

Work by Knibbs et al. (2007) developed a capillary tube based bifurcated diluter for use with the TSI 3007. Knibbs attempted to quantify the effectiveness of the dilution system by using a high concentration, combustion generated aerosol, coupled with a reference counting measurement. Volumetric dilution was determined by direct flow rate measurements through the diluter. No work was done to attempt to ascertain the losses within the diluter. Verification of the diluter was performed using a combustion derived aerosol put into holding chamber from which both a reference CPC, TSI 3302A, and the TSI 3007 with the diluter sampled. The holding chamber was vented to room air, allowing the removed volume by the CPC's to be diluted with room air over a 3 hour period. No work was done to determine the size distribution over the 3 hours, nor was there any systematic determination of why the particle dilution ratio deviated as much 500% of the volumetric dilution ratio. It should noted that the greatest deviation occurs at the highest concentration, which also coincides with the beginning of the test. As the concentration decreases, and the amount of time the aerosol has been in the chamber increases, the influence of coagulation would have increased the particle size. The difference between the volumetric and particle dilution ratios was concluded by Knibbs et al. to be possible due to particle volatility or other loss mechanisms. No work, either theoretical or empirical, was done to determine the effect of particle volatility on losses in the diluter.

1.5 Instrumentation Review

The bulk of the measurements taken for this body of work required the use of both particle sizing and particle counting instruments. For this body of work, the Differential Mobility Analyzer (DMA) was used to generate monodisperse aerosols. The task of particle counting was performed exclusively by a CPC.

1.5.1 Differential Mobility Analyzer

The differential mobility analyzer (DMA) is an instrument which allows for the size selection of particles by their electrical mobility diameter. The electric mobility of a particle, Z_p, is described by Equation 1-9

$$Z_p = \frac{neC_C}{3\pi\eta d} \qquad \textbf{Equation 1-9}$$

where n is the number of charges on the particle, e is the fundamental charge of an electron, C_c is the Cunningham slip correction factor, η is the viscosity of air, and d is the diameter of the particle(Hinds, 1999).

The terminal velocity of a particle in stagnant air exposed to an electric field is described by

$$V_{TE} = Z_p E \qquad \textbf{Equation 1-10}$$

where Z_p is the electric mobility of the particle and E is the electric field. Figure 1-6 shows a simplified drawing of a DMA. Particles introduced in the outer portion of the DMA are pulled towards the inner electrode via the electric field acting on the charged particle. The sheath flow provides the transport medium to move particles down the

length of the electrode. Only particles with the correct mobility, or assuming a singly charged particle, the correct electrical mobility diameter will enter the monodisperse slit. For a fixed electric field resulting from the voltage applied to the center electrode, those particles that are smaller than the correct diameter will deposit on the electrode of the DMA, while those to large travel too slowly and either deposit below the slit, or exit the DMA entirely via the exiting sheath flow.

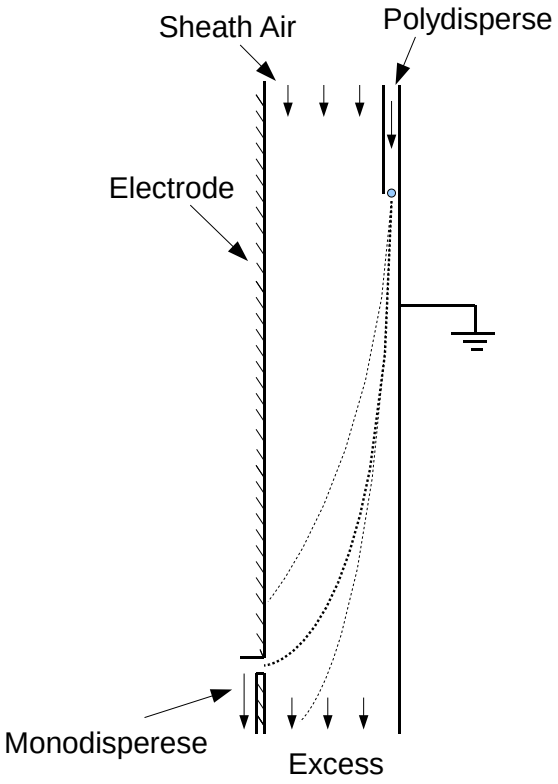

Figure 1-6
Schematic of a typical Cylindrical DMA

There are a variety of other influences in the DMA that effect the standard deviation of the exiting "monodisperse" aerosol. Work by Knutson et al. (1975) investigated the width of the transfer function of the DMA. For the case in which the

polydisperse flow equals the exiting monodisperse flow the transfer function is shown in Figure 1-7, where Ω is the probability of a particle being selected based on the product of electric mobility, Z_p, and the finite electric flux function, .

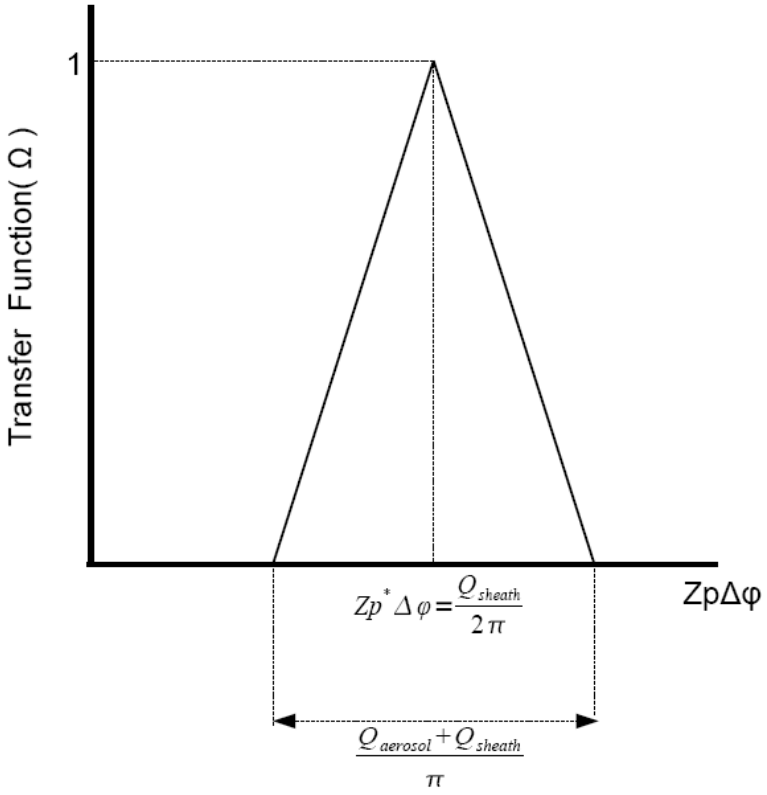

Figure 1-7
Transfer Function for a Cylindrical DMA

The resulting peak occurring where the transfer function is equal to unity is also known as Z_p^*, and such that one can determine the required voltage of the DMA based on the geometry of the DMA and the particle mobility selected such that

$$Z_p^* \Delta\varphi = \frac{Q_{sheath}}{2\pi} = \frac{neC_C}{3\pi\mu d} \frac{LV}{\ln\left(\frac{b}{a}\right)}$$ **Equation 1-11**

where Q_{sheath} is the flowrate of the sheath flow, L is distance between the inlet slit and exit slit of the DMA, b is the outer radius of the housing, a is the radius of the electrode, V is the applied voltage to the electrode.

Work by Knutsen et al. (1975) then described the relative half-width of the transfer function, which effectively describes the size range of particles that will enter the slit at a fixed voltage as

$$\frac{\Delta Z_p}{Z_p^*} = \frac{Q_{aerosol}}{Q_{sheath}}$$ **Equation 1-12**

where ΔZ_p is the half width of the transfer function and $Q_{aerosol}$ is the polydisperse aerosol inlet flow rate. Further work was done by Stolzenburg (1988) investigating the effect of diffusion broadening of the DMA transfer function.

1.5.2 Condensation Particle Counter

Counting particles smaller than 1μm poses a significant challenge as typical optical particle counters do not have enough sensitivity to detect particles below 100 nm due to the small amount of scattered light. Particles in this size range have a scattered light intensity that is proportional to dp^6. This means that the scattered light intensity for a 10 nm particles is $1x10^{-6}$(1/1000000) of that of a 100 nm particle. To overcome this, a liquid is condensed on to the surface of the particle increasing the resulting size of the

particles to be detected optically. This type of instrument is typically referred to as a Condensation Particle Counter (CPC), and sometimes referred in some early literature sources as a Condensation Nucleus Counter (CNC), but are the same device (McMurry 2000).

The general layout for a CPC is shown in Figure 1-8, in which the incoming aerosol passes through the Saturator. This portion adds condensable vapor to the aerosol stream, and to do so, the aerosol is exposed to the working fluid at an elevated temperature either via passing over a liquid bath or passing through a wetted tube. By then passing the now vapor laden aerosol through the cold condenser, the gas temperature decreases which results in a decrease in the saturation vapor pressure of gaseous working fluid. This resulting decrease in saturation vapor pressure results regions of supersaturation within the condenser section. Due to a supersaturated condition, vapor will condense not only on the walls of the condenser, but on the particles as well, causing them to grow. Typically growth is to the super-micron range which is easily detectable by an optical counter.

In the optical portion of the CPC, grown particles are passed through a laser beam and the resulting scattered light is detected by a photo detector. With a know aerosol flow rate, the total number of particles counted over a period of time allows for the calculation of the concentration.

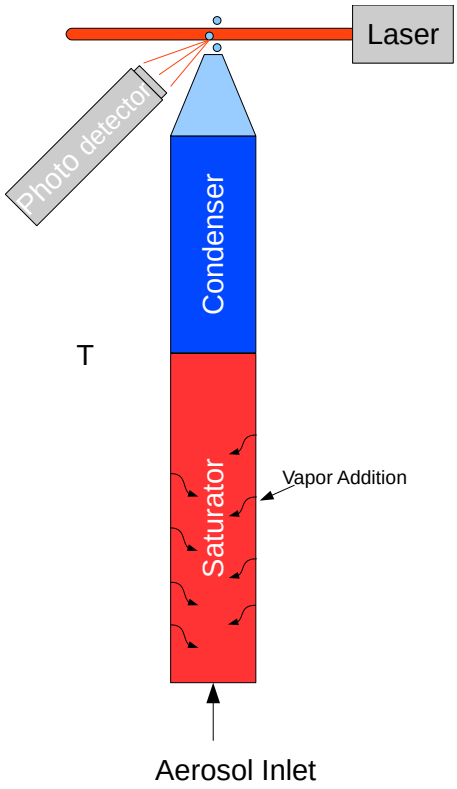

Figure 1-8
Schematic of a typical laminar flow CPC

The operation of the CPC depends upon producing a region within the device in which the vapor form of the working fluid has reached supersaturation. The level of supersaturation, *S*, is defined as

$$S = \frac{P_v}{P_s(T)} \qquad \textbf{Equation 1-13}$$

where P_v is the partial pressure of the working fluid, and $P_s(T)$ is the temperature dependent saturation pressure of the working fluid. The smallest particles on which the

working fluid will begin to condense, termed heterogeneous nucleation, is defined by the Kelvin equation which yields

$$S = \frac{P_v}{P_s(T)} = \exp\left(\frac{4\sigma}{d\rho_l RT}\right) \qquad \textbf{Equation 1-14}$$

where σ is the surface tension of working fluid, d is particle diameter(a.k.a Kelvin diameter), ρ_l is the working fluid density, R is the working fluid specific gas constant, and T is the vapor temperature(Hinds 1999). It is important to note, that as the saturation ratio, S, increases, the smallest particle diameter on which vapor will condense decreases. This operation of the condensation particle counter depends upon particles nucleating and growing large enough to be optically detected. Particles that enter the device which are smaller than the minimum effective Kelvin diameter, or those that do not grow to an optically detectable size will not be counted.

The saturation ratio within the device, however, is not a fixed value and depending on the path through the condenser section the particles may experience a different saturation ratio. Work by Stolzenburg et al.(1991) found the variation of the saturation ratio in the condenser of the TSI 3025, and resulting Kelvin diameter, can range from 2.64 nm to 4.5 nm over the diameter and length of condense. This indicates a large discrepancy in the saturation ratio particles may experience when they pass through a CPC.

The resulting variation in the saturation ratio typically generates a counting efficiency curve that has a slow roll off as the particle size is reduces. An example curve is shown in Figure 1-9, where 50% of particles of size 5 nm are counted by the device.

What this intrinsically means, is that 50% of the particles of 5 nm in diameter are grown to an optically detectable size, which means that the other 50% passed through regions where the supersaturation ratio is not great enough to grow the particles to a sufficient optically detectable size. In practice, the use of the size of particle counted at 50% efficiency is a common reference for comparison of CPCs and is often referred to as dp_{50}.

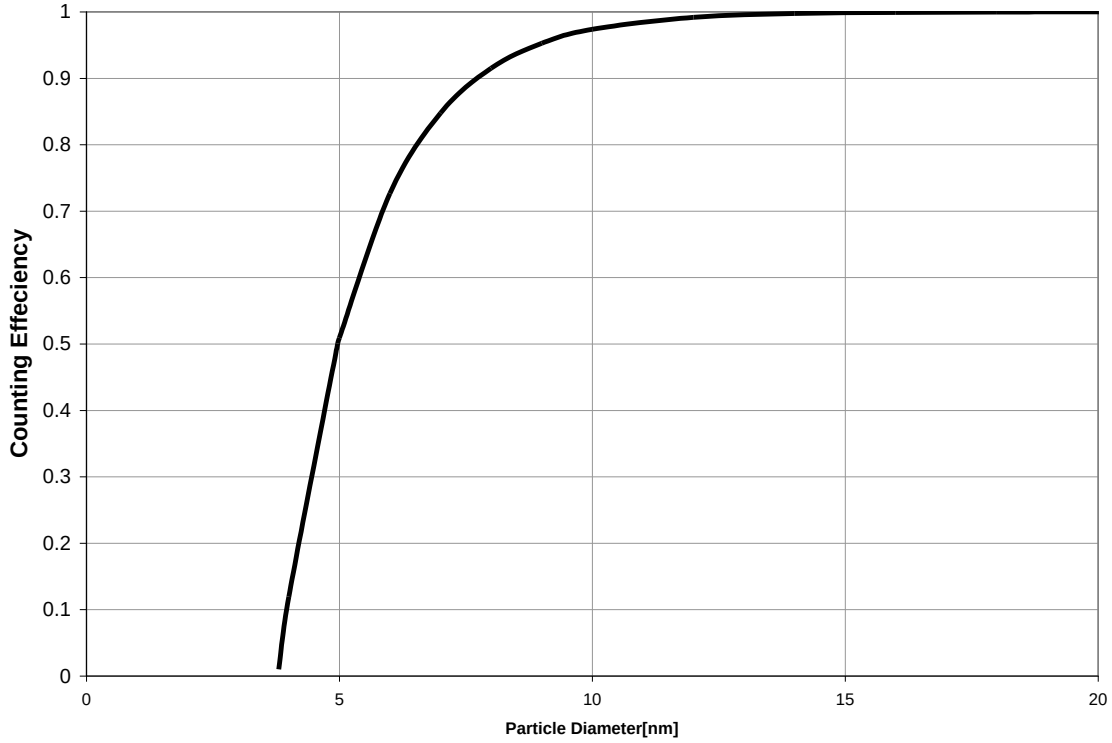

Figure 1-9
Typical CPC Counting Efficiency Curve

It should be further noted, that in all tests in which the CPC counting efficiency curve is determined as a function of particle size and composition it is assumed that the aerosol has spatial homogeneity. This means that concentration profile passing through the regions of supersaturation is assumed to be a constant. This assumption is often not directly stated.

Chapter 2
Particle Loss in Aerosol Diluters

2.1 Introduction

As discussed previously, the effect of losses within an aerosol diluter can significantly affect the performance of the diluter. This portion of the work will focus on determining the losses within aerosol diluters over the particle size range of 9 to 100 nm under various conditions. These test variables include volumetric dilution ratio, aerosol charge state, and downstream mixing. The diluters tested will be the TSI 3302, MSP 1100, "Leaky Filter" diluter and the Orifice Diluter.

2.2 Diluter Particle Penetration Measurement Apparatus

The apparatus used for the measurement of the particle penetration of the tested diluters can be found Figure 2-1. The general concept of the apparatus is based on work Liu and Pui(1974) as a method to calibrate CPC's. A polydisperese test aerosol is generated and small size particle range is classified by electrical mobility to provide a nearly monodisperese test aerosol. Upstream and downstream concentration levels of the diluter are monitored with CPC's.

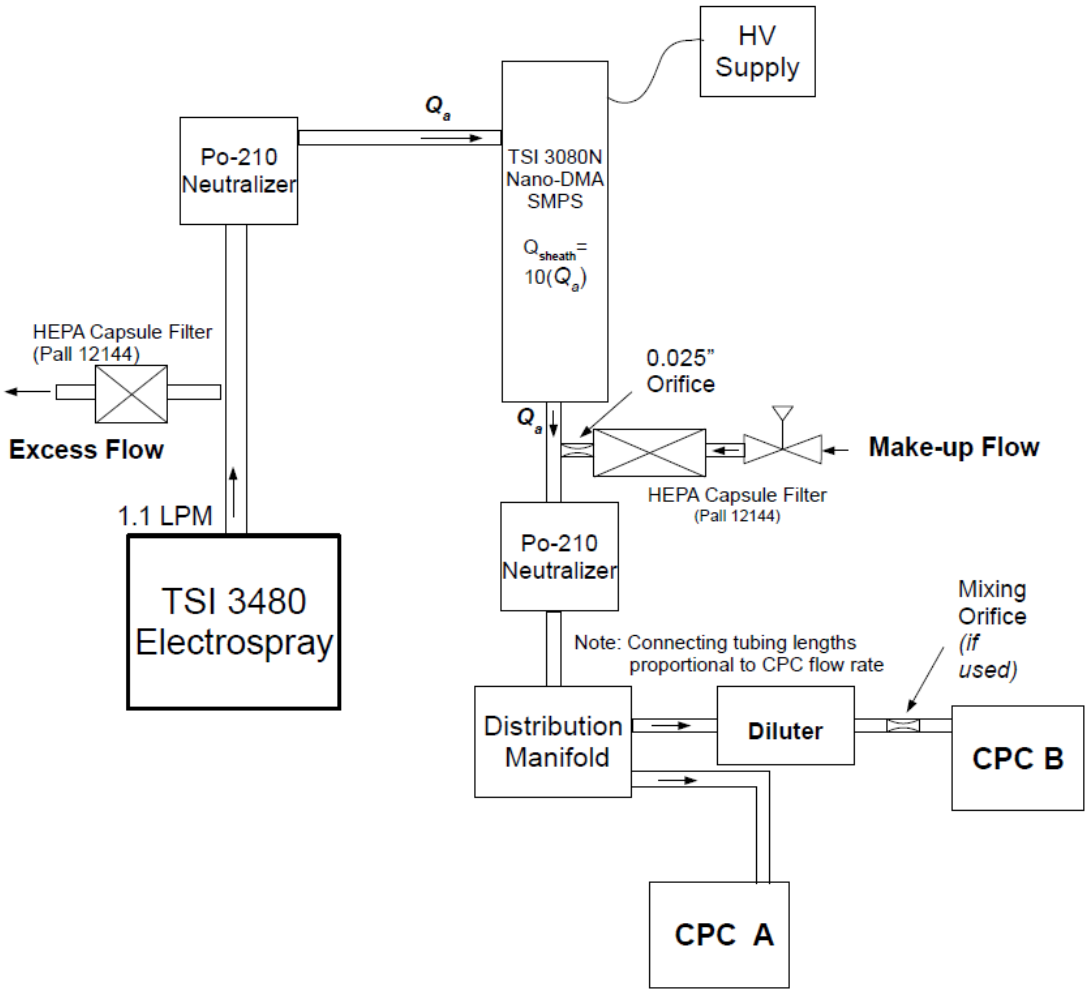

Figure 2-1
Diluter Penetration Test Apparatus

For this apparatus a TSI 3480 electrospray aerosol generator was used with an electrospray solution of sucrose in a 20mM ammonium acetate buffer solution. This solution consisted of a 20mM ammonium acetate solution with the pH adjusted to 8 using ammonium hydroxide. The range of sucrose solutions used is shown in Table 2-1, where the droplet diameter was calculated relative to the peak droplet size for the 0.028% V/V sucrose solution. This peak droplet size was determined to be 10.8 nm using a home-built Scanning Mobility Particle Sizer(SMPS) which measured the size distribution of the

aerosol leaving the TSI 3480. Typically the TSI 3480 generates approximately 150 nm droplets that are allowed to evaporate in dry air leaving behind solid sucrose. The peak size and the concentration of the initial solution allows the initial droplet size to be determined using the following equation

$$D_D = \frac{dp_{peak}}{C^{1/3}} = 163nm \qquad \textbf{Equation 2-1}$$

where D_D is the droplet diameter, dp_{peak} is the peak diameter of the generated aerosol and C is the volume to volume concentration of the initial solution. The droplet diameter agrees well with the TSI 3480 manual(TSI, 2010) which states that for a sucrose solution the typical droplet diameter is 150 nm. The variation of the viscosity of the solution due to the varying concentration of sucrose will affect the final droplet diameter due to a changing capillary flow rate as show by Chen et al.(1995) but for a rough approximation the calculation is sufficient.

Table 2-1
Resulting peak particle size for given concentration of Sucrose solutions (using D_d=165 nm)

Concentration	dp_{peak}(nm)
0.004%	6
0.012%	8
0.020%	10
0.075%	15
0.17%	20
1.42%	40

For all test conditions the compressed air flow rate was set to 1.0LPM via the rotameter included on TSI 3480, furthermore the gaseous CO_2 flow rate was set to

0.1LPM via the included rotameter. The high voltage level applied to the electrospray was varied to maximize the concentration for the given solution concentration.

A Po-210 neutralizer(P-2042 Nuclespot, NRD LLC) was installed within the TSI 3480 in the provided location within the device to remove excess charge and provide a Boltzmann charge distribution to the evaporating droplets.

The polydisperse aerosol then was transported via conductive tubing(SIMST-190250,Simolex Rubber Corp.) to the inlet to the TSI 3080N Nano DMA. For the case in which the aerosol flow rate into the TSI 3080N does not equal the outlet flow rate of the TSI 3480, a make up flow rate is provided via a HEPA filter(12144, Pall Corp) placed between the devices, as shown in Figure 2-1, to keep the inlet pressure of the TSI 3080N at near atmospheric pressure.

The TSI 3080N Nano-DMA was used to classify the incoming polydisperse aerosol. This unit is a stand alone system, which includes the TSI 3085 Nano-DMA, high voltage supply, sheath blowers, and all necessary tubing connections. For the majority of the work the sheath flow rate was fixed at 5.00LPM, but for any test that varied from this the sheath flow, the sheath was set to ten times the incoming aerosol flow rate. The incoming aerosol flow rate was determined via the pressure drop across a 0.073cm orifice impactor used at the inlet to prevent large particles from entering the device. The neutralizer installed into the TSI 3080N was Po-210 neutralizer (Static Master 2U500, NRD LLC) to provide a Boltzmann distribution to the incoming aerosol. Although not completely necessary to have an additional Po-210 neutralizer in the TSI 3080N, it was included simply because that is the standard configuration in which they are used in the lab.

As shown in Figure 2-1, a tee was placed down stream of the TSI 3080N to allow a make up air source. Since the combined flow rate of the two CPC sampling instruments was always greater than the exit monodisperse flow of the TSI 3080N a make up flow is required. To aid in generating a spatial homogenous concentration, the “make-up” air flow was introduced through an orifice which is placed as close to the pass through section of the tee as possible. For this body of work, a 0.035 in(8.9E- 4 m) inner diameter orifice(IC25-SS,O’Keefe Controls) was pressed into a stainless steel swaging tube type tee(SS-400-3, Swagelok Company).

By introducing the orifice, the incoming “make-up” air becomes a high velocity jet, a typical Reynolds number of 1200, in relation to the flow through the rest of the tee at a Reynolds Number of approximately 250.This provides a mixing action to provide spatial homogeneity. To ensure that the incoming make up air was particle free a HEPA capsule filter(12144 Pall Corp.) was used along with a valve to control the amount of makeup air. The valve controlled the amount of aerosol passing through the DMA because the sum of the make up air and the DMA aerosol rate must equal to the total flow entering the CPC’s. For this work the monodisperse aerosol flow rate used was 0.5LPM with the resulting makeup flow dependent upon the CPC combinations used.

For tests in which a Boltzmann equilibrium charge distribution was needed for the monodisperse test aerosol, a Po-210 charging source(Static Master 2U500, NRD LLC) was placed downstream of the mixing tee. Due to the fact that a DMA selects singly charged particles, if no Po-210 source is used, the resulting particles will mostly carry a +1e charge. By selecting to use, or not use, the neutralizer allows for the influence of charge to be investigated.

To distribute the flow to each of the CPC's, a distribution manifold was used. For this work a 7 inch diameter and 1.5 inch height cylindrical manifold was used. The incoming aerosol came in through the axial direction of the cylinder, with both CPC's connected via port connections made radially from the cylinder, 180° opposed to each other.

For this work the CPC's are calibrated relative to each other prior to taking data, however, it is good practice to match the length of tubing to each CPC such that the losses due to diffusional deposition in the transport tubing are the same for each CPC. Assuming that the flow within the tubing is fully developed laminar flow then the losses within the tube are a function of L/Q, where L is the length of the tubing and Q is the volumetric flow rate(Hinds, 1999). To have matched theoretical losses yields

$$\frac{L_A}{Q_A} = \frac{L_B}{Q_B} \qquad \textbf{Equation 2-2}$$

where L_A represents the sample line length for CPC A, Q_A is the volumetric flow rate of CPC A, L_B is the sample line length for CPC B, and Q_B is the volumetric flow rate of CPC B.

Lengths were then reduced to shortest possible value as to minimize losses. As shown in Figure 2-1, with CPC A monitoring upstream concentration, the addition of a diluter, a mixer or both allow for penetration to be determined using the downstream concentration via CPC B. Overall tubing length for the connections made from the distribution manifold to the CPC B remained the same for the duration of that configuration. The addition of the diluter provides additional overall length of sample

transport, but since the same length of tubing is used for all diluters any measured losses would be the result of the addition of a mixer, diluter, or both.

A general overview of the CPC's used for this body of work can be found in Table 2-2. All CPC's used for the test are laminar flow CPC's using Butyl Alcohol, Butanol, as the condensable working fluid. It should be noted that the MSP 1100 CPC has a built in dilution system and was not designed as a standalone CPC.

Table 2-2
CPC Instrumentation Overview

Manufacturer	Model	Serial Number	Flow Rate (LPM)	Working Fluid	dp_{50} (nm)
TSI Inc.	3010	2116	1	Butyl Alcohol	10
TSI Inc.	3010	2136	1	Butyl Alcohol	10
TSI Inc.	3025A	1195	1.5	Butyl Alcohol	3
MSP Corp.	1100	NA	0.3	Butyl Alcohol	5

Data collection for the TSI manufactured CPC's was done via the TSI Aerosol Instrument Manager(AIM) software, and connections to the CPC's were done via a RS-232 serial cable. A personal computer(PC) using Windows 98 software and loaded with the TSI AIM software logged and stored data on to the hard drive.

Data collection for the MSP 1100 was done via the internal data storage of the device. To ensure that the time stamp of the samples matched that of the TSI AIM software, both the time setting of the MSP 1100 and the data collection PC were synchronized to within ±1sec of each other. Data were then compiled after the run completion for data analysis.

Four diluters were tested, these include the TSI 3302(SN:362) Aerosol Diluter, MSP 1100, a commonly used laboratory "leaky filter" diluter, and the Orifice Diluter.

Table 2-3 gives an overview of the diluter tested and the CPC used to provide the sampling flow and to do downstream concentration measurements. It should be noted that the Dilution Range listed in Table 2-3 is only valid for that CPC flow rate and diluter combination. This is due to the fact that the range of dilution ratios is dependent on the aerosol sample flow that the diluter is providing.

Table 2-3
Diluter/CPC Combination Overview

Diluter	Type	CPC	Reference CPC	Dilution Range	Mixing Orifice Diameter(in)
TSI 3302	Bifurcated Capillary	TSI 3010	MSP 1100	8-100	0.040
MSP 1100	Mixing	MSP 1100	TSI 3010	80-25	NONE
"Leaky Filter"	Bifurcated Capillary	TSI 3025A	MSP 1100	15.3	NONE,0.040
Orifice Diluter	Bifurcated Orifice	TSI 3010	MSP 1100	40-80	NONE,0.033, 0.025

.

2.2.1 TSI 3302 Diluter

The TSI 3302 Aerosol Diluter is of the bifurcated flow type. The pressure restriction in this device is a 0.14cm diameter capillary tube with a total length of 13.4cm. This pressure restriction drives a majority of the flow through two HEPA capsule filters placed in parallel and drives flow through a valve placed downstream of the filters. The addition of the valve allows for the pressure drop along the filtered air loop to be increased or decreased by adjusting the valve. This effectively creates a higher, or lower, pressure drop in which drives more, or less, flow through the sample capillary. In the end this allows for the variable dilution ratio by the modification of the pressure drop across the filtered air loop. Additional features of the TSI 3302 include pressure drop

measurements made across the capillary with the first pressure tap at 7.54cm from the end of the capillary and the second tap being at the exit of the capillary tube. This allows for a direct measurement of aerosol flow once the pressure drop and flow rate relation have been determined for the capillary tube. The pressure drop is measured via a 0-1 in H20 Magnahelic pressure gauge which comes pre-installed in the device.

2.2.2 MSP 1100 Diluter

The MSP 1100 is a mixing type diluter packaged along with a CPC. The packaged internal CPC is of a laminar flow style with Butyl Alcohol as the working fluid and a sample flow rate of 0.3LPM. The internally packaged diluters use a mixing style diluter approach with the incoming clean air flow and exiting excess flow being recirculation loops. The MSP 1100 allows for a user selectable dilution ratio of 80:1,100:1 and 125:1 for each of the included diluters. The flow loops have HEPA capsule filters placed before and after a blower, which provides the driving force for the recirculation loop. The MSP 1100 incorporates the ability to have two of the MSP style mixing diluters run in series, but due to internal plumbing this feature was disabled to test the penetration of only one diluter. A user selectable valve on the rear of the device allows for the selection of the inlet flow to travel to the CPC only, to 1 diluter, and to two diluters in series. This valve was disabled and all plumbing connections were made directly the device tested. Since the MSP diluter was designed to handle a matched sample flow that of the included CPC, all tests of the penetration of the diluter were done using the included MSP CPC.

2.2.3 *Laboratory "Leaky Filter" Diluter*

The laboratory "Leaky Filter" diluter is a bifurcated type dilute with the flow restriction being a capillary tube. The diluter construction consists of a glass capillary tube with an inner diameter of 0.069" and a length of 2.41" placed in a HEPA Capsule filter(12144, Pall Corp)The glass capillary acts as a controlled leak of the incoming aerosol to bypass the filter media, hence the term "leaky filter". The major flow in this passes through the filter media removing more than 99.97% of particles and provides the clean air to dilute the bypass aerosol. A schematic of the system of diluter can be found in Figure 2-2.

Due to the nature of the design, once the glass capillary was inserted into the device the tube could not be removed. This results in the diluter having a fixed dilution ratio. Determination of the volumetric dilution ratio can be found in Appendix I. One advantage to using a glass capillary tube, however, results in a near linear dilution ratio as the total inlet flow varied.

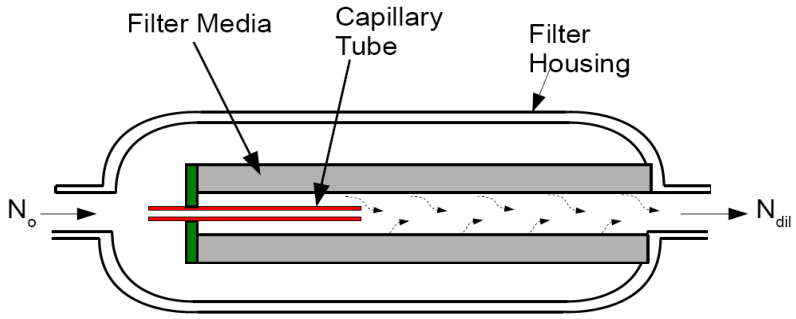

Figure 2-2
Schematic of Leaky Filter Diluter

2.2.4 Orifice Diluter

The Orifice Diluter is a bifurcated type diluter with the flow restriction being a small diameter orifice. The diluter was developed specifically for this work to produce a diluter in which sub-100 nm particle losses are minimized. This unique design allows for a variable dilution ratio to be achieved by modifying the diameter of orifice, while not greatly affecting the penetration of the diluter.

A threaded orifice assembly(Z-10-10/32 Series, O'Keefe Controls) was used as the pressure restriction for this passive style diluter. To allow for an adjustable dilution ratio, the threaded orifice inserts come in variety of orifice diameters as well as the diluter main body allows for easy changing of the orifice by unscrewing from the threaded passage within the diluter. The ideal design parameter for this device would be to have a device with a bypass flow length of zero, however, because of need to have an adjustable dilution ratio and to be able to remove the orifice led to a threaded orifice design. The threaded orifice and internal threaded passage has a length of approximately 0.25" which is the smallest length available with commercial threaded orifice inserts.

The rest of the main body was designed to aid in tubing connections to and from the two HEPA Capsule filters(DFC-06-DV2, Porous Media) used to provide filtered air for dilution as well as to provide tubing connections for the inlet and outlet of the diluter. The choice to use two HEPA filters was driven to reduce the pressure drop across the device to a minimum as well as to allow for larger orifice diameters to be used to provide the 10-80 dilution ratio range with a 1 LPM sample flow. A schematic of the Orifice Diluter can be found in Figure 2-3. Determination of the volumetric dilution ratios can be found in Appendix I.

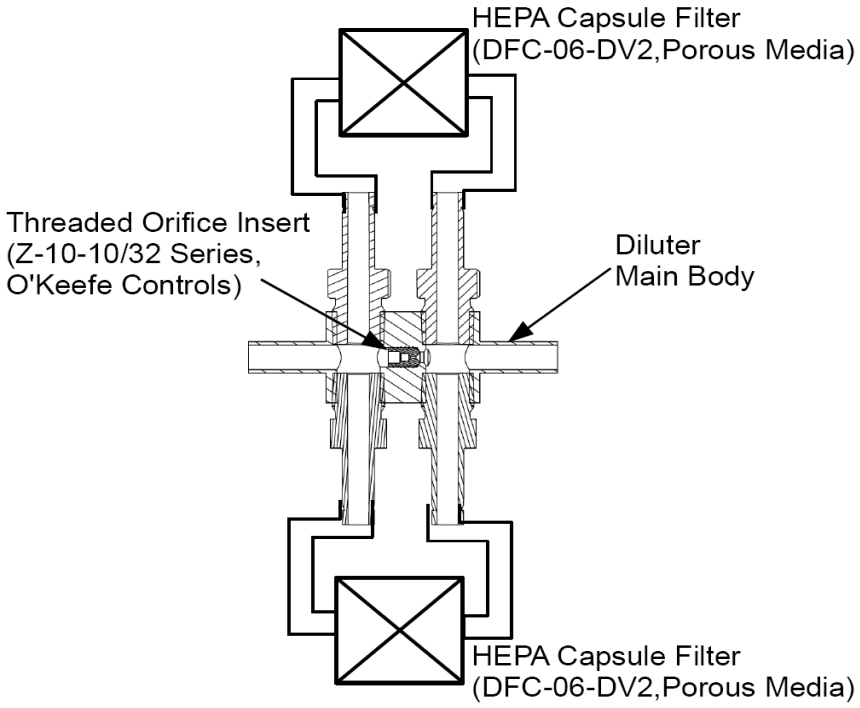

Figure 2-3
Schematic of Orifice Diluter

One additional variable investigated is the downstream mixing of the diluter. The downstream mixing is necessary to provide spatial homogeneity to the aerosol concentration. To provide a mixing, a threaded orifice assembly(Z-10-10/32 series, O'Keefe Controls) is placed into a swaging type port connector(SS-401-PC, Swagelok Company). The port connectors used were not designed to have a threaded orifice put them, to overcome this, a 10-32 UNC tap is run through the port connector to provide threads through the entire length of the connector. The threaded orifice assembly is then threaded into the port connector and conducting tubing provides the connection between the diluter and CPC used.

2.3 Diluter Particle Penetration Measurement Methods

For the measurement of diluter particle penetration it is imperative to have the upstream and downstream CPC's calibrated with respect to one another prior to the installation of diluters and mixers. To do this the apparatus shown in Figure 2-1 is used to generate the monodisperese test aerosol from the size range of 6 nm-100 nm with concentration of the aerosol being less than 3000 particles/cm^3.

The importance of referencing the CPC's to one another prior to installing the diluter, allows for the effects of variables such as charge, and the introduction of a mixing orifice, to be negated during the diluter measurements . The method used is as follows. First the DMA is adjusted to a specific particle electrical mobility diameter. The upstream and downstream CPC's are then referenced for that particle size using the sampling time, inter-sampling time, averaging time described below. The DMA is then adjusted to a new particle diameter, and after waiting the inter-sample transition time, data are collected for the new particle diameter. The process is repeated until the number of samples and particles sizes have been tested.

Additional effects investigated such as down stream mixing, or the addition of a neutralizer, downstream of the DMA was examined during this phase to determine a baseline CPC response over the size range tested with the additional components installed. For example the test in which the test aerosol is to be in Boltzmann charge equilibrium, a Po-210 neutralizer was installed as shown in Figure 2-1, and the CPC's were then referenced to one another to negate any effect of enhanced nucleation due to particle charge(Gamero-Castano,2000).

Once the CPC's are referenced to each other for the particle size range tested, the diluter is then installed before the downstream CPC and before the mixing orifice if used as shown in Figure 2-1. To determine the volumetric dilution ratio, the sample flow of the downstream CPC is measured via a bubble flow meter (Gilibrator-2, Gillian Inc.) and recorded prior to installing the diluter. The dilution ratio is set to a fixed value over the test period, and the upstream and downstream concentrations are measured.

2.4 Sample Time, Inter-sample Time, Number of Samples and Averaging Time

The sample time is defined as the length of time the concentration is logged for a specific condition. The sample time used for a majority of the tests is 60 seconds. Another important parameter is the averaging time which is the CPC counting period over which the number concentration is averaged by the CPC. For all tests in this body of work, the averaging time was 1 second. Using a sample time of 60 seconds and an averaging time of 1 second results in the total number of data points for that sample time being 60. This allows for a larger sample population to provide a better average concentration. The inter-sample time is the time period between samples of different particle diameter and is the time waited for the previous particle size to be purged from the sampling system. An appropriate value for this time was determined by introducing room air aerosol with a number concentration of 14,000 particles/cm^3 into the system by disconnecting the tubing connection at the monodisperse exit of the DMA, and then at time zero a filter was then placed at the inlet of the disconnected tubing introducing only particle free air. Figure 2-4 shows the concentration versus time profile for a particular CPC flow rate and internal sampling volume. For the data collected in Figure 2-4 the

CPC's used were the MSP 1100 and TSI 3010, which have a combined flow rate of 1.3 LPM. The combined flow rate for that test was 1.3 LPM and this was the lowest combined flow rate tested for this body of work. Thus combined flow rates greater that 1.3 LPM will result in decreased decay time.

The decay in concentration can also be displayed as a percentage of the initial starting concentration, N/N_0, as shown in the secondary axis of Figure 2-4. This represents the percent of the aerosol that will be present in the sampling system and CPC's once the particle diameter has been changed. Based on the results from this work the inter-sample time period was selected to be at minimum 120 seconds which results in less than 0.7% of the initial concentration from the previous sample still in the internal volume of the sampling system and CPC's. This value is judged to be minimal and therefore for all calculations the influence of the previous sample condition is assumed to be negligible and is ignored.

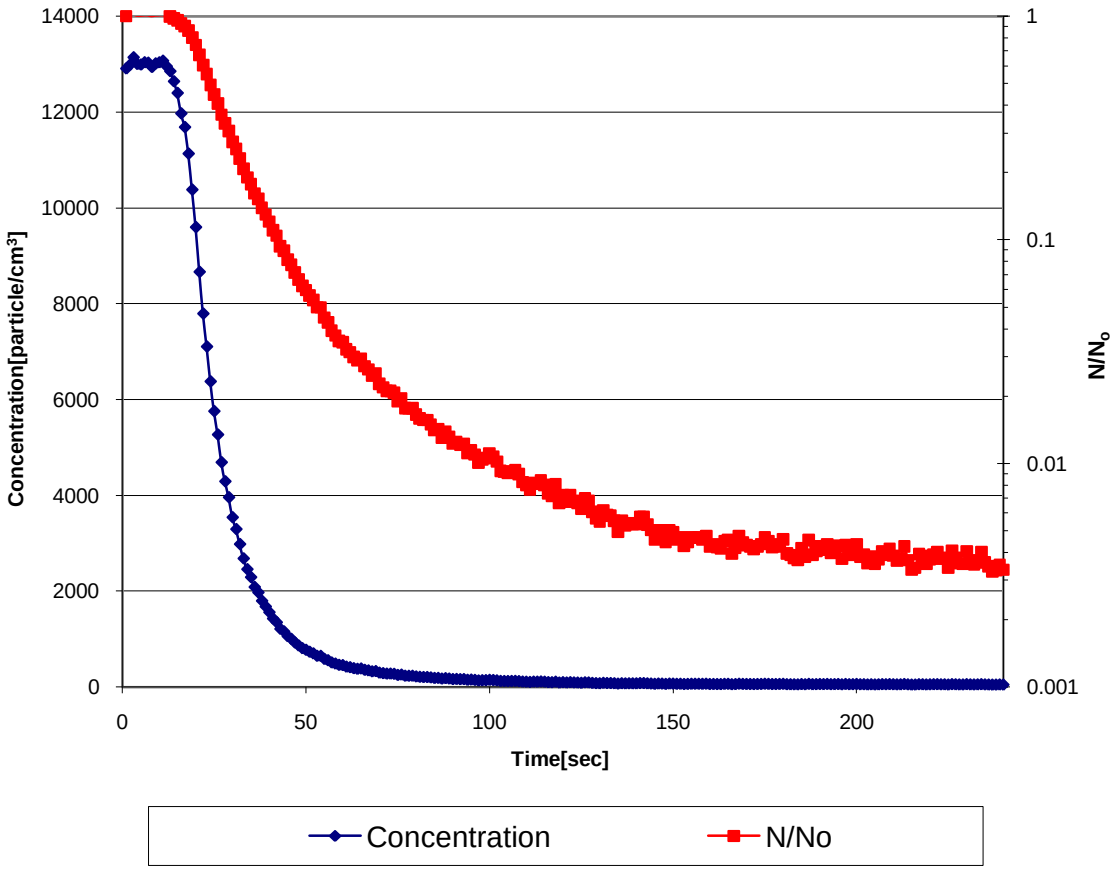

Figure 2-4
Determination of Sample System Time Response for 1.3 LPM Flow

The number samples is simply defined as the number times the same particle size is tested. For this work the number of samples tested for each particle size is three. This is to provide a better average of the particle penetration and CPC reference measurements and helps to determine measurement uncertainty.

2.5 Test Aerosol Concentration

The concentration of the monodisperese aerosol for this body of work was kept as close to 3000 #/cm^3 as possible by reducing, or increasing, the high voltage setting used on the electrospray. In cases where the CPC's responded considerably different the

reading of CPC that displayed highest value was reduced until it was below 3000 particles/cm^3.

The logic for keeping the aerosol concentration lower than 3000 #/cm^3 is due to the method in which CPC's count particles, and more specifically coincidence error. Coincidence error is the result of a particle being missed by the optical counters due to proximity to another particle. This can be due to two particles being in the laser beam at the same time, or it can be due to the counting electronics missing a particle due to the time it takes for the electronics to refresh after counting a particle. This electronic refreshing time is often referred to as blanking time. For the TSI CPC's used in these tests, all had less than 2% coincidence up to 3000 #/cm^3(TSI,2002). The MSP 1100 specifications did not give the level of coincidence as a function of concentration but it is assumed to be comparable to that of the TSI 3010 and TSI 3025A tested.

Ensuring that the upstream concentration was kept as close to 3000 #/cm^3 also ensured that the downstream concentration would remain high enough to provide a statistically significant number of counts.

The upstream concentration was monitored closely to ensure a near constant level as to avoiding large concentration spikes. Large concentration spikes occurred from random changes in the electrospray operating conditions. The transient response of the system, and the inherent delay in the concentration readings between the two CPC's when a diluter is installed then results in inaccuracies when determining the particle dilution ratio. For this work upstream concentrations were monitored live while sampling, and in the event that a large change in concentration occurred the test condition was repeated.

2.6 Leak Check

When measuring the penetration of a diluter it is imperative that the system does not have leaks that allow aerosol to enter or exit the internal sampling system. It is even more imperative due to the large difference in concentration between upstream and downstream of the diluter and because the ambient concentration are much higher than either upstream or downstream levels. A small leak that allows particles to enter the system downstream of the diluter can skew the results considerably. Consequently the system was leak checked prior to any measurements each day. This was done by placing a filter downstream of the DMA mondisperse exit, and upstream of the mixing make up air. This ensured that all air entering the system, both from the DMA sample flow and mixing make up air is HEPA filtered. The system was deemed leak tight if the concentration read by both CPC's could be reduced to less than 0.01 #/cm^3.

2.7 Particle Size Test Order

Due to the fact that a considerable time used for the inter-sample time, the effect of sample hysteresis was minimized and therefore there is no significant effect on the previous sample. The particle test order was then dictated by the necessity to change electrospray solutions to get the desired particle size range. Since a higher sucrose concentration was necessary for a larger particle diameter the testing was order was done from the lowest sucrose concentration to the highest to prevent cross contamination of the solutions. Although a buffer solution was installed between sucrose solutions, concern that if a high concentration solution was used prior to a low concentration that any amount of cross contamination would result in an increase in the sucrose concentration.

Therefore as an additional safety measure the particle diameter testing order was then tested from smallest electrical mobility diameter to the largest.

2.8 Calculation Methods

The average concentration over the sample period tested is computed for each particle size. The average concentration over the sample period is the data used for all calculations for CPC reference and penetration measurements. CPC locations and nomenclature are in reference to Figure 2-1

The CPC reference correction is calculated as follows

$$C_{B,A}(dp) = N_B(dp) / N_A(dp) \qquad \textbf{Equation 2-3}$$

where $C_{B,A}(dp)$ is the CPC Reference Correction Factor, $N_B(dp)$ is the concentration recorded by CPC B, $N_A(dp)$ is the concentration recorded by CPC A and dp is the particle electrical mobility diameter.

Once the CPC Reference Correction Factor is determined the calculation to determine the particle dilution ratio is as follows

$$DR_{particle}(dp) = \left(\frac{N_{B,dil}(dp)}{N_{A,dil}(dp)} \right) C_{B,A}(dp) \qquad \textbf{Equation 2-4}$$

where $DR_{particle}(dp)$ is the Particle Dilution Ratio, $N_{A,dil}$ is the concentration recorded by CPC A with the diluter installed and $N_{B.dil}$ is the concentration recorded by CPC B with the diluter installed

Using the computed $DR_{particle}(dp)$, and the previously determined $DR_{Volumetric}$, the particle penetration can be determined. Particle penetration is defined as

$$P(dp) = \frac{DR_{volumetric}(dp)}{DR_{particle}(dp)} \qquad \textbf{Equation 2-5}$$

2.9 Results

2.9.1 Lab "Leaky Filter" Diluter

2.9.1.1 Effect of Spatially Homogenous Aerosol

The influence of downstream mixing, and its effect on spatial homogeneity, was investigated using a singly charged, nearly mondisperese aerosol. For this series of experiments, as stated previously, the laboratory "leaky filter" diluter was placed upstream of a TSI 3025 CPC, with the MSP 1100 CPC monitoring upstream concentration.

As shown in Figure 2-5 the $DR_{particle}$ is measured both with, and without, a 0.040" orifice mixer downstream of the diluter. The resulting $DR_{particle}$ measurements show considerable deviation below 40 nm when comparing that of the mixed and non-mixed test conditions. The largest deviation occurs at 11 nm with a factor 143 between that tested without an orifice to that of the 0.040" orifice. It should also noted that at the largest size tested, for this experiment at 80 nm, also shows a similar deviation but of less magnitude, with the 0.040" curve being roughly 30% more than that of the test without the orifice installed.

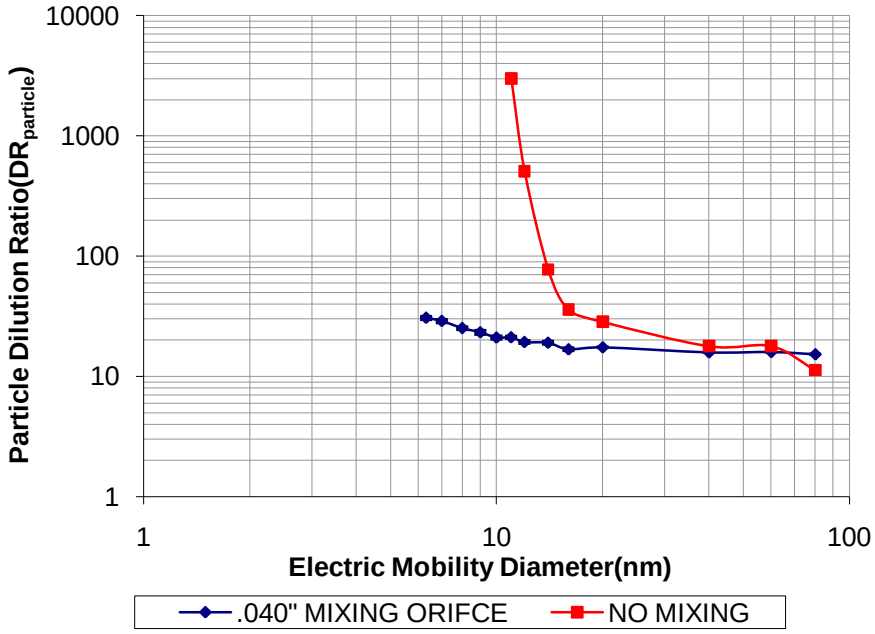

Figure 2-5
Particle Dilution Ratio for the "Leaky Filter" diluter

Since no modifications were done the diluter itself, only the addition of the mixer downstream, the large variation indicates that it is due to the method of sampling the diluted aerosol. In this case the particular CPC used to sample downstream, the TSI 3025A, has multiple flow splits within the inner workings of the device. Spatial concentration homogeneity is a large issue with these types of devices. The flow splits two times within the device, first a large flow split where 0.30 LPM of the incoming total flow of 1.50 LPM is sampled. This 0.30 LPM is the primary sample flow for the CPC, and from this smaller flow it further splits again to .03 LPM for the actual sample flow in which the concentration of the aerosol is determined. The requirement that is not explicitly stated when using this CPC is the fact that concentration of the 1.5 LPM flow must be spatial homogenous.

In the case of test without the mixing orifice placed after the diluter, it is clear that the particle dilution ratio is both less than, and greater, than that of the mixed test case, which yields itself to indicate that it is due to a poorly mixed flow.

As shown in Figure 2-2, the capillary tube allows the aerosol to enter into the core of a converging flow. Assuming the diluter is axis symmetric, and due to the low Reynolds number within the diluter, the aerosol would remain near the axis of the diluter and would only diffuse out into the sheathing particle free air over time. Effectively this would produce a very non-homogenous mixture of the aerosol, and with the multiple flow splits could result in a majority of the particles eventually making it into the actual sample flow of the CPC, or in the case of Figure 2-5, a large amount of the aerosol never making it into the CPC. This will result in an artificial $DR_{particle,}$ due to artificially increased or decreased concentration measurement downstream of the diluter

Due to this discovery, the remaining portions of the test include the use of a 0.040" diameter orifice placed downstream of the diluter as shown in Figure 2-1. To ensure that the level of mixing was sufficient to supply homogenous mixing, tests using the same experimental setup were repeated over a period of a week in which and were within a half of the sample standard deviation of the previous results.

2.10 Effect of Aerosol Charge

With the sampling of the downstream aerosol corrected to provide a spatially homogenous mixture of the aerosol into the downstream CPC, the effect of particle diameter on the particle dilution ratio could then be determined accurately. Due to the nature of the DMA, however, it provides an aerosol comprised mostly of singly charged

particles. Figure 2-6 shows the particle dilution ratio for an aerosol comprised mostly of singly charged particles, as well as a aerosol that was brought to an a Boltzmann charge distribution by exposure to a Po-210 neutralization source. The resulting curves show an increase in the particle dilution ratio for a decrease in particle diameter. Both the case of a singly charged aerosol and that of an aerosol at Boltzmann equilibrium charge have a similar particle dilution ratio for a particle size greater than 40 nm. Below 40 nm, however, a clear separation occurs with the singly charged test aerosol resulting in a maximum difference of 40% at 6 nm.

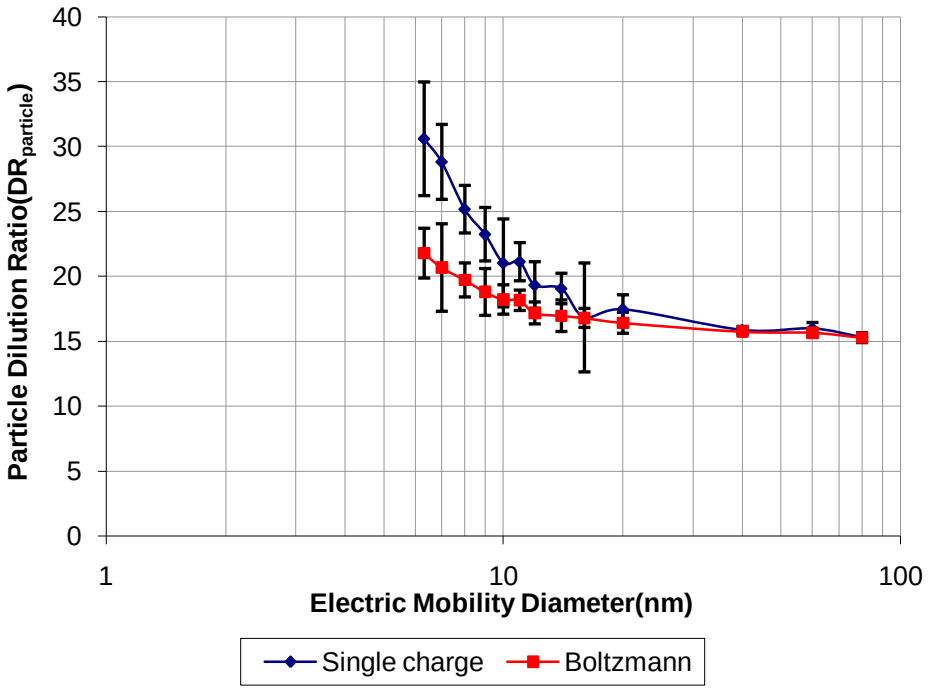

Figure 2-6
Influence of aerosol charge on $DR_{particle}$ for the "Leaky Filter" Diluter

The resulting measured volumetric dilution ratio was determined to be 13.11(Appendix I). The volumetric dilution ratio, however, does not agree with the particle dilution ratio at 15.2 at 80 nm, resulting in a 16% difference. This error is most

likely due to the measurement of the internal capillary flow rate. Due to the nature of the diluter, direct measurement of the capillary flow was difficult to perform and was constrained by the method of measurement of the pressure drop, as discussed in Appendix I. Attempting to recreate the flow and pressure drop from penetration testing mostly likely resulted in the measured capillary pressure drop being slightly greater than was actually present. To overcome this, the dilution ratio at 80 nm is then assumed to be the same as the volumetric dilution ratio. With this assumption the resulting value can be converted into penetration as discussed in Section 1.2.

Figure 2-7 represents the penetration through the diluter. The resulting effect of the increasing particle dilution ratio as particle size decreases, as observed in Figure 2-6, results in a reduction of particle penetration. The reduced penetration is likely mainly due to increasing diffusion losses with decreasing size with additional losses due to electro-static effects with a singly charged aerosol.

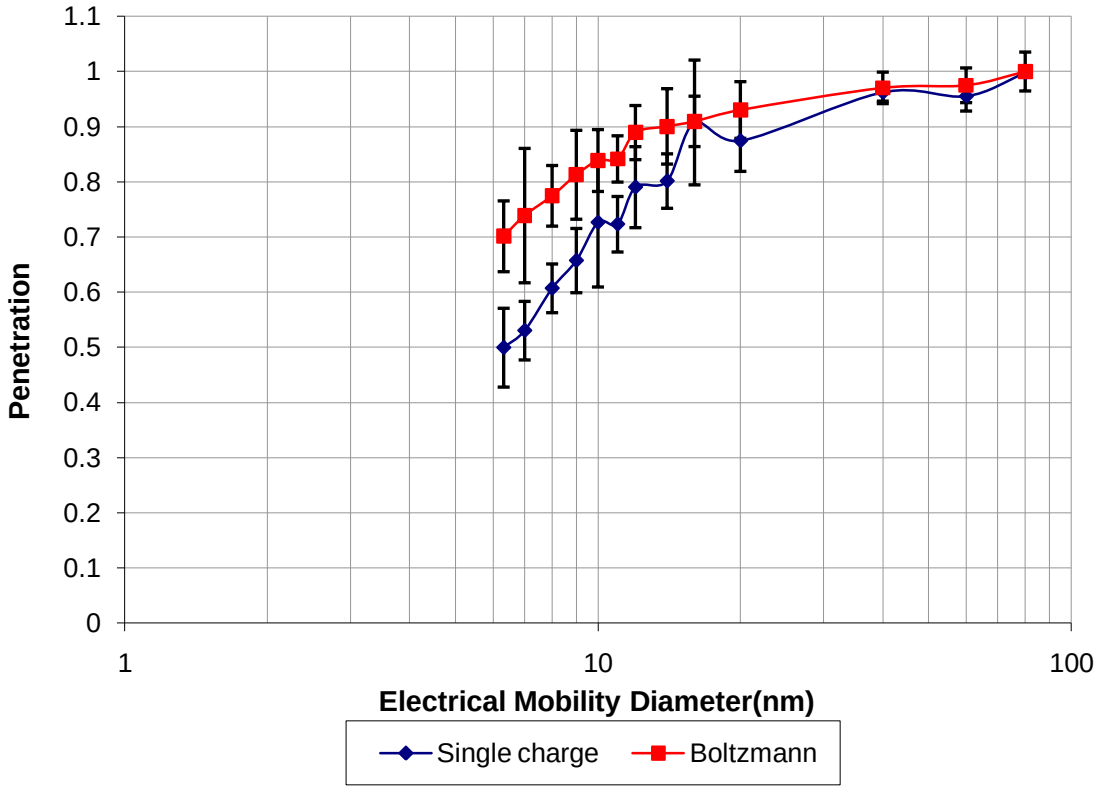

Figure 2-7
Particle penetration as function of aerosol charge for the "Leaky Filter" diluter

For the case of the laboratory "leaky filter" diluter, the diffusion loss shown in Figure 2-7 are primarily due to particle loss in capillary tube. This is evident by the design of the diluter, shown in Figure 2-2, with bypass flow carrying the aerosol that will be diluted through the capillary tube.

To attempt to characterize the losses for these two cases, a model for diffusion losses within tube with fully developed laminar flow is fitted to the data by minimizing the Sum of Squares Error(SSE) results in Figure 2-8. The equation that describes this model is as follows

$$\mu = \frac{DL}{Q}$$ **Equation 2-6**

$$P = 1 - 5.50\mu^{0.667} + 3.77\mu \quad \text{for } \mu < 0.009$$
$$P = 0.819\exp(-11.5\mu) + 0.0975\exp(-70.1\mu) \quad \text{for } \mu \geq 0.009$$

where P is the particle penetration, Q the volumetric flow, D is the diffusion coefficient of the particle and L as the length of the tube.

The resulting curves show good agreement with their respective data set indicating diffusion driven particle loss as the primary mechanism. As shown in Figure 2-8 the theoretical diffusion loss show a near unity penetration for particles greater than 80 nm with both theoretical curves at more than 98% penetration for that particle size. This matches the logic used earlier, that for diffusion driven losses, particles greater than 80 nm have a very high penetration due to their low diffusion coefficient. This is also evident in the equation that describes the model, in such that μ is only dependent upon the diffusion coefficient, length, and flow through the tube. In the case of a diluter the effective loss length and flows are constant so the only particle dependent value is that of the diffusion coefficient.

Using the particle dilution ratio, and the assumption that at 80 nm the volumetric dilution ratio and particle dilution ratio are equal, the flow rate through the capillary tube is determined to be 0.0982 LPM. Using the measured length of the capillary tube, 0.0613 m, the theoretical ratio of tube length to flow rate(L/Q) is 3.74E4 sec/m^2. Using Equation 2-6 the theoretical losses in the tube is calculated and can be found in Figure 2-8.

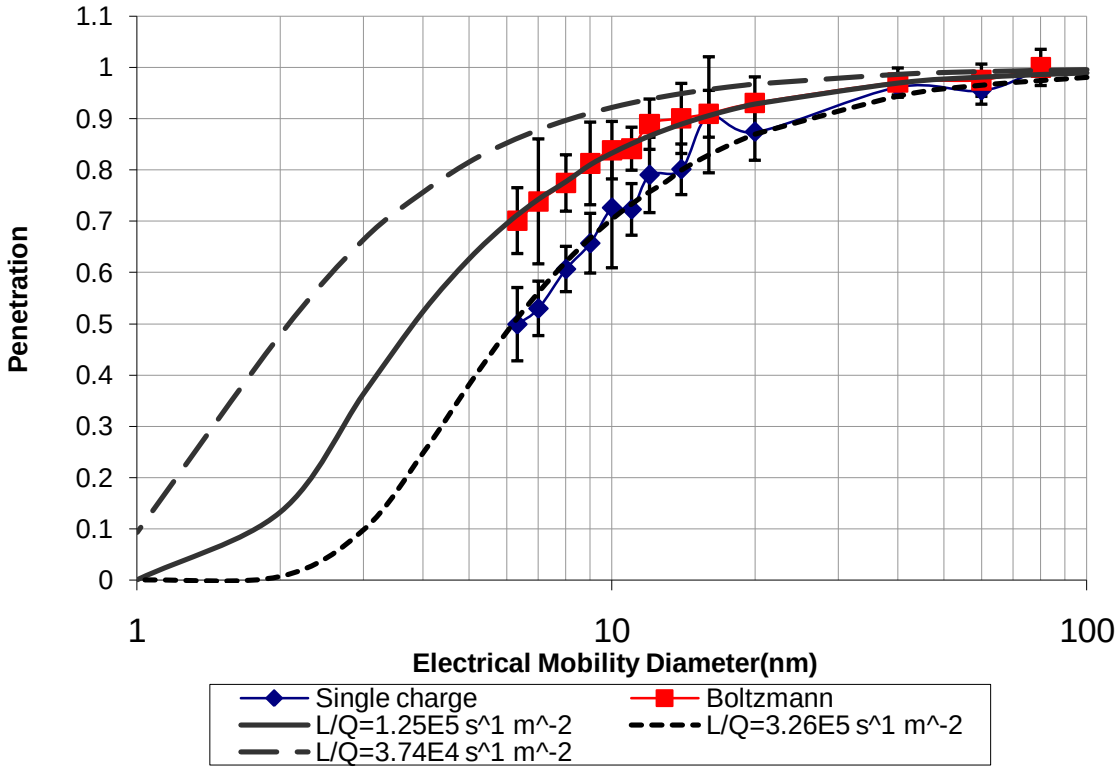

Figure 2-8
Laminar Tube Diffusion model fit to "Leaky Filter" diluter penetration data

As shown in Figure 2-8, the measured penetration values for both the singly charged and Boltzmann equilibrium aerosol are less than that of the theoretical results with the values of L/Q equal to 1.25E5 s/m^2 for the Boltzmann aerosol, 3.3 times the theoretical value. The singly charged aerosol curve fit at a L/Q value of 3.26E5 s/m^2 which is 8.7 times the theoretical value. All three curves, however, indicate that particles greater than 80 nm have low diffusion coefficient that the resulting penetration is near unity. Furthermore this indicates that in most cases, penetration can be assumed to be near that of the volumetric dilution ratio up to about 300 nm before particle inertial effects become important.

One important topic that has not been discussed is the significant influence of particle charge on the particle dilution ratio and the resulting penetration. In the case of the singly charged test aerosol there is an increase in the resulting μ when a curve fit using Equation 2-6 is used. Since the diffusion coefficient is calculated only based on thermal energy and particle mobility, there is no influence of charge described by the model. To attempt to quantify the effect of particle charge, an additional term will be added to Equation 2-6 such that it yields

$$\mu = \frac{\alpha DL}{Q} \qquad \textbf{Equation 2-7}$$

where α is the correction for charge term. To do this, the original diffusion model is fit to the Boltzmann charge equilibrium test aerosol using the diffusion coefficient as determined by the Stokes-Einstein equation, such that α is equal to unity . The resulting L/Q values, as shown above, are found to be 1.25E5 s/m^2. Then using this value of L/Q the curve is fit to the singly charged test data by minimizing the SSE. The resulting determined charge correction term is 2.61. This is effectively similar to increasing the tube length by a factor of 2.61 when compared to the Boltzmann charged aerosol.

To better ascertain the influence of charge the work by Yu and Chandra(1978) is used determined theoretical deposition rate for charged particles in a cylindrical tube due to image force. Using this theoretical calculation yields greater than 99% penetration of particles of 9 nm which clearly does not agree the empirical work described above. Kasper(1981) described the effect of space charge, a mutual repulsion by a charged aerosol. However, the influence of this effect is determined to be less than 1% due to the low aerosol concentration and low number of charges per particle. Work by Liu et al.

(1985) showed similar effects in transport tubing with increased deposition due to aerosol charge and tubing material but did not indicate a working model for the enhanced deposition. Liu et al. did notice an enhancement to particle deposition in non-conducting tubing. This may possibly be evident in this as well due to the fact that quartz tubing is a non-conducting material. Further work by Alonso et al. (2007) examined effects of image force deposition on single fiber collection efficiency; further noting the that the effect of space charge was negligible in their work. Therefore based on previous works, it is indicative that the increase in diffusion driven losses within the capillary are due electrostatic effects acting on the charged particle, however currently no model accurately predicts the loss.

2.11 MSP Diluter

In testing the MSP 1100 dilution system the investigation of spatial homogeneity of the exiting diluted aerosol was not performed. This is due to the one primary requirement for this type of dilution, as discussed in Section 1.5, is that the resulting diluter must have spatial homogeneity of the aerosol concentration after the internal mixing. Therefore the work focused on sub-100 nm particle dilution ratios for this device.

For this work, the size dependent particle dilution ratio was investigated at a dilution ratio of 80:1. The dilution ratio for this instrument is user selectable and also internally monitored via the MSP software. As shown in Figure 2-9, the resulting particle dilution ratio over the particle size range tested shows an increasing particle dilution ratio with a decreasing particle size. This trend indicates losses within the diluter which cause an increase the particle dilution ratio. At these test conditions the 9 nm particle dilution

ratio is 129:1, which is 48% greater than the dilution ratio at 100 nm. One point of interest is that for the largest particle size tested, 100 nm, the measured particle dilution ratio was 87, when compared to the volumetric dilution ratio recorded at 80. This could be due to an error in the measured volumetric flow rates resulting in volumetric dilution ratio being 87:1. This is further substantiated as possibility when examining the particle dilution ratio for 100 nm, 80 nm and 60 nm which results in a particle dilution ratio within 87±1. This would tend to indicate that the losses within the diluter are independent of size for particles greater than 60 nm, indicating an error in the volumetric dilution ratio measurement. However, the resulting CPC flow rate measurements, and indicated dilution flow into the MSP diluters was within a dilution ratio of 80±2, with the variability due to a non steady reading from the flow meters. The losses could be still due to an improper calibration of the flow meters, software error, but since there is no clearly evident source for the error the assumption that the volumetric dilution ratio measured by the MSP diluter is accurate will be used.

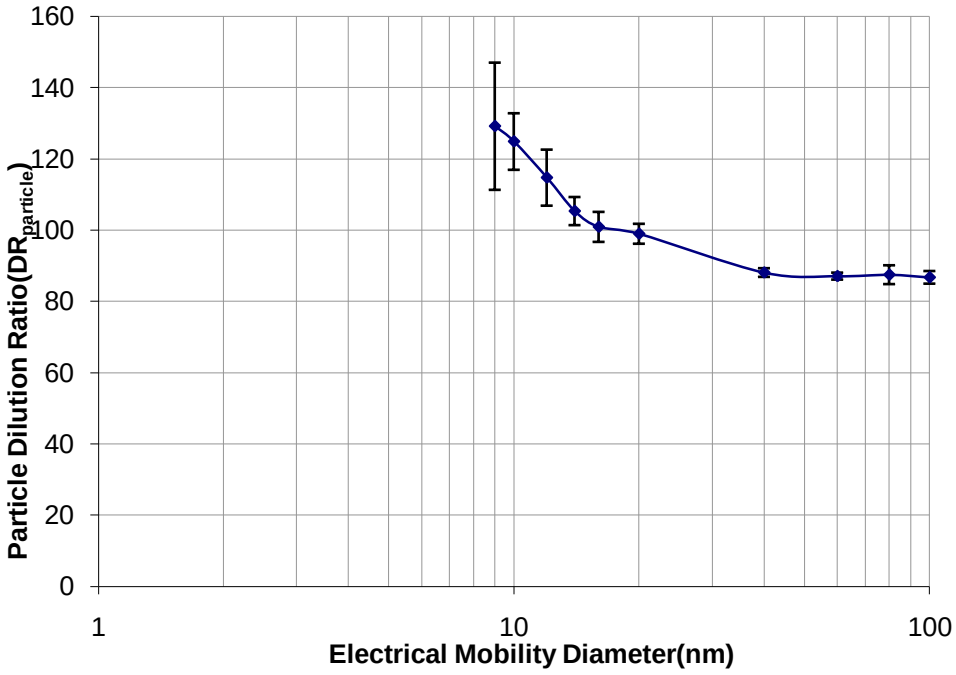

Figure 2-9
MSP 1100 $DR_{particle}$ with aerosol at Boltzmann equilibrium charge, DR_{vol}=80

Using the volumetric dilution ratio determined by the MSP 1100 the resulting penetration can be found in Figure 2-10. Notably the penetration is greatest at 100 nm at 0.92 and decreasing to 0.62 at 9 nm. This is an expected trend as seen in the previous diluters, and again the effect of diffusion deposition is clearly evident by the trend.

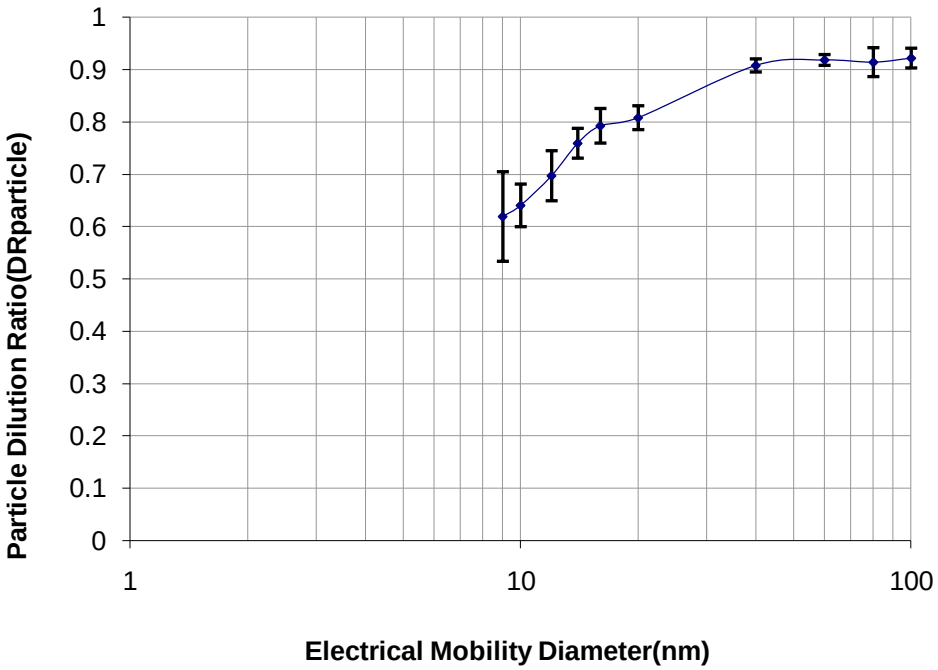

Figure 2-10
Diluter Penetration with aerosol at Boltzmann equilibrium charge, DRvol=80

One additional feature of the MSP diluter when compared to that of the laboratory "leaky filter" diluter discussed prior, is that the MSP diluter has the ability to vary the dilution ratio. Due to the time required to do a full measurement of the particle dilution ratio the measurements were abbreviated to include only 100 nm and 9 nm particle dilution over the volumetric dilution range of 80 to 125. As shown in Figure 2-11, the resulting 100 nm particle penetration decreases from 0.93 at a volumetric dilution setting of 80, to 0.86 at a volumetric dilution ratio of 125. This rate can be determined by fitting a linear curve to the data with the resulting rate of particle loss shown in Figure 2-11.

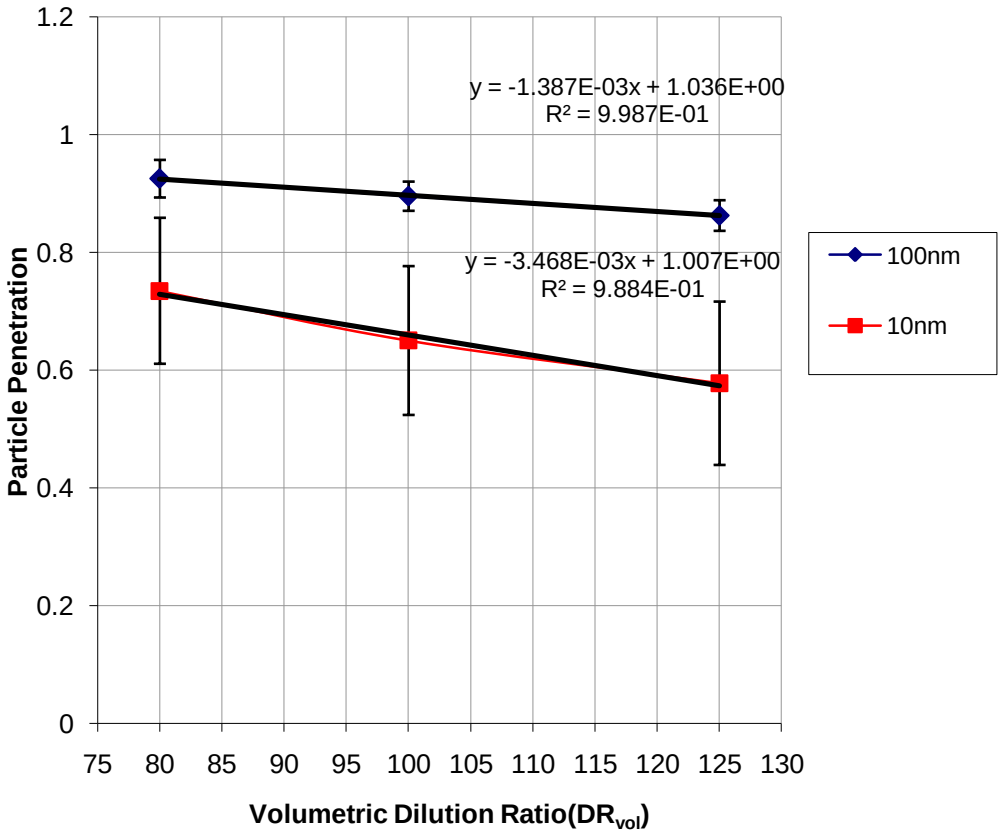

Figure 2-11
Particle Dependent Dilution with aerosol singly charged

The relative slopes for particles sizes of 9 nm and 100 nm results in value of 2.25, indicating that the rate of 9 nm particle penetration as a function of volumetric dilution ratio decreases at a rate that is 2.25 times that of 100 nm.

When compared to a simply turbulent deposition model however, there is inverse relation to flow rate and penetration. In a turbulent deposition model described by Hinds(1999) the increase in volumetric flow through the tube results in a increase in the particle penetration as shown by

$$P = \exp\left(\frac{-0.16L}{d_t \,\mathrm{Re}^{1/4}}\left(\frac{\rho_g D}{\eta}\right)^{2/3}\right) \qquad \textbf{Equation 2-8}$$

where L is the tube length, d_t as the tube diameter, η is the gas dynamic viscosity, D is the particle diffusion coefficient and ρ_g is the gas density. The clear relation shown by this equation, with the Reynolds number as the denominator, is that as the flow increases within the tube the resulting penetration is increased. This in relation to the mixing diluter, would predict that as the dilution ratio increases, the particle penetration would also increase.

Since the empirical data for the diluter shows the opposite trend, the simplistic model as that of a turbulent flow in a pipe, may not be sufficient to model the flow within the device. One argument that could be made, however, is that a fixed percentage error in the flow rate measurement may result in a similar trend. This seems plausible when looking at the 100 nm aerosol where the rate of reduction in particle penetration is linear. As described prior, the rate of reduction is approximately -0.0016 DR_{vol}^{-1}. If this was the case however, then the error and the resulting effective rate of reduction in penetration would be evident in the 9 nm case as well. This is not the case, however, with the rate of reduction in particle penetration greater at a value of -0.0036 DR_{vol}^{-1}. This indicates that 9 nm particles are more likely to be lost to the walls of diluter with an increasing flow rate at an increasing rate when compared to that of a 100 nm particle. The relationship between the flowrate and particle penetration may indicate a strong correlation to the internal flow of the device.

Work by Chen et al.(2007) analyzed the flow through a orifice and found a significant influence on penetration due on the flow field on the back side of the orifice,

more specifically due to regions of recirculation. Due to the design of a mixing style diluter, a similar effect may be present within the diluter. With increasing flow rate, regions of recirculation may develop that enhance particle loss on the walls.

One additional parameter investigated for this diluter was the influence of particle charge on the particle dilution ratio. This test performed at a volumetric dilution ratio of 80, and the results can be seen in Figure 2-12. Using the volumetric dilution ratio as determined by the instrument, the particle penetration is then determined as per Section 1.2.

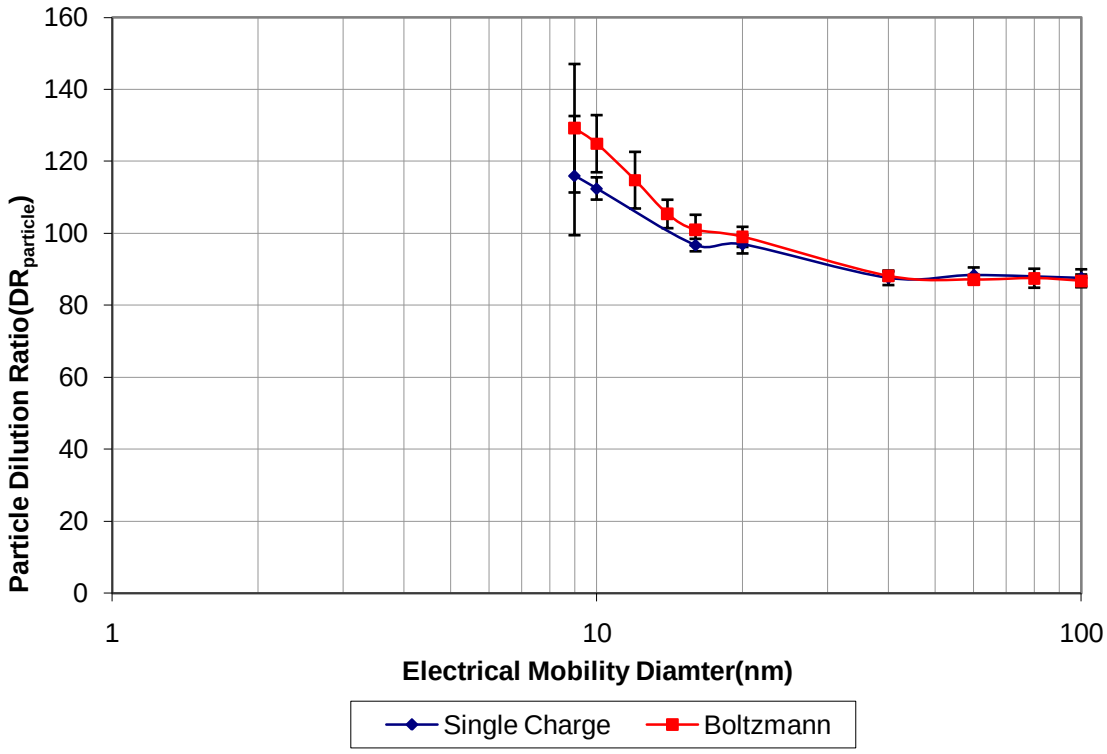

Figure 2-12
MSP 1100 $DR_{particle}$ as function of aerosol charge

The resulting particle penetration indicates a small difference between an aerosol carrying a single charge per particle to that of an aerosol at Boltzmann equilibrium, with the singly charged aerosol having a greater penetration. As shown in Figure 2-13 the

difference in particle penetration for the two test aerosol above 40 nm shows no significant difference. The two curves, however, diverge below 40 nm with a maximum difference occurring at 9 nm with a 9% difference between the values. Although indicating the opposite trend of charge effects as shown by other diluters, it should noted that the two values do lie within one standard deviation of the propagated error and the small difference could be due to measurement error alone.

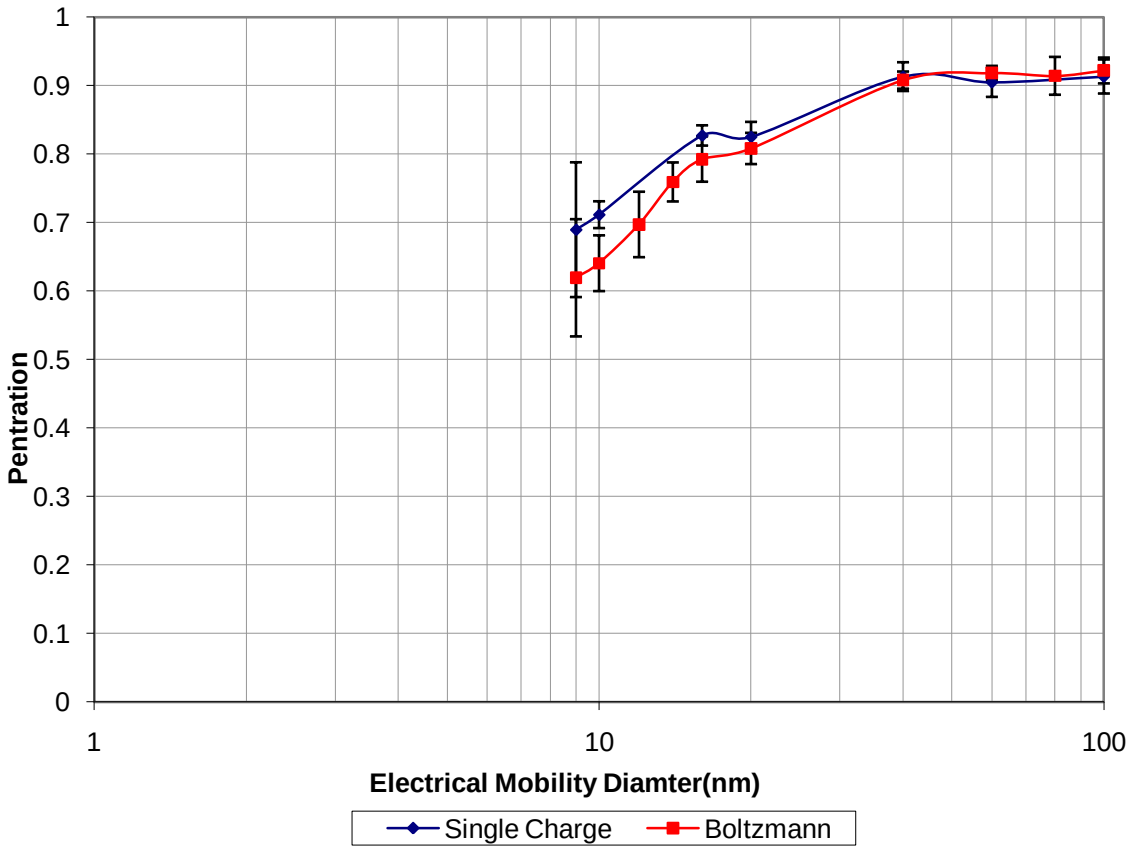

Figure 2-13
MSP 1100 Diluter Penetration as function of aerosol charge

2.12 TSI 3302A

The particle dilution ratio as a function of particle size was tested for the TSI 3302A diluter with the aerosol at Boltzmann equilibrium. The resulting particle dilution ratio for a fixed volumetric dilution condition of 18.2 can be found in Figure 2-14. The resulting figure shows a similar trend to other diluters tested resulting in an increasing particle dilution ratio as particle size decreases. The resulting 100 nm particle dilution was measured to be 17.2 while the resulting 9 nm particle dilution ratio resulted in 22.2. This difference of roughly 29% between the 100 nm and 9 nm is again due to internal losses within the diluter.

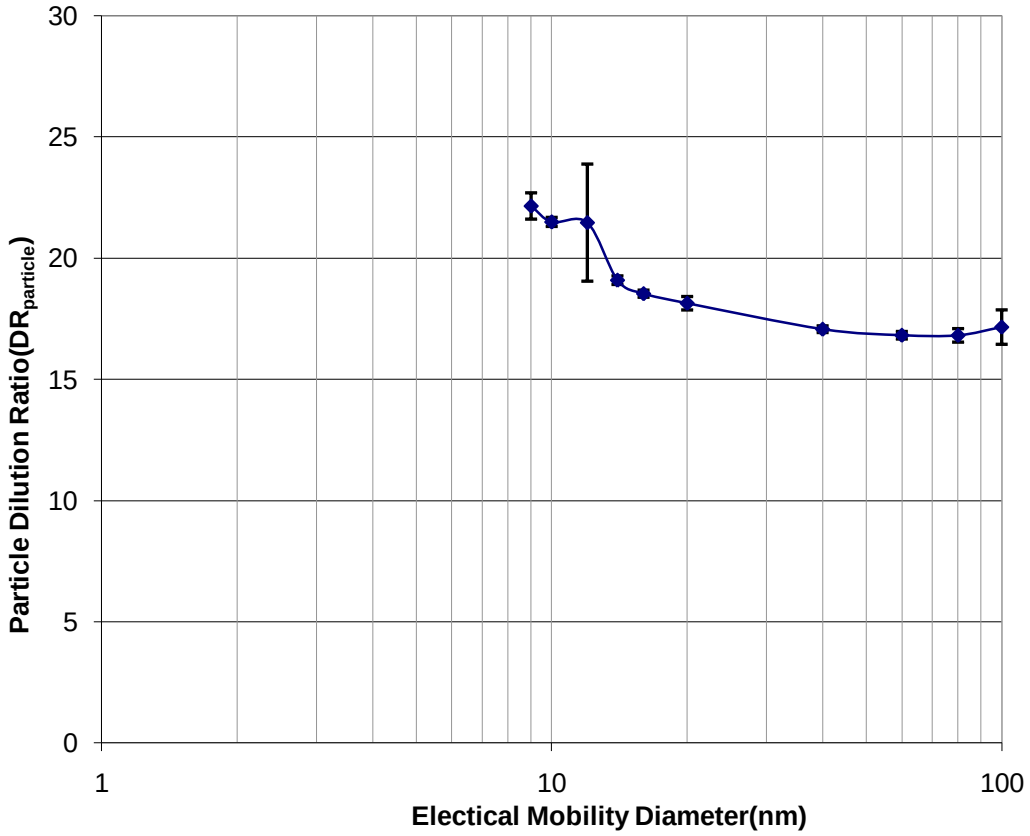

Figure 2-14
TSI 3302 $DR_{particle}$ with a Boltzmann charge aerosol, DR_{vol}=18.2

To better display these losses the particle dilution ratio, as well as the volumetric dilution ratio, is used to determine the particle penetration through the diluter. The resulting values can be found in Figure 2-15. The resulting calculated value for the Boltzmann aerosol is greater than unity for particles sizes greater than 20 nm. This means intrinsically that particles greater than 20 nm are produced by the diluter and in the case of this diluter is not physically possible. This therefore is assumed to be an error, and is most likely due to experimental error of measuring the capillary aerosol flow and total sample flow of the CPC. Furthermore, due to the adjustable dilution ratio of this diluter, error in setting the dilution ratio could also result in a similar trend. To correct for this error the diluter penetration is normalized to unity for the particle size of 80 nm as shown in Figure 2-15.

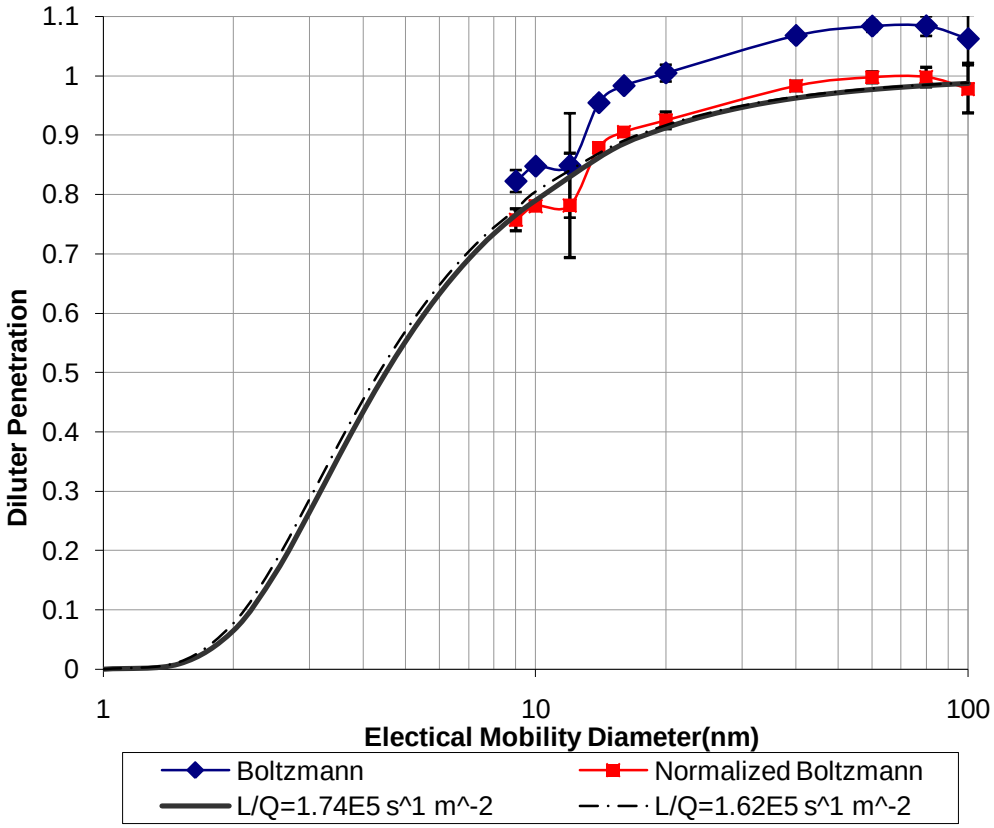

Figure 2-15
TSI 3302 Diluter Penetration for DR_{vol}=18.2

The resulting curve, as can be seen in Figure 2-15, shows a similar trend to the other diluters tested. The resulting downward curve as the particle size decreases is expected as particles deposit on the inner capillary of the diluter and are lost. This results in the penetration being less than unity.

The theoretical values of penetration are calculated using Equation 2-6 with a measured capillary length of 13.4 cm and a measured capillary flow of 49.72 cm^3/min resulting in a theoretical L/Q to be 1.62E5 s/m^2. The curve fit of the normalized penetration data, using Equation 2-6, results in a L/Q value of 1.74E5 s/m^2. A plot of the resulting theoretical values can be found in Figure 2-15.

The numerical difference between the L/Q values is only 8%, furthermore over the size range tested, the greatest penetration difference between the curves results in a difference of only 2% at 9 nm. This is small difference and well within the error of the test data.

An investigation of the influence of particle charge on the particle dilution ratio was done using a singly charged aerosol as discussed previously. The resulting particle dilution ratio is shown in Figure 2-16. Two things are evident when comparing the singly charged test aerosol data to that of the Boltzmann equilibrium charge data. First, the 80 nm and above the data for both the single charge test aerosol and Boltzmann equilibrium data are in good agreement with less than 2% difference between them. Second is the divergence between the data as the particle diameter is reduced, such that there is a 34% difference between the singly charged and Boltzmann test data at 9 nm.

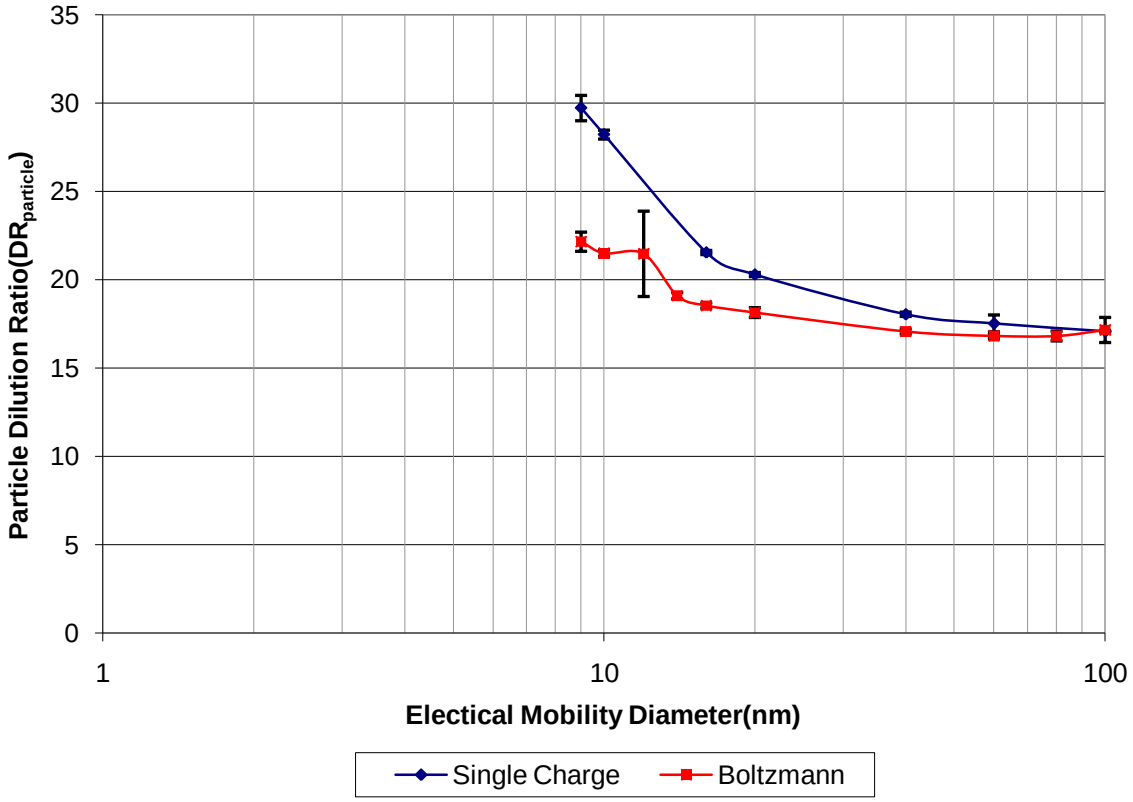

Figure 2-16
Effect of aerosol charge on $DR_{particle}$ for TSI 3302 diluter, DR_{vol}=18.2

To better interpret the data, the results are converted to particle penetration using the volumetric dilution ratio. It should be noted, that like the previous penetration dataset, the values are normalized. The results for the particle penetration as a function of particle size can be found in Figure 2-17. The resulting difference between the singly charged aerosol and that of an aerosol at Boltzmann Equilibrium is largest in particles less than 40 nm. To better analyze the difference between the two data sets, Equation 2-6 is used to curve fit the respective datasets. The resulting value of L/Q for the singly charged aerosol was determined to be 5.36E5 s/m^2. Using the same comparison made previously, the resulting diffusion correction for charge(α) for the singly charged aerosol is determined to be 3.1. This is similar to that found for the leaky filter diluter in which the diffusion

correction for charge was determined to be 2.61. Although the system is similar in terms of the dilution method, it should be noted that TSI 3302 uses a stainless steel capillary tube, while the laboratory leaky filter diluter uses a quartz capillary tube. This difference in material may account for the difference in the charge correction factor.

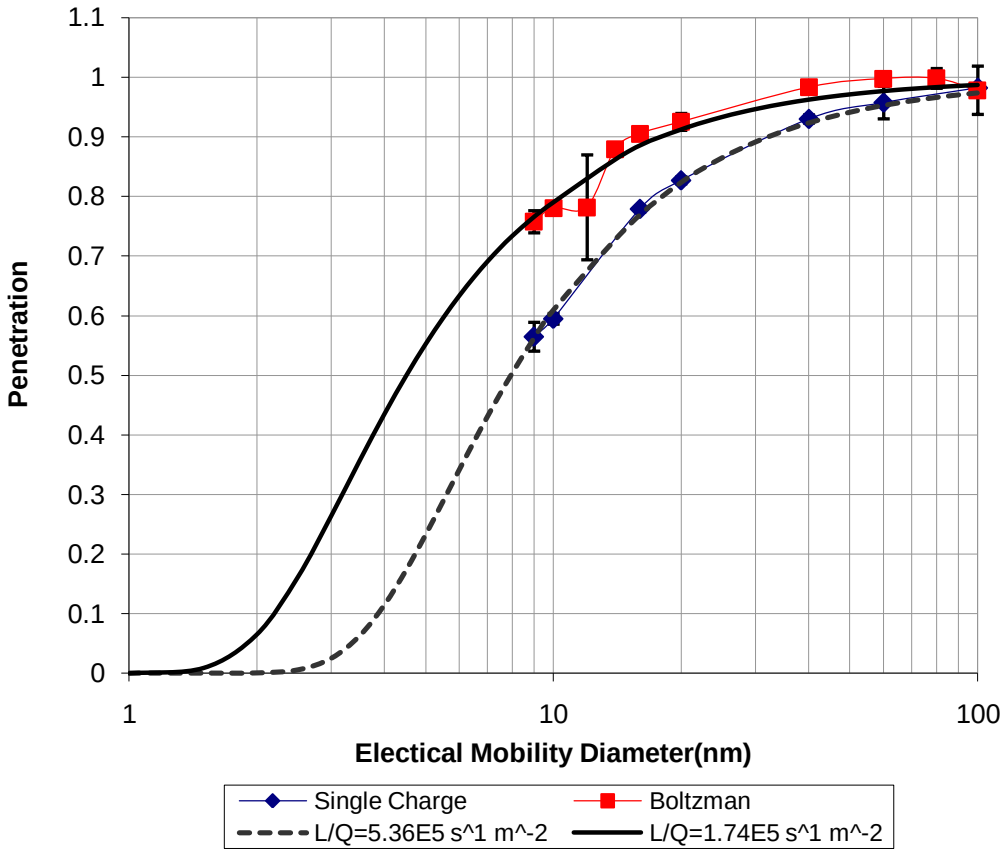

Figure 2-17
Effect of aerosol charge on Diluter Penetration, DR_{vol}=18.2

The ability to change the dilution ratio with this diluter, or effectively the flow through the capillary tube, allows the influence of the dilution ratio on particle penetration to be examined. Shown in Figure 2-18 is the particle penetration for both 100 nm and 9 nm particles, for a Boltzmann equilibrium aerosol, over a range of volumetric

dilution ratio conditions. Due to the experimental error, as previously discussed, the resulting particle penetration for the diluters at 100 nm test condition is greater than unity, but in this case was not normalized. The penetration for the 100 nm particles is relatively independent of dilution ratio, while the 9 nm particles show decreasing penetration with increasing dilution ratio. This is expected because increasing dilution ratio results from reducing the amount of flow through the capillary and increasing the L/Q ratio.

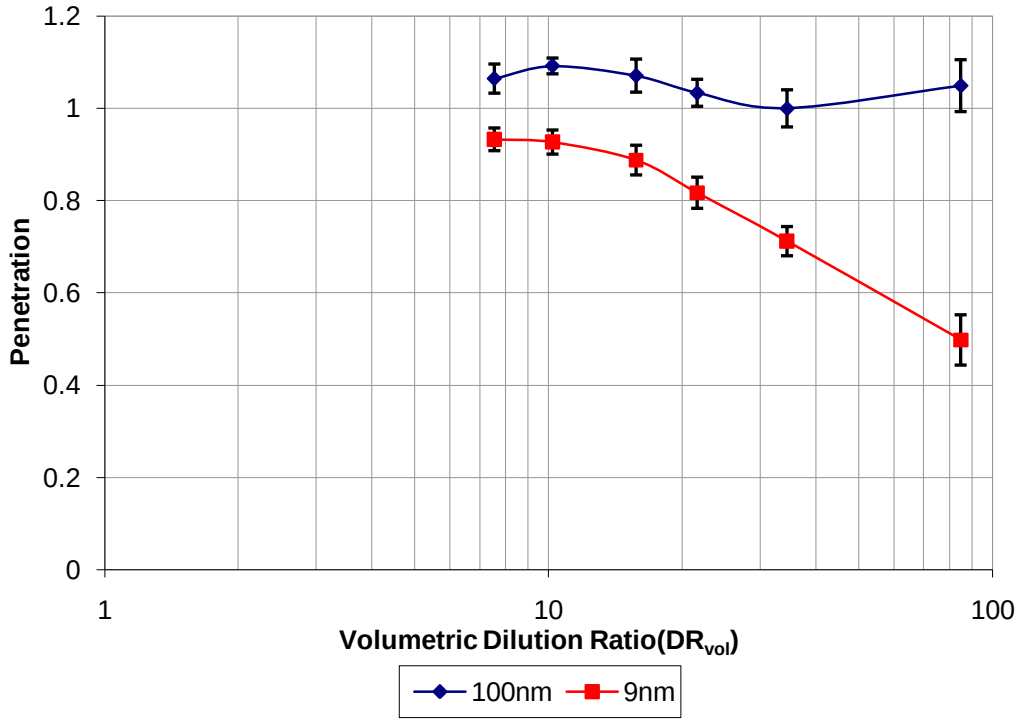

Figure 2-18
Effect of DR_{vol} on Diluter Penetration with a Boltzmann charged distributed aerosol

To remove the effect of error of volumetric dilution ratio in the determination its use can be bypassed by using a relative penetration. This is done be comparing the relative penetration between 100 nm particle test case and 9 nm test case. This assumes that the 100 nm particle penetration is near unity and based on the previous test data it is

fair assumption over the values tested. A plot of the 9 nm/100 nm relative penetration can be found in Figure 2-19.

As shown in Figure 2-19, the resulting relative penetration decreases with increasing dilution. From the data set, the highest penetration occurred at a volumetric dilution ratio of 7.6 with a resulting relative penetration of 0.88. This compared to the lowest relative penetration of 0.47 at a volumetric dilution ratio of 84.8.

Using the measured length of the capillary, as well as the theoretical flow through the capillary tube for the resulting volumetric dilution ratio, a theoretical value of the relative penetration can determined using Equation 2-6. A plot of the theoretical 9 nm/100 nm relative penetration can be found in Figure 2-19. The measured relative penetration and the theoretical value is in good agreement, with the greatest difference occurring at a volumetric dilution ratio 22.6 and a resulting difference in the relative penetration of 0.03, less than a 4% difference.

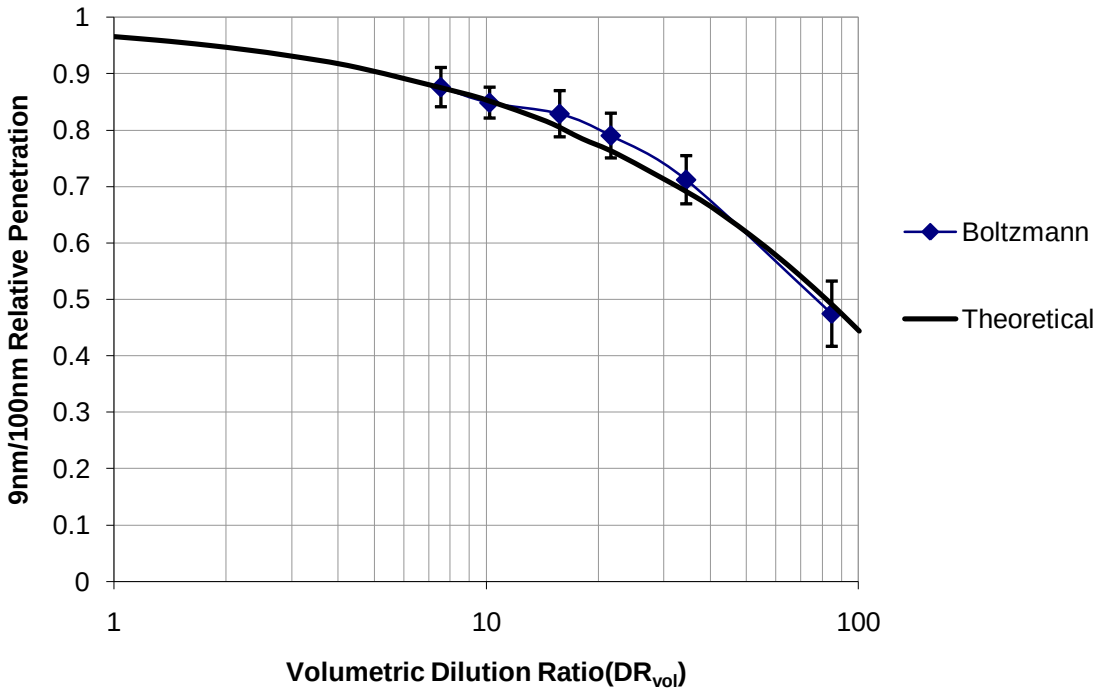

Figure 2-19
Effect of DR_{vol} on 9 nm/100 nm Relative Diluter Penetration

2.13 Orifice Diluter

The effort to develop a diluter in which sub-100 nm particle losses could be minimized, led to the Orifice Diluter. Testing was done using the TSI 3010 CPC as the downstream reference. The reason for selecting the TSI 3010 CPC is that it is a full-flow laminar CPC, in which the entire 1.0 LPM sample flow is used for the concentration measurement. The 3010 was preferred over the 3025A CPC with its internal flow splits because it eliminated the need for downstream mixing, as discussed above for the laboratory leaky filter.

The results of measurement of the particle dilution ratio as a function of particle size for orifice diameters of 1.6 mm, 0.64 mm and 0.41 mm are shown in Figure

2-20,Figure 2-21, and Figure 2-22 respectively. The particle dilution ratio for the 1.6mm diameter orifice has a resulting particle dilution ratio of 3.51 at 100 nm. The particle dilution is essential size independent over the particle size range tested with a maximum deviation from the mean particle dilution ratio, a value of 3.54, is found to be 4.1% for the 16 nm test case.

The results from the 0.64mm orifice test case, as shown in Figure 2-21, shows a similar trend as the 1.6 mm test case for particle size greater than 20 nm, with a fairly flat profile hovering around a particle dilution ratio of 23. What is striking in this data set is for the first time the measured particle dilution ratio decreased as particle size was reduced below 20 nm. This suggests decreasing losses below 20 nm or this device is generating particles. This is unlikely and suggests a measurement flaw that will be discussed below

The results from the 0.41 mm diameter orifice, as shown in Figure 2-22, shows a more similar curve for the particle dilution ratio with values fairly constant at particle dilution of 74. Expected losses in the diluter result in an increase in the particle dilution ratio, and as expected the losses should occur at the smaller particle size tested. What is suspicious of this data, however, is the rate of change of the curve. Since this type of diluter would again be dominated by diffusion losses, it is uncharacteristic to have minimal losses at 12 nm and suddenly losses evident at 10 nm as indicated by an increase in the particle dilution ratio. This is not characteristic of a diffusion loss curve, as discussed above for the other diluter test cause, and the results hint at a fundamental measurement error.

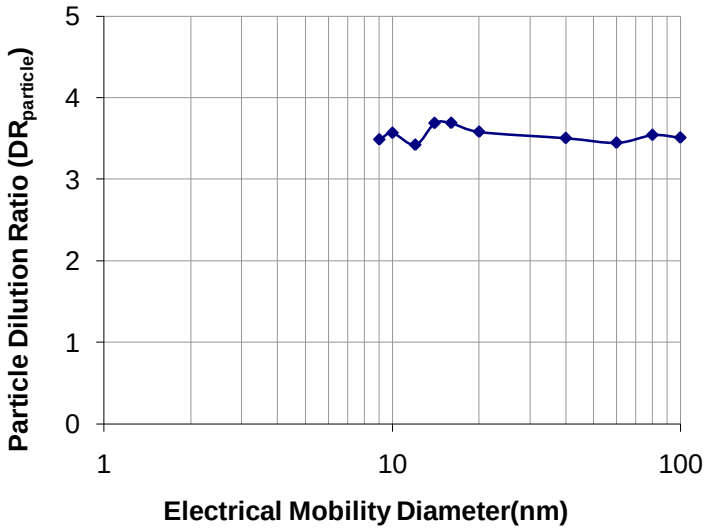

Figure 2-20
$DR_{particle}$ for 1.6 mm orifice installed in the Orifice Diluter

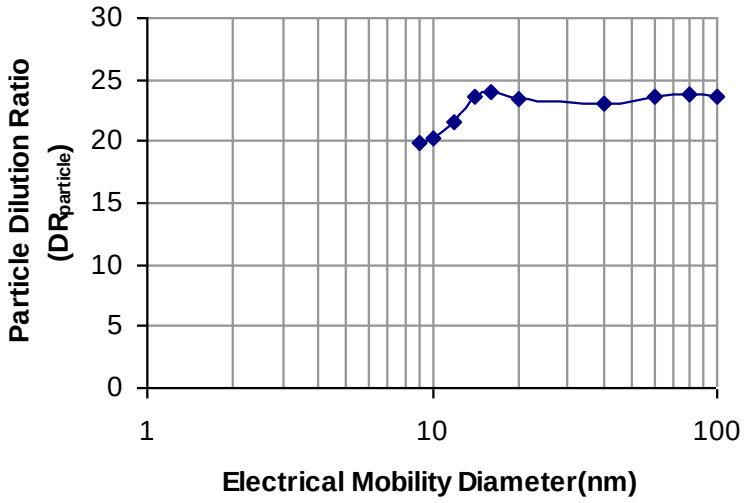

Figure 2-21
$DR_{particle}$ for 0.64 mm orifice installed in the Orifice Diluter

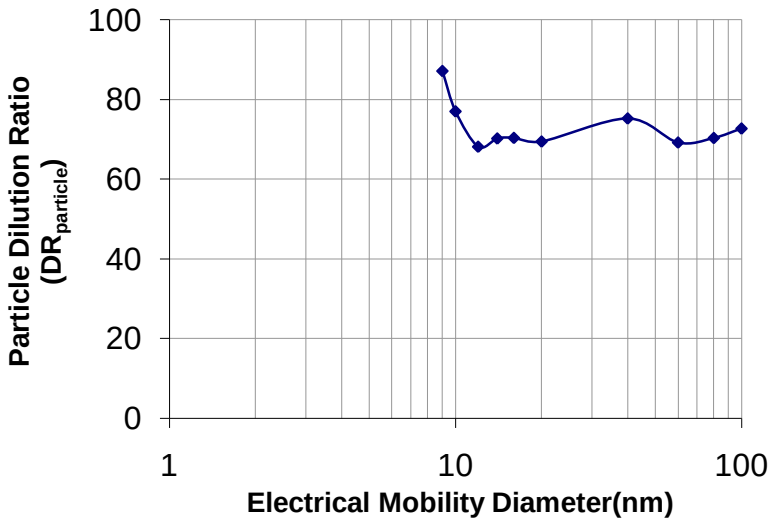

Figure 2-22
$DR_{particle}$ for 0.41 mm orifice installed in the Orifice Diluter

One possible area investigated in the measurement technique was in the downstream mixing of the orifice diluter. Although not initially evident, the use of a full flow laminar CPC did not resolve the need for mixing at all particle sizes. Downstream mixing is still required when particle size approach the edge of the response curve of the CPC. Figure 2-23 shows results for the 0.41mm orifice diluter with and without downstream mixing orifices.

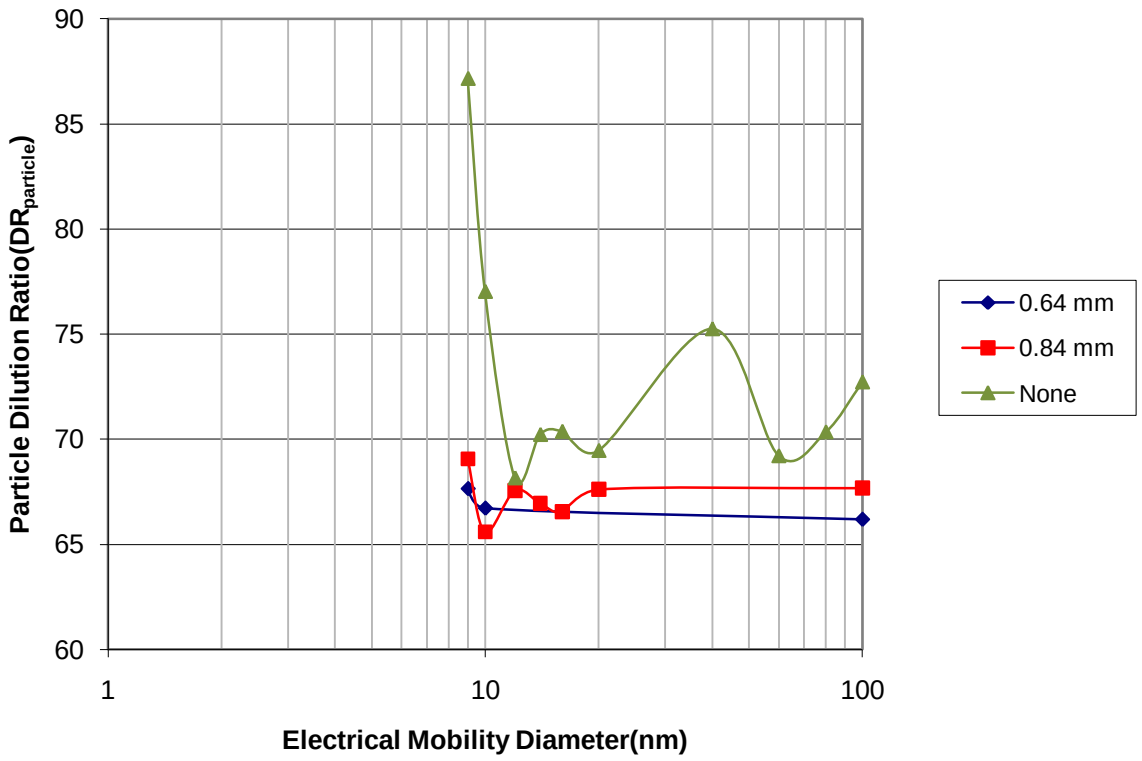

Figure 2-23
Effect of downstream mixing diameter on $DR_{particle}$ measurements for a 0.41 mm diluter orifice

The addition of a 0.84 mm diameter mixer downstream of the orifice diluter provided a more uniform particle dilution over the values tested when compared to the results of using no dilution. To see what further mixing could provide, the 0.84 mm diameter mixing orifice was replaced with a 0.64 mm diameter orifice. Since it was apparent that most of the discrepancy occurred below 10 nm, the test was constrained to 100 nm,10 nm and 9 nm particle diameters. The resulting values show a near uniform particle dilution ratio from 100 nm to 9 nm for the 0.64 mm downstream mixer. This result indicated that the losses within the diluter are minimal, and furthermore that the response of the CPC has a dependence on spatial homogeneity.

Due to the nature of the orifice diluter, the particle concentration downstream is not homogenous. This is due to the effect of introducing a small aerosol laden flow into a much larger dilution flow at low Reynolds number resulting in the particles constrained to the streamlines of the bulk flow. A computational fluid model was generated using CFX 10.0 and particle tracking added to provide a graphical representation of this, as shown in Figure 2-24. As shown in Figure 2-24 the 100 nm particles with density of $1g/cm^3$, shown in black, enter the dilution flow on the right with the particle free dilution air coming from the top. Although there is a region with a vortex, the low Reynolds number of this flow does not provide adequate mixing. The exit flow clearly shows the particles still only occupying a small region of the flow, and is clear that the resulting concentration is not homogenous. It should be noted that this model did not include the diffusive effect of that particles which would help reduce the non-homogenous concentration, but as described previously, the diffusion coefficient for a 100 nm particle is minimal.

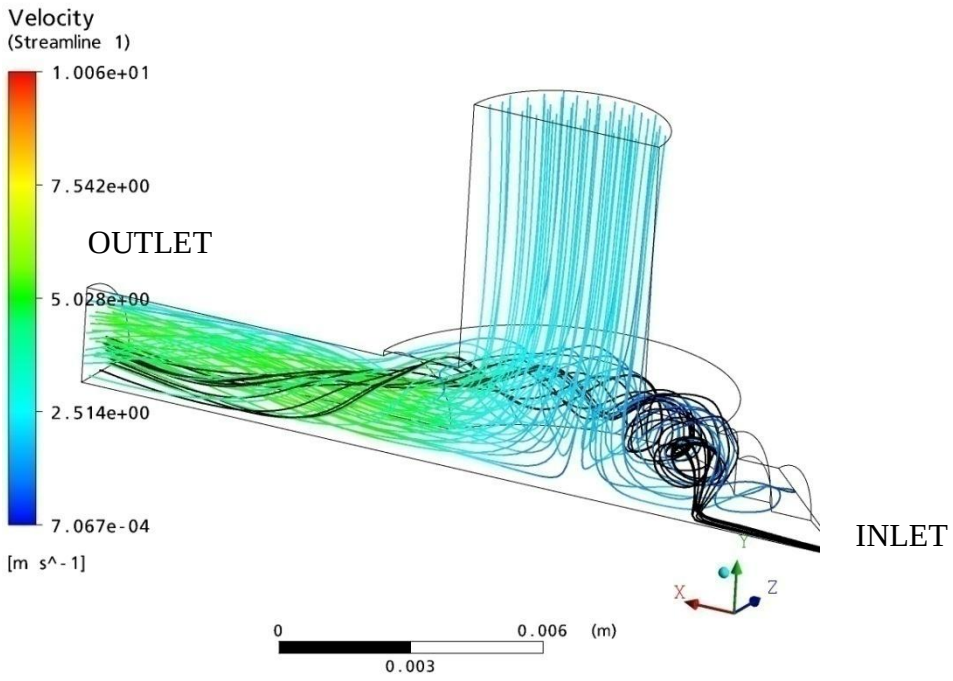

Figure 2-24
Fluid flow model of the orifice diluter at the exit of the orifice

This effect results in particles primarily being bound to a region within the tubing, and in the case of no mixing device downstream, the only force to provide a homogenous profile is diffusion. This is a relatively slow method of creating a homogenous mixture and therefore the particles will remain constrained in a section of the flow.

Furthermore, particles that are trapped in a small portion of the flow then pass through the CPC under the same condition. This can result in large difference in particle number counts from what would be expected from a homogenously mixed aerosol. This

resulting number count difference is due to variation in supersaturation conditions within the condensing portion of the CPC, as discussed in Section 1.5.2.

Particles that are trapped in one portion of the flow can pass through regions in the condenser where the supersaturation is not sufficient to grow the particles resulting in the particles passing through the CPC undetected. This is only occurs, however, for particle diameters in which the CPC counting efficiency is less than unity. In the case of the TSI 3010 used, this occurs below 30 nm as shown in Figure 2-25. The inverse can also happen as well, where a large percentage of the particles pass through regions sufficient for growth and the CPC over counts relative to an aerosol that had a spatially homogenous concentration.

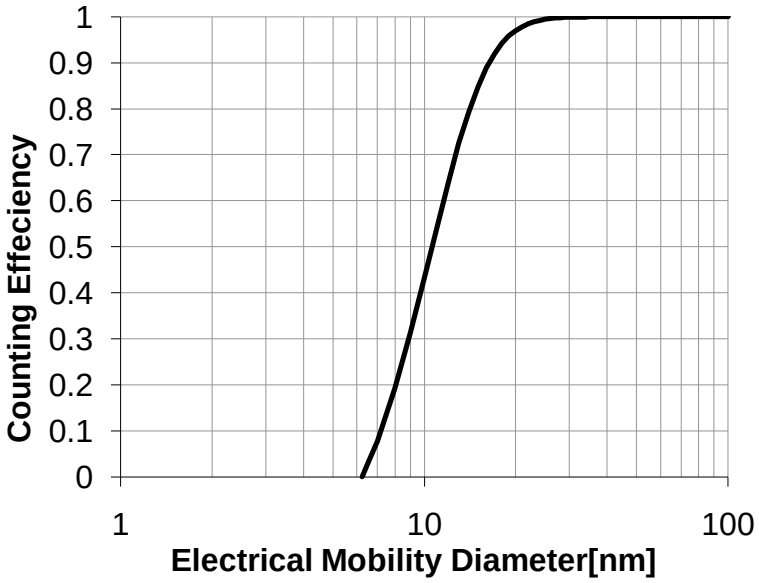

Figure 2-25
TSI 3010 Counting Efficiency as a function of particle diameter(Mertes 1995)

To mitigate this effect, the introduction of a mixing orifice insures that the incoming aerosol entering the CPC is spatially homogenous. This allows the CPC

reference measurements to be used correctly and the particle dilution ratio to be accurately measured. As shown in Figure 2-23, the effect of including a downstream mixing orifice on the apparent particle dilution ratio results in a substantial decrease in variability of result. The use of a 0.084 mm diameter mixing orifice leads to a substantial reduction in the particle dilution ratio for particles less than 12 nm. This indicates clearly the effect of a non-homogenous aerosol in a full flow CPC.

It is however, still clear that even with a 0.084 mm orifice there is still some variability in the data such that the 10 nm particle dilution is less than that of particle dilution at 100 nm. To further increase the spatial homogeneity of the aerosol a smaller orifice of 0.064 mm was selected and allowed for further reduction in the variability.

It should be noted that by decreasing the mixer diameter also resulted in a reduction of the 100 nm particle dilution ratio. This may be due to reduced variability with the introduction of mixing resulting in a more accurate determination of the particle dilution ratio . Furthermore, a reduction in total flow rate through the CPC and diluter could have altered the particle dilution ratio produced by the Orifice Diluter. Using the volumetric flow data for the Orifice Diluter, located in Appendix I, this flow rate reduction would be approximately 9%. The factors of decreased variability could still have some effect on the data and the actual reduction in flow rate could have been significantly less than this.

Using the experimentally determined volumetric dilution ratio curve for this orifice diameter, see Appendix I, and a resulting measured CPC sample flow rate of 906.1 cm^3/min the volumetric dilution ratio is determined to be 68.3. Using the data collected using the 0.41 mm diameter mixing orifice the resulting penetration for this

diluter can be found in Figure 2-26. The resulting penetration is greater than unity for all particle sizes tested, and is theoretically impossible, since this would indicate particle production. This error is due to the determination of the volumetric dilution ratio and is corrected for by normalizing that data for the 100 nm results. The resulting normalized data indicate only small amount of losses at the 9 nm test case with the resulting penetration of 0.979. This effectively indicates of a loss of only 2.1% at a dilution ratio of 68:1.

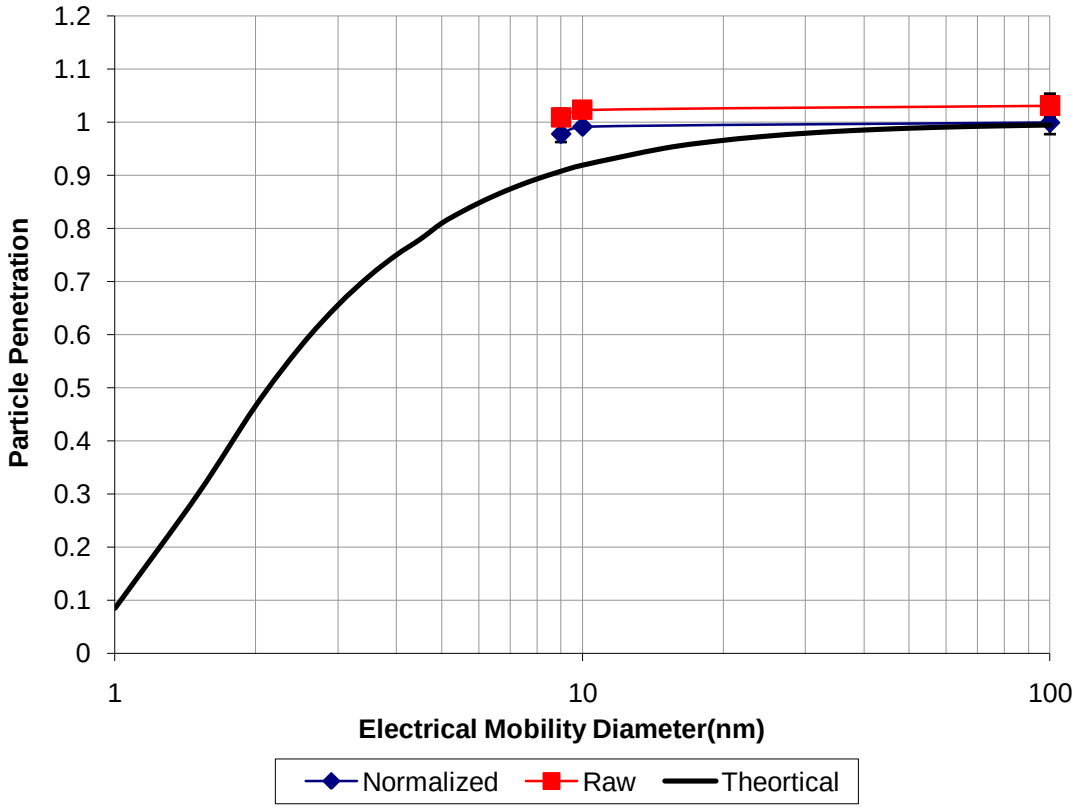

Figure 2-26
Diluter penetration for the Orifice Diluter with 0.41mm diameter orifice using a Boltzmann charge equilibrated aerosol with a 0.64mm mixing orifice

As shown in Figure 2-26, the theoretical losses using the determined flow through the orifice and the geometry of the orifice diluter are determined using

Equation 2-6. The determination of the internal tube length is done by the summation of the total path length that the minor bypass flow experiences and is determined to be 0.89 cm. This theoretical model predicts lower penetration at 9 nm than observed. This is most likely due to the fact that Equation 2-6 may not be most suited for this model since it assumes that the flow is fully developed. In the case of this device that most likely is not the case since the total minor flow transport length is 0.89 cm in length with a majority of that in the developing flow region. One additional issue is the changing diameters within the device since the threaded passage and the resulting inner diameter of the orifice assembly all fall within this 0.89 cm length, as shown in Figure 2-3

2.14 Summary

This work suggests that for bifurcated diluters, the transport of the minor flow and the resulting diffusion deposition is the key factor for aerosol loss within the diluter. As was shown by both the TSI 3302A diluter, and the laboratory "leaky filter" diluter, the losses within the dilution system are dominated by the diffusion losses within the capillary flow by diffusion deposition. In the case of these two diluters, losses below 10 nm can be significant with losses greater than 40%. To address this issue the orifice diluter was created with the transport length of the minor flow minimized. This type of dilution design yielded losses of 9 nm particles to less than 5% at a dilution ratio of 68.3:1.

In the case of the mixing style diluter tested, the MSP 1100, the resulting data indicated considerable losses within the diluter for particles smaller than 10 nm, at the lowest dilution ratio condition more than 25% of particles 10 nm particles are lost. As

with the bifurcated diluters the losses are attributed to the diffusion driven deposition of the aerosol within the diluter

Further work was performed to investigate the influence of dilution ratio on particle penetration. This investigation was focused on systems in which the dilution system provided the ability to vary the dilution ratio. The results for the TSI 3302A diluter, a bifurcated style diluter, showed the expected results of increased dilution resulting in increased losses. The resulting losses compared well with theoretical predictions. The MSP 1100 also showed the same trend of increased losses for increased dilution. This was unexpected, however, as the theoretical models predicted a decrease in losses within the diluter. This increase in aerosol loss with increasing dilution for MSP 1100 is attributed to internal flow kinetics within the device.

The final investigation was the influence of particle charge on the aerosol loss within the diluter. For the capillary style bifurcated diluters, TSI 3302A and the laboratory leaky filter diluter, the influence of charge resulted in a significant increase in particle loss within the diluter. The resulting calculations indicated a charge correction value of 3.10 and 2.61 for the TSI 3302A and Leaky Filter diluters respectively. This increase in losses was attributed to electrostatic forces and internally generated electric fields in the diluters. This resulted in enhanced deposition of the particles resulting in a reduce diluter penetration.

Chapter 3

Diluter Performance with Combustion Aerosols

The objective for this portion of the work is to use the previously determined particle penetration curves to correct concentration measurements when sampling a high concentration aerosol. The test aerosol selected was that of a combustion generated aerosol from a diesel engine. Using the previously tested CPC and diluter combinations, the concentration measurements of a conditioned diesel aerosol is compared among the CPC and diluter combinations. Furthermore, using the measured size distribution, correction to the concentration measurement is determined based on the measured particle dilution ratio.

3.1 Correction Methodology

To apply corrections to concentration data measured by a CPC four pieces of information are required: the size distribution of the aerosol entering the diluter, volumetric dilution ratio, particle size dependent diluter penetration and the CPC particle size dependent counting efficiency. This effective modification to the size distribution from incoming aerosol to the final total number count is summarized in Figure 3-1

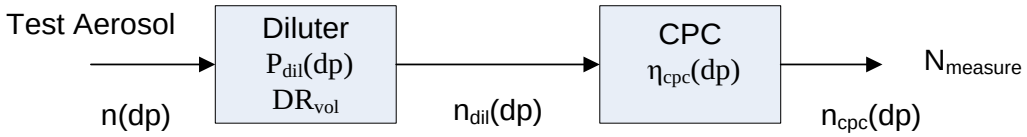

Figure 3-1
Block diagram representing the effects of the diluter and CPC on incoming aerosol

To determine the correction factor for the CPC and the resulting total measured number count, $N_{measure}$, all these pieces of information have to be combined such that the resulting concentration factor is a single number. To do so the following methodology is used.

To quantify the correction factor for losses within the diluter yields,

$$C_{DIL} = \frac{\int n(dp)ddp}{\int n(dp)\eta_{DIL}(dp)ddp} \qquad \textbf{Equation 3-1}$$

where $C_{DIL\ is}$ Diluter Penetration Correction Factor. This quantifies the percentage losses due to the diluter for a given particle size number distribution, *n(dp)*, and a diluter penetration curve give by η_{DIL}. The resulting value of C_{DIL} is a value greater than unity when losses are present.

Unfortunately using this correction factor alone could results in a correcting for losses within the diluter only and not the inherent measurement loss in the CPC due to the particle response curve. Since the goal of this correction methodology is to generate one correction term to be applied to the measured CPC count, the inclusion of the CPC response curve provides the additional information to apply a single number correction

$$C = \frac{\int n(dp)ddp}{\int n(dp)\eta_{DIL}(dp)\eta_{CPC}(dp)ddp} \qquad \textbf{Equation 3-2}$$

where C is the Count Correction Factor, η_{CPC} is the CPC counting efficiency curve and η_{DIL} is the diluter penetration. This value is comparing the ratio of the total number count of the incoming aerosol to the total number count as would be counted by a diluter and CPC combination. The resulting value of C will always be a number greater than or equal to unity as the resulting numerator should always be greater than denominator for typical diluter and CPC counting efficiency curves.

The end use of such corrections, are to correct total number concentration from a diluter and CPC combination. This then yields the resulting total number concentration value such that

$$N_{corrected} = N_{measured} DR_{vol} C \qquad \textbf{Equation 3-3}$$

where $N_{corrected}$ is the Fully Corrected Number Concentration which is the product of the experimental total CPC number concentration, $N_{measured}$, volumetric dilution ratio, DR_{vol}, and the Concentration Correction Factor, C.

It should be noted that the neutralized aerosol diluter penetration curves will be used for this correction. This is based on work by Jung et al.(2005) who found that the aerosol charge distribution is near a Boltzmann distribution at a gas temperature of 300-500K.

3.2 Apparatus

The aerosol generation system comprised of a John Deere 4045H 4.5L diesel engine coupled to a 200HP General Electric DC dynamometer for load control. A system schematic of this apparatus can found in Figure 3-2. A small portion of the exhaust was sampled using a 2 stage micro-dilution system similar to the one described elsewhere(Abdul-Khalek, 1999). Primary dilution was set to operate at a dilution ratio of approximately 13:1. It should be noted that the dilution ratio was not directly measured during the full duration of testing because measurement of engine out emissions was not within the scope of this project. The wall temperature of the diluter was maintained at 20°C to provide a consistent aerosol size distribution over the test conditions. To quench the condensation growth and coagulation of the particles a secondary dilution ratio of approximately 20:1 was selected. The diluted and quenched aerosol was then transferred via conductive tubing to a distribution manifold.

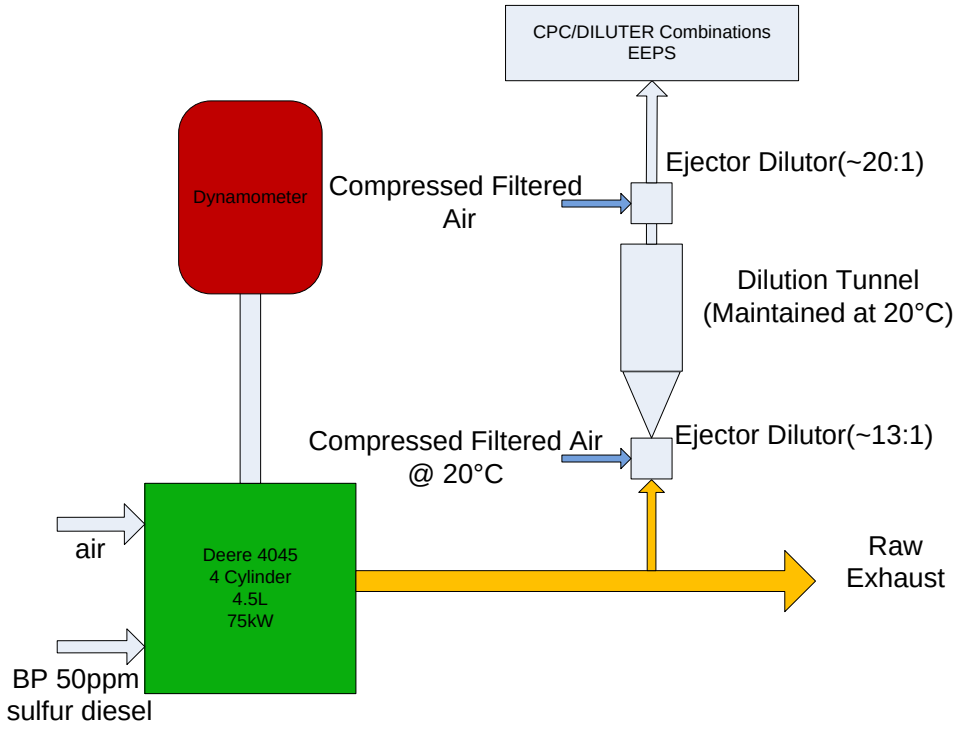

Figure 3-2
Diesel Aerosol Generation Schematic

3.2.1 Aerosol Measurement Apparatus

The aerosol measurement battery consisted of both particle size distribution measurements as well as number count measurements. To ensure proper flow splitting a 12" diameter, stainless steel, radial manifold was used with each instrument separated equidistance along the circumference of the manifold as shown by Figure 3-3.

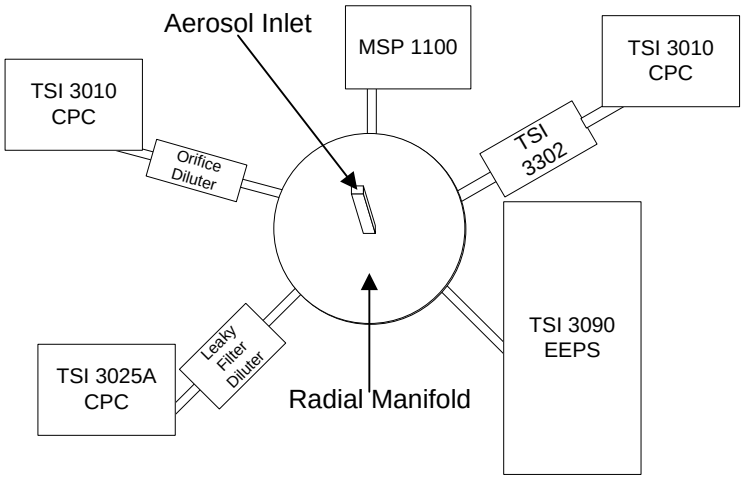

Figure 3-3
Aerosol Instrumentation and Flow Configuration

The particle size distribution was measured using the TSI 3090 Engine Exhaust Particle Sizer that was connected to the distribution manifold using conductive tubing. Since the objective of the experiment was to correct total CPC number count for diluter losses, a variety of CPC and diluter combinations were used. A summary of the diluter and CPC combinations can be found in Table 3-1.

Table 3-1
Diluter and CPC Combinations

Diluter	Type	CPC	CPC Nominal Flowrate(LPM)
TSI 3302	Bifurcated Capillary	TSI 3010	1
MSP 1100	Mixing	MSP	0.3
Laboratory Leaky Filter	Bifurcated Capillary	TSI 3025	1.5
Orifice Diluter	Bifurcated Orifice	TSI 3010	1

The diluters were connected to the distribution manifold via conductive tubing, and were located equidistance along the circumference of the radial distribution manifold. The CPC's were then connected to their respective diluter, as shown in Table 3-1 via conductive tubing. Care was taken to ensure that the length of aerosol tubing was inversely related to total sample flow of the CPC to reduce the influence of diffusion losses in the transport tubing. Thus the resulting connections to each of the CPC and diluter combinations resulted in equal residence time.

CPC counting efficiency curves are required for the method of correction, as described in Section 3.1. The curve for the TSI 3010 CPC comes from Mertes et al.(1995) and for the TSI 3025A the curves is taken from Wiedensohlet et al(1997). The MSP CPC counting efficiency curve was determined experimentally for this body of work and can be found in Appendix II.

3.3 Methods

3.3.1 Engine Test Conditions

Three engine test conditions were tested at a fixed 1400RPM. The three conditions were 0 N-m, 150 N-m and 300 N-m. These test conditions were selected based on the expected aerosol distribution at each load condition. It was expected to see the nucleation mode dominate in the 0 N-m load case, as well as the accumulation mode dominate at 300 N-m (Kittelson, 1998). The selection of 150 N-m was selected to provide a mixture of both the nucleation and accumulation mode.

Test conditions were deemed stable when the exhaust gas temperature stabilized within less than 0.1°C over a one minute span which based on previous measurements

was a good indicator of a stable particle number count. Once deemed at a stable test condition the aerosol sampling devices began logging.

3.3.2 Data Acquisition

Data were collected and logged for each TSI brand CPC using a serial port connection and the included software on a dedicated personal computer(PC). The MSP 1100 has an internal data collection system and all data were stored on the internal storage device included. To ensure accuracy when compiling data, both the internal clock of the personal computer and MSP 1100 were synchronized to ensure accurate data collection.

Data collection for the TSI 3090 was performed using a dedicated personal computer connected via the Universal Serial Bus (USB) to the device. Data were stored onto the internal data storage of PC, and to ensure accurate data collection the internal clock was synchronized with the MSP 1000 and the PC logging CPC data.

3.3.3 CPC and Diluter Reference Calibration

To ensure accurate results the concentration measurements made by the CPC's where all referenced to the TSI 3025A. A Dioctyl Sebacate (DOS) aerosol was generated using a mixture of Isopropyl Alcohol and DOS in a collision atomizer. A TSI 3081 long column DMA then electrically classified the aerosol at 100 nm. This aerosol passed through a Polonium-210 source before entering axially into the radial distribution manifold. Each CPC line length was determined based on the inverse of flow rate and the length of line used for the TSI 3025 to ensure equal particle loss within the connection.

All CPC concentration data were logged simultaneously for a three minute period where the average concentration over the three minute period was the value used for the calculation. The reference concentration calibration factor($F_{a/3025}$) was determined as follows,

$$F_{a/3025} = \frac{N_{a,ref}}{N_{3025,ref}} \qquad \textbf{Equation 3-4}$$

where $N_{a,ref}$ is the three minute average concentration of a CPC and $N_{3025,ref}$ the three minute average concentration for TSI 3025.

The same apparatus was used to determine dilution ratio of the various CPC and diluter combinations tested using the 100 nm electrically classified DOS aerosol. Using the TSI 3025 CPC as the reference CPC, the dilution ratio of the TSI 3302, Laboratory Leaky Filter and Orifice Diluter was determined using the total measured count over a one minute period. For the test in which the TSI 3025A and Leaky Filter diluter combination was to tested to determine its correction factor the MSP CPC was used. \

It should be noted that based on previous measurements for the TSI 3302, Laboratory Leaky Filter and Orifice Diluter the 100 nm particle dilution ratio is near that of the volumetric dilution. Using this information, a simplification was made such that the 100 nm particle dilution ratio is equal to the volumetric dilution ratio. For the MSP 1100, the volumetric dilution ratio was taken directly from the instrument as it a measured value for this instrument. The results from the calibration can be found in Table 3-2.

Table 3-2
CPC Concentration Calibration and Volumetric Dilution Ratio

CPC	$F_{a/3025}$	Diluter	DR_{vol}
TSI 3010	0.948	TSI 3302	69.4
TSI 3010	0.824	Orifice Diluter	67.3
MSP	0.958	MSP 1100	81.2
TSI 3025	1	Laboratory Leaky Filter	15.6

3.4 Results

3.4.1 350N-m Load

For the 1400RPM, 300N-m test condition, the resulting concentration measurements corrected for the volumetric dilution ratio plotted over time can be found in Figure 3-4. The resulting concentration measurements indicate a stable engine condition by the low coefficient of variation, at 5.2% for the 3025a and "Leaky Filter" combination. The size distribution given EEPS can be found in Figure 3-5. The resulting distribution indicates a strong accumulation mode with a peak diameter at 60.4 nm. The resulting error bars also verify a stable test condition.

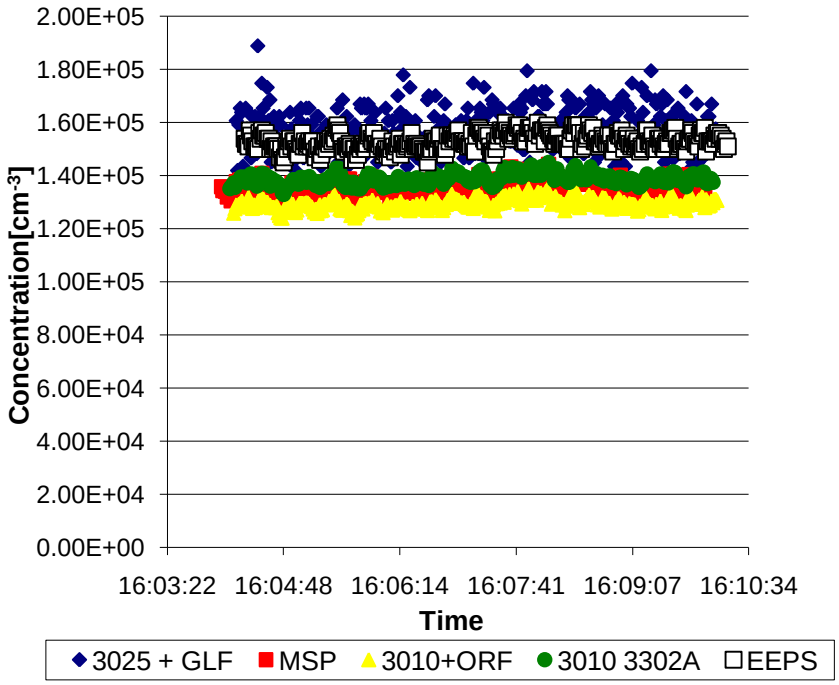

Figure 3-4

350N-m Load: Volumetric Dilution Ratio Corrected Concentration Measurement

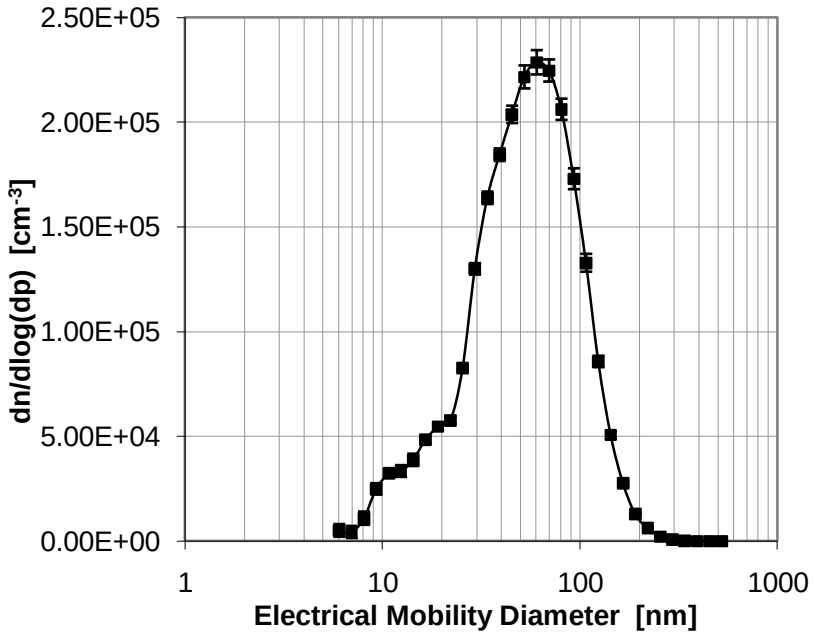

Figure 3-5
350N-m Load: EEPS Particle Size Distribution

Discrepancies between the various CPC and diluter combinations are evident in Figure 3-4. To quantify the difference, the average concentration over the sample period of 16:04:30 to 16:10:30 is determined for each combination. The values are then referenced to the 3025A/"Leaky Filter" diluter combination to provide a relative measurement of agreement between CPC's as shown in Table 3-4.

Table 3-3
350N-m Load Case Concentration Correction Factors

Diluter/CPC	C_{DIL}	C
Orifice/3010	1.000	1.032
3302A/3010	1.096	1.118
MSP/MSP	1.116	1.123
Leaky Filter/3025A	1.035	1.035

As shown by the Dilution Ratio corrected row in Table 3-4, the resulting average concentration ratio for all the CPC's is less than unity, with a range of 82% to 88% of the concentration counted by the 3025A and "Leaky Filter" combination.

To attempt to reduce variation between the CPC and diluter combinations, the 3025A reference correction, as found in Table 3-3 will be applied. The resulting agreement between CPC's is further improved for all CPC and diluter combinations as shown in Table 3-4. The most evident improvement is by the TSI 3010 and Orifice Diluter combination with no difference in counting efficiency against the reference CPC and diluter combination. This is to be expected due to the fact that orifice diluter has almost no loss in the range detectable by the 3010 CPC and therefore gives the most

accurate concentration measurement. A notable improvement in relative concentration is had by both the MSP combination, and the 3010/3302 combination, with roughly a 4% improvement in agreement.

The remaining discrepancy among diluters is attributed to the resulting losses within the aerosol diluter. To correct this, the resulting $\boldsymbol{C_{DIL}}$ correction is calculated for each CPC and diluter combination. The resulting correction values can be found in Table 3-3.

Table 3-4
350N-m Average Relative Concentration

	(CPC+DIL)/(3025+LF)			
Applied Corrections	**3010+ORF**	**3010+3302**	**MSP**	**EEPS**
$\mathbf{DR_{vol}}$	0.823	0.882	0.864	-
$\mathbf{DR_{vol}}$, $\mathbf{F_{a/3025}}$	0.999	0.931	0.902	-
$\mathbf{DR_{vol}}$,$\mathbf{F_{a/3025}}$,$\mathbf{C_{DIL}}$	0.965	0.986	0.973	-
$\mathbf{DR_{vol}}$, $\mathbf{F_{a/3025,}}$**C**	0.996	1.01	0.979	0.939

The dominate correction factor for the MSP,3302 and Leaky Filter diluter is the correction for particle losses within the diluter as given by the C_{DIL} correction factor. However, the effect of the CPC counting efficiency curve is still evident, albeit small, for the MSP and 3010/3302 and 3010/Orifice. The resulting difference in the $\boldsymbol{C_{DIL}}$ and $\boldsymbol{C}$ correction factor is due to the effect on the CPC counting efficiency curve. To fully correct the data set the Concentration Correction Factor, $\boldsymbol{C}$, is applied to the concentration data.

The resulting relative concentration with both the C_{DIL} and C , are shown in Table 3-4, indicate improved inter agreement among the CPC and diluter combinations with all three combinations within less than 2.1% of the reference 3025/Leaky Filter combination

using the fully corrected data. This also validates the Concentration Correction Factor used, as agreement is greatly improved over just dilution ratio corrections, and still improved from using the diluter loss correction.

The fully corrected concentration for each CPC/diluter combination over the test duration can be found in Figure 3-6.

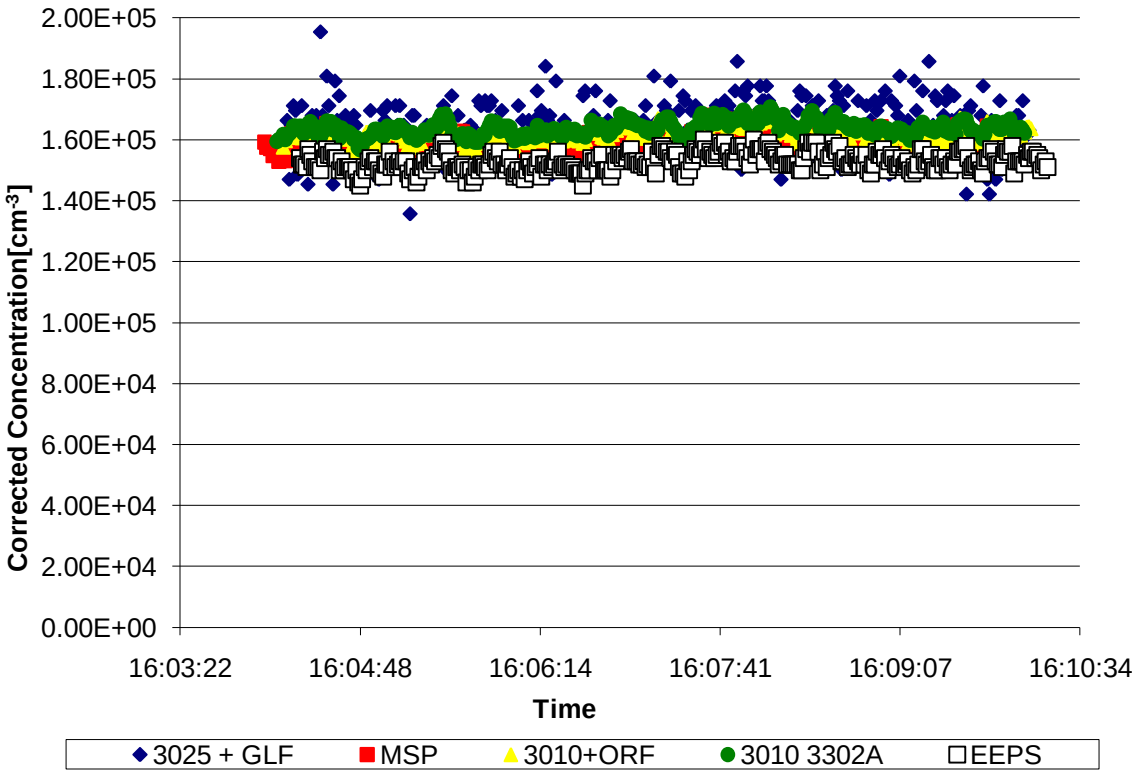

Figure 3-6
350N-m Load: Fully Corrected Concentration Measurements

3.4.2 100N-m Load

For the 100N-m load case, the same method as described above is used to analyze the concentration measurements made by the diluter and CPC combinations. The resulting dilution corrected concentration as a function of time can be found in Figure 3-7. The resulting corrected concentration indicates a large discrepancy for all CPC and diluter combinations when compared to the 3025A and "Leaky Filter" combination. This is also evident by the relative counting efficiency for the average concentration over the sample period, as shown in Table 3-6. There is fairly reasonable agreement between the Orifice, 3302 and MSP diluter with the range from 80.5% to 82.6% relative counting efficiency.

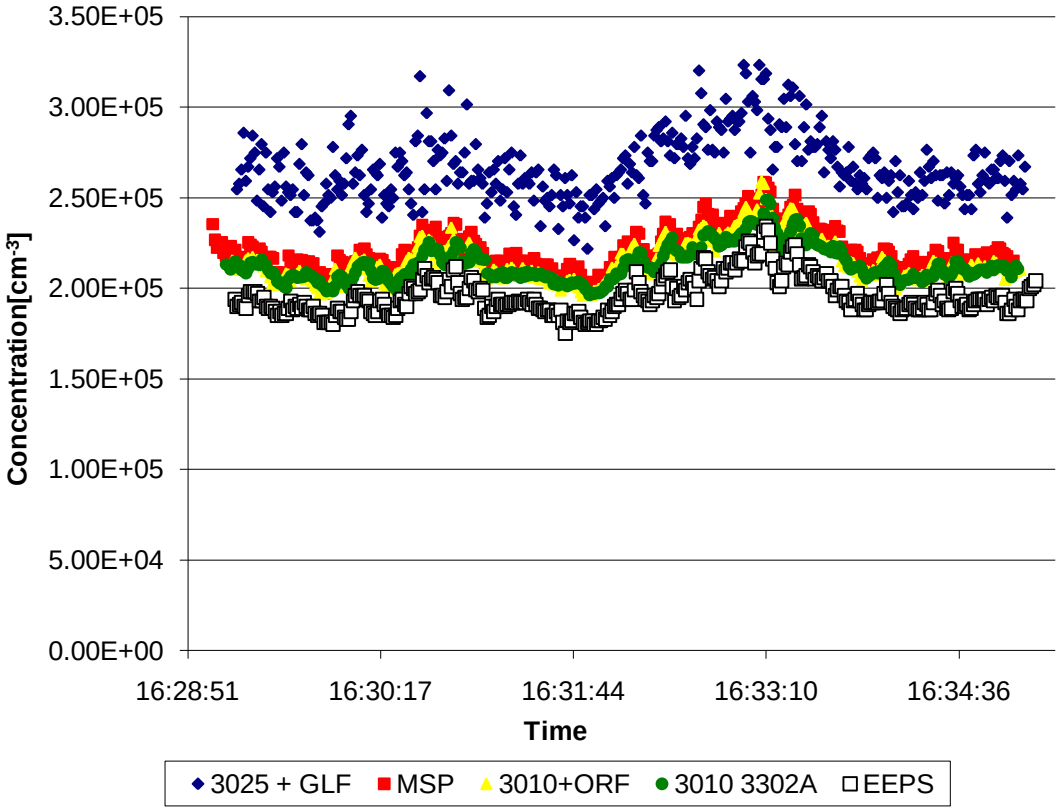

Figure 3-7
100N-m Load: Volumetric Dilution Corrected Concentration

Applying the 3025A reference correction, as determined previously, relative counting efficiency for the 3010/Orifice combination is greatly improved to 97.8% of the 3025A/Leaky Filter combination. The relative counting efficiency of both the 3010/3302 combination and MSP combination also improved to 84.3% and 86.2% respectively.

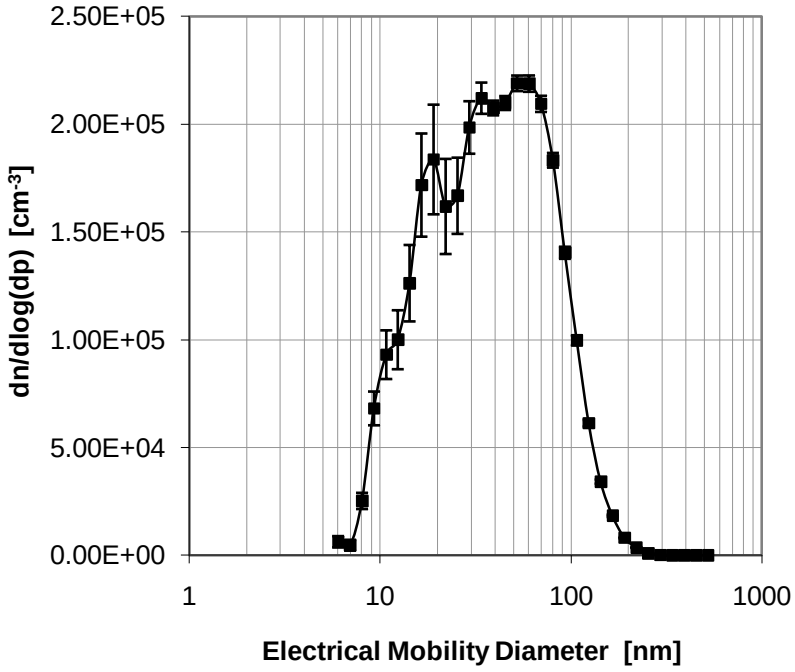

Figure 3-8
100 N-m Load: EEPS Particle Size Distribution

To attempt to further reduce variability between CPC and diluter combinations, correction for particle loss within the diluter will be applied using the size distribution as measured by the EEPS, found in Figure 3-8. The magnitude of the corrections can be found in Table 3-5 and are derived as described previously.

Table 3-5
100N-m Load Case Concentration Correction Factors

Diluter/CPC	C_{DIL}	C
Orifice/3010	1.000	1.069
3302A/3010	1.148	1.203
MSP/MSP	1.155	1.172
Leaky Filter/3025A	1.052	1.052

Again the diluter penetration for the Orifice Diluter is assumed unity and therefore results in no corrections being applied. The 3302A and MSP diluters also have the largest correction with the resulting final correction of 1.148 and 1.155 respectively.

To fully correct the data using the CPC counting efficiency curve the Count Correction Factor is determined for each diluter and CPC combination. These results are found in Table 3-5, and as previously noted; the difference between the $\boldsymbol{C}$ and $\boldsymbol{C_{dil}}$ is due to the counting efficiency of the associated CPC. The Leaky Filter has no effective CPC correction required due to the fact that 3025A has no reduction in counting efficiency over the size range given by the EEPS hence why the $\boldsymbol{C}$ and $\boldsymbol{C_{dil}}$ are equal.

Table 3-6
100N-m Load Case Average Relative Concentration

	(CPC+DIL)/(3025+LF)			
Applied Corrections	**3010+ORF**	**3010+3302**	**MSP**	**EEPS**
$\boldsymbol{DR_{vol}}$	0.805	0.799	0.826	-
$\boldsymbol{DR_{vo}I,F_{a/3025}}$	0.978	0.843	0.862	-
$\boldsymbol{DR_{vol},F_{a/3025},C_{DIL}}$	0.929	0.919	0.947	-
$\boldsymbol{DR_{vol},F_{a/3025},C}$	0.993	0.964	0.961	0.698

The resulting relative counting efficiency after applying the final Concentration Correction Factor gives good inter agreement between the MSP, 3302A and Orifice diluter combinations at 96.1%, 96.4% and 99.3% relative counting efficiency respectively. A graph of the corrected concentration measurements can found in Figure 3-9.

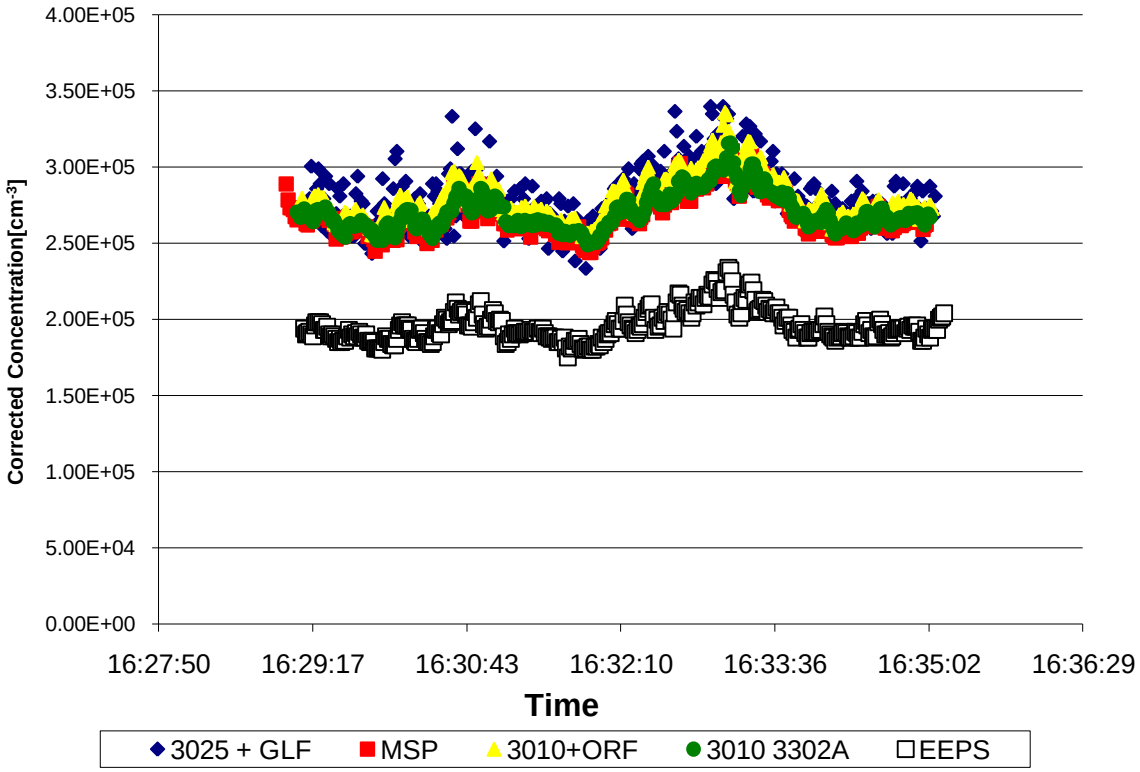

Figure 3-9
100N-m Load: Fully Corrected Concentration Measurements

3.4.3 0-m Load

The final test condition was the 0N-m load case. The objective of this load case was to generate a test aerosol with a large nucleation mode and was accomplished as shown by the size distribution as generated by the EEPS, found in Figure 3-11.

Figure 3-10 is the time resolved plot of concentration measurements by the CPC and diluter combinations corrected for the dilution ratio. As can be seen the test condition yielded fairly stable test condition with a coefficient of variance for the 3025/LF at 3.7% and 2.0% for the MSP system.

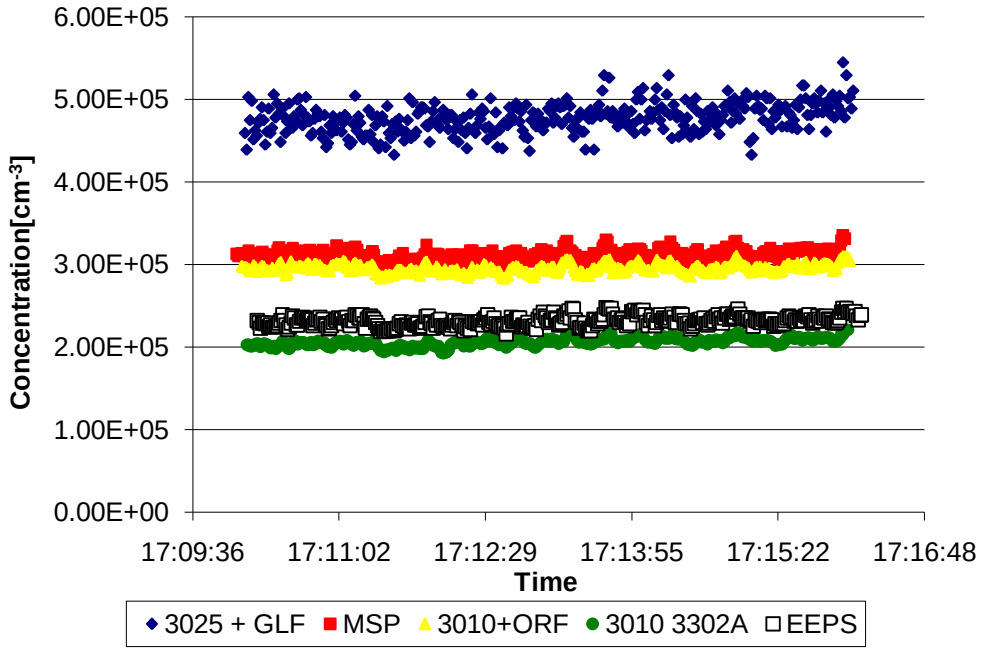

Figure 3-10
0N-m Load Case: Volumetric Dilution Corrected Concentration

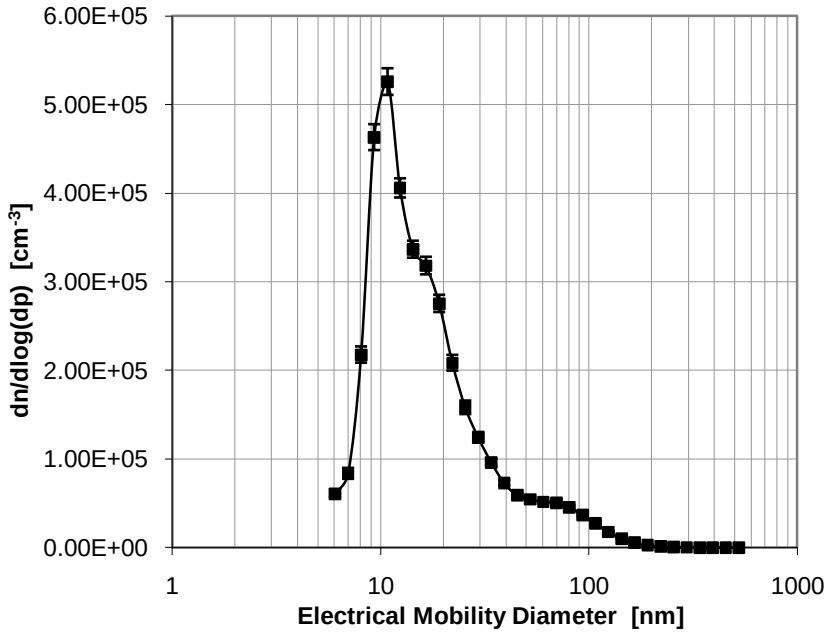

Figure 3-11
0N-m Load Case: EESP Particle Size Distribution

Using the same method as described above, the discrepancy between CPC and diluter combinations will attempted to be reduced by using correction factors. The relative counting efficiency of each diluter is referenced to the 3025 and Leak Filter diluter. Using the size distribution collected by the EEPS and the methodology described above the correction factors for each diluter can be determined as shown in Table 3-7

The resulting correction factors are larger than the previous conditions and this is due the fact that peak diameter of the aerosol was 10.4 nm. As can be seen in the penetration tests, the losses at this level for the MSP,3302 and LF diluter are substantial at this size and therefore a large correction results. It should also be noted that the resulting CPC counting efficiency curves will also have a large impact for the 3302A and Orifice diluters Concentration Correction Factor due to the fact that 3010 CPC has a cut point(50% counting efficiency) of roughly 10 nm(Mertes et al.). The resulting correction, ***C***, has to take into account the fact that the CPC would not have counted all the particles that should have passed through the diluter. That is that if the diluter had 100% efficiency at 10 nm, that is it lost no particles, the CPC still would have only counted 50% of those particles. This is why the resulting final correction is enhanced from the just the diluter correction.

Table 3-7
0N-m Load Case Concentration Correction Factors

Diluter	C_{DIL}	C
Orifice/3010	1.000	1.426
3302A/3010	1.402	1.841
MSP/MSP	1.327	1.424
Leaky Filter/3025A	1.131	1.131

To summarize the effects of applying the correction and quantify the result the reference combination of the 3025A and LF are again used. This summary of relative counting efficiency as a function of the correction used can be found in Table 3-8.

Table 3-8
0N-m Load Case Average Relative Concentration

	(CPC+DIL)/(3025+GLF)			
Applied Corrections	**3010+ORF**	**3010+3302**	**MSP**	**EEPS**
DR_{vol}	0.619	0.432	0.652	-
DR_{vol} ,$F_{a/3025}$	0.751	0.456	0.680	-
DR_{vol} ,$F_{a/3025}$,C_{DIL}	0.664	0.565	0.798	-
DR_{vol} ,$F_{a/3025}$,C	0.947	0.742	0.856	0.429

Most notably is the fact that even with all the correction applied agreement among the CPC and diluter combinations is relatively good with the lowest relative counting efficiency of 74.2% for the 3302A diluter and 3010 CPC combination. This is in comparison to the 94.7% for the orifice diluter, in which the same model 3010 CPC is used. The MSP diluter and CPC combination had a final agreement of 85.6% relative counting efficiency.

A plot of the fully corrected concentration over the sample period is shown in Figure 3-12. Here graphically the differences in counting efficiency are evident, but it should be noted that the diluter and CPC combinations do track well to changes in the measured concentration.

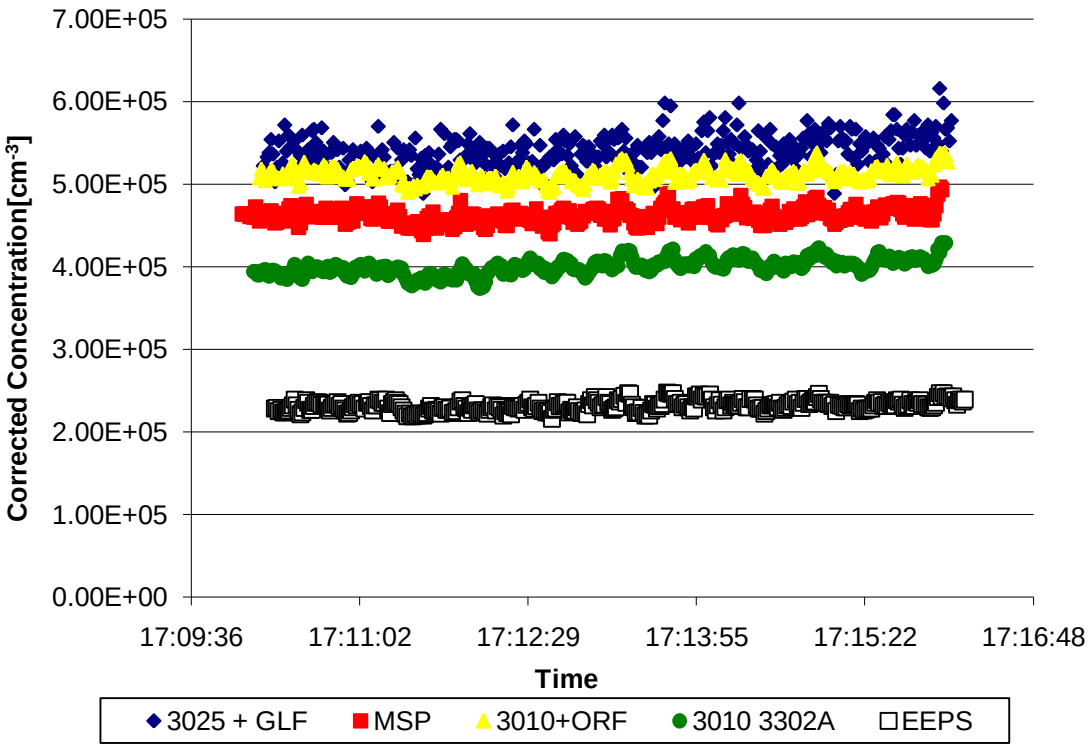

Figure 3-12
0N-m Load Case: Fully Corrected Concentration Measurements

3.5 Discussion

While it clear that for the load conditions of 350 N-m, the use of correction factors to remove the effect of particle loss in diluters, and CPC counting efficiency curves was effective with all CPC and diluter combinations. This is indicated by the fact that the agreement among all CPC and diluter combinations are within 2.1%.

The 100 N-m load case also resulted in good inter agreement among the MSP,3302 and Orifice diluter combinations with the range of values of 96.1% to 99.3% of the reference combination of the Leak Filter and 3025A CPC.

This trend, however, does not continue to the 0 N-m load case, as previously described with a significant difference among CPC's with a range of 74.2% to 94.7%

agreement. This not completely unexpected as the size distribution for the 0 N-m load case has a peak diameter of 10.8 nm and the resulting correction factors for the diluter and final Concentration Correction Factor are large due to the diluter loss and reduction in CPC counting efficiency.

One key assumption of this method is that the size distribution information and the literature values for the CPC counting efficiencies are accurate. Errors in these will result in errors in the calculation of the correction factors. One method to estimate the accuracy of the correction factors is to compare the total number count, determined by the size distribution, to the total number count by a CPC and diluter combination. The logic being, that if the size distribution and CPC counting efficiencies are accurate, then the ratio of the concentrations should be unity.

To test this method, the total number count is determined at the sample frequency of the EEPS, which for this test case was 1 s, for each load case. Figure 3-6, and Figure 3-12, show the resulting concentration determined from the size distribution as a function of time for the test loads of 350 N-m, 100 N-m and 0 N-m respectively. The summarize the results, the average concentration over the sample period is determined and compared to the resulting average concentration as measured by the 3025A and Leaky Filter diluter combination. The results of these values for each for the Concentration Correction Factor and load cases can be found in Table 3-4,Table 3-6, and Table 3-8.

Table 3 9 shows the relationship between engine load, the geometric mean diameter (GMD) measured with the EEPS for the sample averaged size distributions, and the ratios total EEPS number to the corrected CPC plus diluter measurements for the 3025 + LF and the 3010 + Orifice. It is clear that as the load on the engine is reduced and

the distribution shifted to smaller particles size, the ratio of the EEPS concentration to the corrected CPC concentrations decreases. This suggests errors in the EEPS distribution, the CPC counting efficiencies or a combination of the two for the smallest size particles. The agreement between the corrected 3025+ Leaky Filter and the 3010 + Orifice results suggests that the CPC counting efficiencies are unlikely to be the problem and that the discrepancy arises from errors in the EEPS calibration at the lower end of its sizing range. The magnitude of this error is quite large with the size distribution determined number concentration, off by more than a factor of two, when compared to the 3025A and leaky filter combination for the 0 N-m load case.

Table 3-9
Inter Agreement Comparison of EEPS to Fully Corrected CPC and Diluter Combinations

Engine Load (N-m)	GMD of EEPS Size Distribution (nm)	EEPS/3025+LF	EEPS/3010+ORF
350	50.0	0.939	0.942
100	36.5	0.698	0.702
0	16.3	0.429	0.453

One possible explanation for the undercounting by the EEPS could be the existence of a third peak size distribution below the lower sizing limit of the EEPS. The lower detection limit of the EEPS is 5.6 nm (TSI,2010) while the lower limit for the TSI 3025 CPC is 2.5 nm (Wiedensohlet,1997) However, the author knows of no reports of a split in the nucleation mode of a Diesel exhaust aerosol. Furthermore the agreement between the 3025 results and those of the 3010, which has a detection limit of about 10 nm, indicates that there is not a significant fraction of the aerosol below 10 nm. Thus it appears that, at least for EEPS used in this study, the manufacturers calibration for the

lower size channels, those less than about 20 nm, underestimate the actual concentration. For the zero load case the EEPS number concentration is more than a factor of two too low. Here the indicated fraction of particles below 20 nm was 78%. On the other hand at the 350 N-m load, when the indicated fraction of particles below 20 nm was 11%, the EEPS number concentration was only low by approximately 6% when compared to the CPC diluter combinations. This suggests that the EEPS size channels greater than about 20 nm provide accurate determination of size and number concentration.

The apparent errors in the EEPS response in the lowest size range raise other issues. The diluter and CPC response correction factors are based on the measured size distributions and if the size distributions are wrong the corrections will be wrong. This does not appear to be a significant problem for the 350 and 100 N-m cases shown in Figures 3.6 and 3.9 because the number concentrations fully corrected CPC and diluter combinations fall essentially on top of each other but there are clearly problems with the zero load results shown in Figure 3-12.

3.6 Conclusion

The observed disagreement among the CPC and diluter combinations could be due to a variety of errors including errors in the penetration measurements, CPC counting efficiency curves and the measured aerosol size distributions. However, based on analysis of the data collected from the 350 N-m, 10 0N-m and 0 N-m load cases, the accuracy of the correction is most dependent on the size distribution and its accuracy. Overall the use of diluter penetration curves to correct for losses and determine the total CPC number

concentration can be done, provided an accurate size distribution in the size range where diluter and CPC losses are important.

Furthermore, this method does provide a consistent way to check the accuracy of the size distribution. The convergence of the total number count determined by the size distribution and the corrected total number count as measured by the CPC and diluters will indicate an accurate measurement from all instruments.

Chapter 4 Summary

Size dependent particle loss in aerosol diluters has been found to have a significant effect on diluter performance when used with ultrafine aerosols. Diluters tested include the TSI 3302, MSP 1100 and the "Leaky Filter" diluter which were found to have significant particle loss. Losses were found to be mainly due to diffusion and increased with decreasing size. Penetration of 9 nm particles was found to be in the range of only 40% to 60% for these diluters. These losses can have a significant effect on the actual dilution of the aerosol, and can skew measurements when only volumetric dilution is used.

Other factors that can have a significant effect on particle losses include the total dilution ratio in the device, as well as the charge state of the aerosol. This effect was most notable in the TSI 3302 with the penetration reduced by more than a factor of 2 when adjusted from minimum dilution ratio to maximum, although all adjustable diluters has shown the effect to some degree. The effect of aerosol charge was also found to have a significant impact on diluter performance with the effect found to increase particle loss in capillary tube based bifurcated diluters by as much as 40%.

A new diluter was developed, the Orifice Diluter, which minimized aerosol loss by minimizing transport time of the diluting aerosol. Loss of 9 nm diameter particles was determined to be less than 3% for this diluter when tested with a neutralized aerosol.

A high concentration diesel aerosol was sampled using the diluter and CPC combinations described above. Using a measured size distribution, diluter penetration and CPC counting efficiency curves, concentration correction factor for the CPC and dilute

combinations were determined. The resulting inter-agreement between CPC and diluter combinations was found to be less than 3% when an accurate size distribution was available.

This method, however, has a significant dependence on the measured particle size distribution. As a verification of accuracy, the values of the total number concentration, as determined by the particle size distribution, and those calculated using fully corrected concentration for diluter and CPC combinations were compared. The worst case was for an engine exhaust aerosol with approximately 80% of the particles below 20 nm. In this case, the number concentration determined with the different CPC and diluter combinations differed by as much as a 33% difference, and integrated number concentration determined from the EEPS size distribution was more than a factor of 2 lower than the highest CPC and diluter combination.

The use of the characterization methods described above can provide the information necessary to determine the true aerosol concentration when using a diluter with particle losses present provided the shape of the aerosol size distribution is known. This provides a tool to researchers in determining the true aerosol concentration when it is out of the typical measurement range of particle counters, thereby increasing the accuracy and repeatability of their measurements.

References

Abdul-Khalek, I.S., Kittelson, D.B., Brear, F. (1999). The Influence of Dilution Conditions on Diesel Exhaust Particle Size Distribution Measurements. *Society of Automotive Engineers*. 1999-01-1142.

Alonso, M., Alguacil, F., Santos, J., Jidenko, N., & Borra, J. (2007). Deposition of ultrafine aerosol particles on wire screens by simultaneous diffusion and image force. *Journal of Aerosol Science,*

Brockmann, J. E., Liu, B. Y. H., & McMurry, P. H. (1984). A sample extraction diluter for ultrafine aerosol sampling. *Aerosol Science and Technology, 3*(4), 441-451.

Chen, S.C.; Tsai, C.J.; Wu, C.H.; Pui, D.Y.H.; Onischuk, A.A.; Karasev, V.V.(2007). Particle loss in a critical orifice. *Journal of Aerosol Science, 38*(9),935-949.

Chen, D. R., Pui, D. Y. H., & Kaufman, S. L. (1995). Electrospraying of conducting liquids for monodisperse aerosol generation in the 4 nm to 1.8 μm diameter range. *Journal of Aerosol Science, 26*(6), 963-977.

Fuchs, N. A., & Sutugin, A. G. (1965). Coagulation rate of highly dispersed aerosols. *Journal of Colloid Science, 20*, 492-500.

Gamero-Castano, M., & de la Mora, J. F. (2000). A condensation nucleus counter (CNC) sensitive to singly charged sub-nanometer particles. *Journal of Aerosol Science, 31*(7), 757-772.

Hinds, W. (1999). *Aerosol Technology: Properties, behavior, and measurement of airborne particles* 2nd ed. New York, NY: Wiley-Interscience

Jung, H., & Kittelson, D. B. (2005). Measurement of electrical charge on diesel particles. *Aerosol Science and Technology, 39*(12), 1129-1135.

Kasper, G. (1981). Electrostatic dispersion of homopolar charged aerosols. *Journal of Colloid and Interface Science, 81*, 32–40.

Kiljanski, T. (1993). Discharge coefficient for free jets from orifices at low reynolds number. *Journal of Fluids Engineering, 115*(4), 778-781.

Kittelson, D. B. (1998). Engines and nanoparticles a review. *Journal of Aerosol Science, 29*(5-6), 575-588.

Kittelson, D. B., Watts, W. F., & Johnson, J. (2002). Diesel aerosol sampling methodology-CRC E-43: Final report. *University of Minnesota, Report for the Coordinating Research Council, 19*

Kittelson, D., Watts, W., Johnson, J., Remerowki, M., Ische, E., Oberdörster, G., et al. (2004). On-road exposure to highway aerosols. 1. aerosol and gas measurements. *Inhalation Toxicology, 16*(s1), 31-39.

Knibbs, L. D., de Dear, R. J., Morawska, L., & Coote, P. M. (2007). A simple and inexpensive dilution system for the TSI 3007 condensation particle counter. *Atmospheric Environment, 41*(21), 4553-4557.

Knutson, E. O., & Whitby, K. T. (1975). Aerosol classification by electric mobility: Apparatus, theory, and applications. *J.Aerosol Sci, 6*(6), 443–451.

Liu, B. Y. H., & Pui, D. Y. H. (1974). A submicron aerosol standard and the primary, absolute calibration of the condensation nuclei counter. *Journal of Colloid and Interface Science, 47*(1), 155-171.

Liu, B., Pui, D., Rubow, K., & Szymanski, W. (1985). Electrostatic effects in aerosol sampling and filtration. *Annals of Occupational Hygiene, 29*(2), 251.

McMurry, P. H. (2000). The history of condensation nucleus counters. *Aerosol Science and Technology, 33*(4), 297-322.

Mertes, S., Schröder, F., & Wiedensohler, A. (1995). The particle detection efficiency curve of the TSI-3010 CPC as a function of the temperature difference between saturator and condenser. *Aerosol Science and Technology, 23*(2), 257-261.

Oberdörster, G. (2000). Pulmonary effects of inhaled ultrafine particles. *International Archives of Occupational and Environmental Health, 74*(1), 1-8.

Penttinen, P., Timonen, K., Tiittanen, P., Mirme, A., Ruuskanen, J., & Pekkanen, J. (2001). Number concentration and size of particles in urban air: Effects on spirometric lung function in adult asthmatic subjects. *Environmental Health Perspectives, 109*(4), 319.

Stoeger, T., Reinhard, C., Takenaka, S., Schroeppel, A., Karg, E., Ritter, B., et al. (2006). Instillation of six different ultrafine carbon particles indicates a surface area threshold dose for acute lung inflammation in mice. *Environmental Health Perspectives, 114*(3), 328.

Stolzenburg, M. R. (1988). An ultrafine aerosol size distribution measuring system. (Ph.D Thesis, University of Minnesota).

Stolzenburg, M. R., & McMurry, P. H. (1991). An ultrafine aerosol condensation nucleus counter. *Aerosol Science and Technology, 14*(1), 48-65.

TSI. August 2002. Model 3010 condensation particle counter instruction manual.

TSI. *Model 3302a diluter instruction manual.* Retrieved Jan 04, 2010, from http://www.tsi.com/uploadedFiles/Product_Information/Literature/Manuals/1933786b-3302A.pdf

TSI. (2008). *Model 3480 electrospray aerosol generator user manual.* Retrieved Jan 04, 2010, from http://www.tsi.com/uploadedFiles/Product_Information/Literature/Manuals/1933793e-3480.pdf

Weber, R., Marti, J., McMurry, P., Eisele, F., Tanner, D., & Jefferson, A. (1997). Measurements of new particle formation and ultrafine particle growth rates at a clean continental site. *J.Geophys.Res, 102*(D4), 4375-4385.

Westerdahl, D., Fruin, S., Sax, T., Fine, P. M., & Sioutas, C. (2005). Mobile platform measurements of ultrafine particles and associated pollutant concentrations on freeways and residential streets in los angeles. *Atmospheric Environment, 39*(20), 3597-3610.

Wiedensohlet, A., Orsini, D., Covert, D., Coffmann, D., Cantrell, W., Havlicek, M., et al. (1997). Intercomparison study of the size-dependent counting efficiency of 26 condensation particle counters. *Aerosol Science and Technology, 27*(2), 224-242.

Yu, C., & Chandra, K. (1978). Deposition of charged particles from laminar flows in rectangular and cylindrical channels by image force. *J.Aerosol Sci, 9*, 175-180.

Appendix I. Volumetric Dilution Ratio Measurements

TSI 3302

Measurements of the flow rate were performed according to the manufacturer's suggested method(TSI, 2003). The flow through the capillary tube was measure by placing a vacuum source on the exit of the TSI 3302 diluter and connecting a Gillian Gilibrator 2(Gillian Corp) directly to the capillary tube via 1/16" ID Tygon R-22 tubing. The vacuum supplied the pressure drop necessary to draw the flow through the capillary tube, the pressure drop was then varied via the included valve on the filtered air loop, and the flow through the capillary was measured. The pressure drop and flow rates were recorded at 6 different conditions and the test was repeated three times. The average values of the flow rate as function of pressure drop can be found in Figure A1-1. A linear regression model was used to fit a trend line to the data for the purposes of interpolation of the data. The trend line can be found in Figure A1-1 and has coefficient of determination(R^2) of 0.9995.

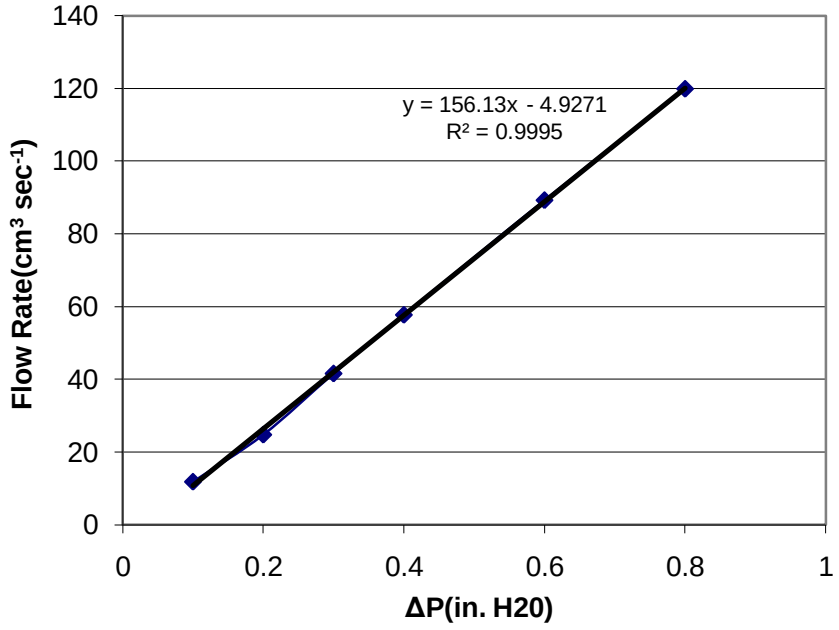

Figure A1-1
Flow rate through TSI 3302 capillary as a function of measured pressure drop.

The resulting volumetric dilution ratio was then calculated such that

$$DR_{vol} = \frac{Q_{total}}{Q_{cap}} \qquad \text{Equation A1-1}$$

where:

DR_{vol}= Volumetric Dilution Ratio

Q_{total}=Total Volumetric Flow(CPC Flowrate)

Q_{cap}= Capillary Flow Rate

Leaky Filter Diluter

Measuring the volumetric dilution ratio of the leaky filter diluter was performed similarly to that of TSI 3302. The first test to provide a known total volumetric flow, and in this case, the TSI 3025A provided the sample flow. The total sample flow using this setup was measured to be 1.495LPM using a bubble flow meter(Gilbrator 2, Gillian). The pressure drop across the diluter was measured using a pressure gage(Magnahelic 2000-6MM, Dywer) and was found to be 2.6mm of water. Using 3/16" ID Tygon R-22 tubing the bubble flow meter was connected directly to the capillary tube and a vacuum pump with throttle valve was used to produce a pressure drop across the tube to 2.6mm of water. Using Equation A1-1 the resulting volumetric dilution ratio for this configuration is determined to be 13.11.

Orifice Diluter

Due to the nature of the design of the orifice diluter, direct measurements of the volumetric dilution ratio are near impossible. A method to determine the volumetric dilution ratio was derived using a combination of direct measurements of flow and assumptions on the flow through the orifice.

As shown in Figure 2-3, the pressure drop across both filters will be equal to the pressure drop across the orifice. Therefore if the relation of the amount of flow going through the filters, and the resulting pressure drop is know, then the flow going through the orifice can be found by

$$Q_{orifice} = C_d A_{orifice} \sqrt{\frac{(2\Delta P}{\rho}} \qquad \text{Equation A1-2}$$

where:

$Q_{orifice}$= Orifice Flow Rate

C_d= Discharge Coeffecient

$A_{orifice}$= Area of orifice

ΔP= Pressure Drop

ρ= Air Density

The pressure drop to flow rate characteristics of the filter setup was determined by placing a plug in the orifice location. This forces all of the flow to pass through the filters and connecting tubing. Using a MSP 180 Flow resistance monitor to measure the pressure drop, and a TSI 4010 flow meter to provide the volumetric flow, yields Figure A1-2.

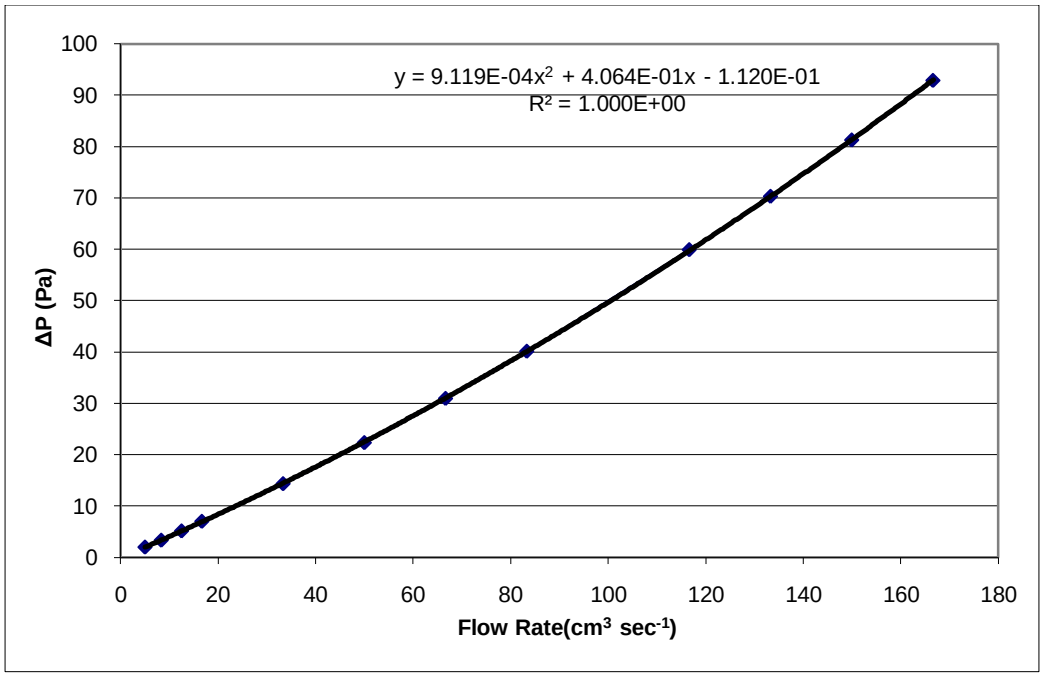

Figure A1-2
Pressure Drop characteristics for filter and connections used within the orifice diluter.

The remaining missing information is that of the discharge coefficient(C_d) which for the flowrates and sizes used is Reynolds number and geometry dependent (Kiljansk el al., 1993). To determine the discharge coefficient for the orifices used, the flow rate and pressure drop were recorded for the orifice sizes of 0.011",0.015",0.028" and 0.065". To provide a interpolation method for orifices not tested, the discharge coefficient is determined as per equation A1-2 and plotted as a function of 1/Re as shown in Figure A1-3. Using a polynomial fit provides a curve interpolation and indicates comparable discharge coefficients to those measured by Kiljanski et al (1993).

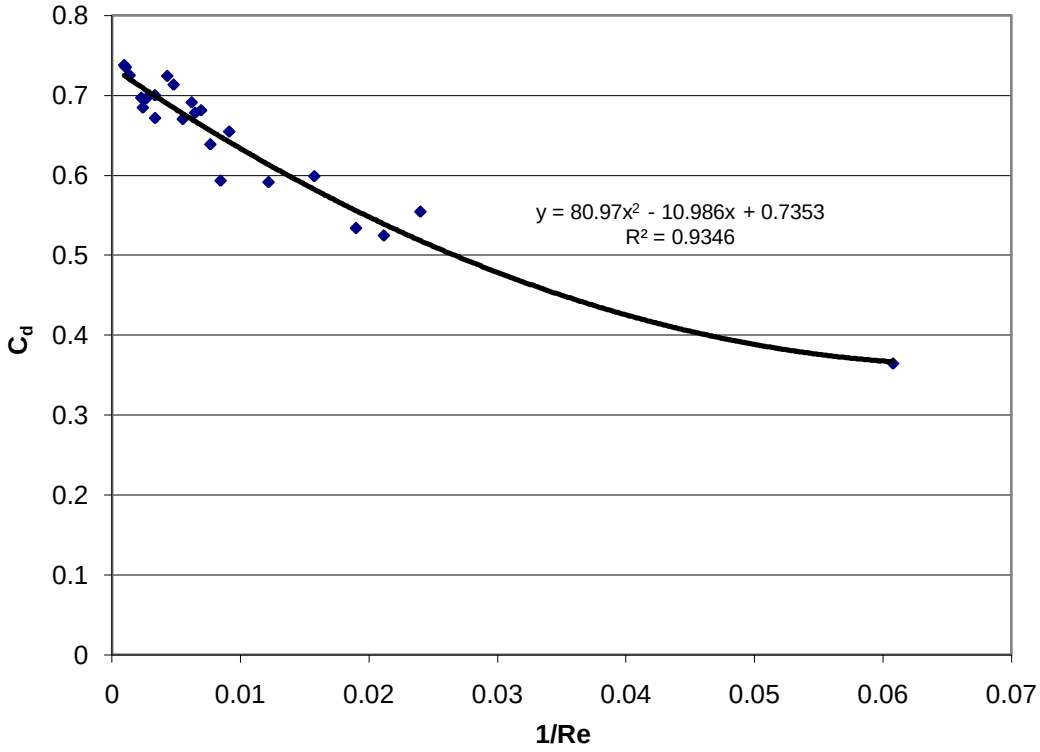

Figure A1-3
Discharge coefficient for O'Keefe orifices as function of 1/Re

To aid in calculations, the use of the software package Engineering Equation Solver(EES) is used for the determination of volumetric dilution ratio given the orifice diameter and total sample flow.

EES Code

```
{Conversions}
Q_total=Q_total_LPM*1.6666667E-5
D_orifice=D_orifice_in*0.0254

{Calculations}
C_d=80.97/Re^2-10.968/Re+0.7353

DELTAP=9.119E-4*(Q_bypass/1E-6)^2+4.064E-1*(Q_bypass/1E-6)-1.120E-1

Re=rho_air*U_orifice_*D_orifice/mu_air

U_orifice_=Q_orifice/(A_orifice)

A_orifice=(PI/4)*D_orifice^2

Q_orifice=C_d*A_orifice*sqrt(2*DELTAP/rho_air)

Q_total=Q_bypass+Q_orifice

DR=(Q_bypass+Q_orifice)/Q_orifice

rho_air=Density(Air,T=T,P=P)

mu_air=Viscosity(Air,T=T)
```

Appendix II. MSP CPC Counting Efficiency Curve

Not provided by the manufacturer, is the CPC counting efficiency curve as a function of particle diameter. To determine the counting efficiency curve the apparatus shown in Figure 2-1 was used. Since the data required for this calculation was collected when referencing the CPC response over the particle sizes tested in Section 2.2.2 it can also be used to determine the CPC particle response curve if the reference CPC, a TSI 3025A , is also known.

Work by both Stolzenburg et al.(1991) and Wiedensohlet et al.(1997) et al. analyzed the particle size dependent counting efficiency of the TSI 3025A with both authors finding the resulting response to be unity for particle sizes greater than 4nm. This effectively allows the TSI 3025A reference CPC to act as absolute measurement of performance of the MSP CPC over the particle size of 6nm to 100nm.

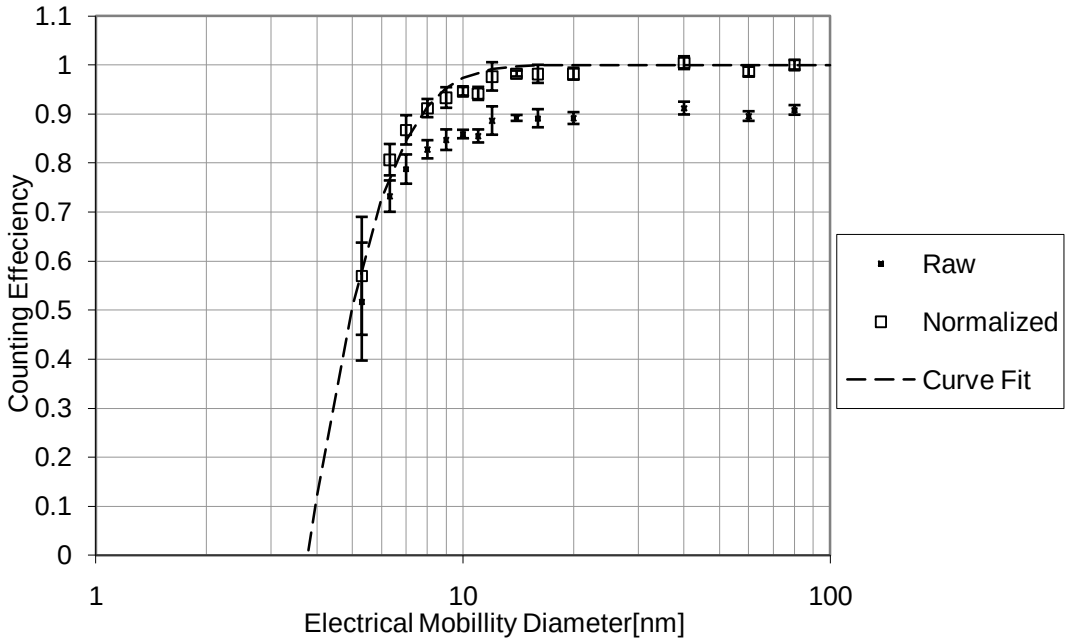

Figure A2-1

Particle detection efficiency for MSP CPC using TSI 3025A as the reference. Error bars represent std. deviation of test data.

The raw data collected, as shown in Figure A2-1, resulted less than unity counting efficiency for particles greater than 20nm. Since this error is most likely due to miscalibration in the CPC sample flows. Due to the resulting trend indicating this for particles as large as 80nm, which are well away from the resulting roll off of the CPC detection curve, the data is normalized to allow the fitting of a three parameter curve as shown by equation A2-1.

$$\eta_{CPC} = 1 - be^{\frac{D_1 - dp}{D_2}} \qquad \textbf{Equation A2-1}$$

The resulting curve fit and fitted parameter values can be found in Table A2-1. Most notably is the fact that the resulting particle size for 50% counting efficiency (dp_{50}) using the fitted curve results in 5.0 nm.

Table A2-1
Fitted Parameters for Equation A2-1

Parameter	Value
b	-3.3447
D1	1.7179
D2	1.7103